UNIVERSITÀ
DEGLI STUDI
DI CAGLIARI

Ph.D. DEGREE IN

Industrial Engineering

Cycle XXXV

TITLE OF THE Ph.D. THESIS

Monitoring and control for NGL recovery plant

Scientific Disciplinary Sector(s)

ING-IND/26

Ph.D. Student — Marta Mandis

Supervisor — Prof. Roberto Baratti

Co-Supervisor — Prof. Stefania Tronci

Final exam. Academic Year 2021/2022
Thesis defence: April 2023 Session

"Marta Mandis gratefully acknowledges the Sardinian Regional Government for the financial support of her PhD scholarship (P.O.R. Sardegna F.S.E. - Operational Programme of the Autonomous Region of Sardinia, European Social Fund 2014-2020 - Axis III Education and training, Thematic goal 10, Investment Priority 10ii), Specific goal 10.5"

I would like to acknowledge the support of Professors Francesco Corona and José A. Romagnoli for hosting me during my time abroad in their departments in Espoo (FI) and in Louisiana (US) as well as for their guidance and assistance.

Table of Contents

Abstract

In this Thesis, the production of natural gas liquids (NGLs) and the challenge of monitoring and controlling the fractionation process are thoroughly explored. NGLs are the C2+ Hydrocarbon fraction contained in natural gas, which comprehend useful feedstocks for industrial production processes. The production and utilization of natural gas have become crucial topics in recent years for several reasons. Foremost, the technological advancements in extraction techniques have led to an increase in the availability of natural gas from unconventional reservoirs. Since NGLs have greater economic value compared to natural gas, their recovery has become increasingly economically significant, leading to a need for efficient NGL fractionation. This energy-intensive process is typically conducted in separation trains that include cryogenic distillation columns. NGL recovery processes widely used in industry have been simulated through the process simulator HYSYS® and analyzed under the imposition of typical process disturbances. The fractionation process considered in this work uses multicomponent distillation for NGL recovery, which is linked to the need for composition analyzers to achieve purity targets. Given the high cost of composition analyzers and the significant delays introduced in composition controllers it makes it unfeasible to profitably achieve the desired control goals. This study first aims to develop a proper and feasible control strategy for the process under investigation without the need for concentration analyzers. Different indirect quality control structures were developed and evaluated under the presence of changes in the inlet plant feed flowrate and composition, with the primary objectives of achieving an ethane recovery of 84 % and low levels of methane impurity in the bottom of the demethanizer column. In particular, the control strategies compared the use of direct temperature controllers widely used in industry, with the implementation of pressure compensator and cascade control using a regression boilup estimation. Also, a hybrid cascade control that updates the reference of the column temperature controller using in-line delayed concentration measurements at each sampling period is presented. The results indicate that besides the control structure developed without the use of composition analyzers, shows optimum performances under inlet feed flow disturbances, the hybrid cascade control schemes provide superior control performance in the presence of composition disturbances, allowing the new steady state offset elimination. To eliminate the offset obtained in the control of the methane concentration at the bottom of the demethanizer without the use of composition

analyzers, a data-driven control strategy based on soft sensors were developed by using Feedforward (FNN) neural networks and implemented in the HYSYS® simulation. Finally, the focus of the research work moves on towards exploiting the multitude of data made available by using the process simulator to develop a digital twin for the NGL recovery process evolving in the cold residue reflux (CRR) process scheme. The goal was to obtain a surrogate model using Long Short-Term Memory (LSTM) neural networks in non-conventional arrangement with incorporated physical knowledge to approximate the real dynamics of the column with reduced computation time. Several neural network architectures were compared, the best of which were integrated with two additional LSTM models for the digital twin realization. The models were trained and tested with realistic measurement noise, and only easy-to-measure variables were used as input data. The results showed that the digital twin effectively reconstructed the column's actual operations quite accurately, proving successful estimation for the considered target variables. Overall, the presented research proposes to exhibit the feasibility of attaining energy-efficient Natural Gas Liquid (NGL) recovery without using composition analyzers, offering a cost-effective and efficient alternative to traditional measuring instruments. Furthermore, the study introduces a novel application of LSTM neural networks in the development of digital twins for distillation columns, providing a valuable tool for optimization, monitoring and quality control by employing only easily and economically available plant measurements.

Chapter 1

Introduction

The introductory chapter explains the motivation behind the development of this thesis. Next, a list of related publications and presentation in international and national conferences are shown. Finally, the state of art of control and estimation in multicomponent columns and the application of Neural Network modeling in chemical processes is summarized.

1.1. Motivations

The industrial sector heavily relies on measurement sensors to provide insight into the state of ongoing processes. However, the actual status of all variables remains elusive due to the high cost of purchasing and maintaining measurement devices and the infeasibility of their installation within the equipment. The composition analyser represents one of the required instruments for product quality control and monitoring in multicomponent distillation columns. However, these measuring instruments are associated with a high cost of purchasing and maintenance, as well as long sampling time and measurement delays. These related disadvantages lead to the pursuit of different control and monitoring solutions, such as the use of temperature measurements to infer or indirectly control the desired composition. Since in multicomponent distillation columns, the concentrations achieved in each column tray are not uniquely related to the tray temperature, the use of temperature measurement does not always allow adequate composition control and estimation. The research project focuses on a natural gas treatment plant that uses multicomponent distillation columns for producing high-value by-products: natural gas liquids (NGLs). This is a complex system which is greatly influenced by operating conditions such as pressure, temperature, and feed conditions, the process is also impacted by various disturbances, such as changes in the inlet flowrate and composition.

In literature, the NGL recovery process has been extensively studied with many authors contributing to the understanding of the major aspects of natural gas field processing. Manning & Thompson (1991) and Kidnay et al. (2011) provided an overview of NGL recovery, while Mehrpooya et al. (2010) and Chebbi et al. (2010) presented different NGL recovery process optimization based on cost analysis. Other authors, such as Getu et al. (2013), Park et al. (2015), Kherbeck & Chebbi (2015), and Olsen et al. (2012), compared different NGL separation schemes employing Joule-Thompson expansion, turbo-expansion, and cryogenic distillation. In this field, the research has focused recently on the dynamics and control of product quality indices, mainly in the demethanizer column bottom product.

The demethanizer column product quality control is particularly challenging due to the localized concentration drop in the column ends and the flat composition profiles in the central zone of the column. The proximity of the concentration drop to the column ends makes the problem of composition control difficult with only the use of indirect temperature control, as the temperature at the column ends also depends on the variation of non-key components, which are greater in the column end zones. Also, the presence of methane in supercritical

conditions in the last stages of the column contributes to obstacles to the use of indirect composition control through temperature measurement, largely influencing the temperature gradient and leading to enormous temperature variability in this part of the column due to his presence as mixture gas solute increasing the need of energy for the separation.

Various works in the literature, including Chebeir et al. (2019) and Luyben (2013), have examined the NGL separation process dynamics and the demethanizer bottom product quality control in the presence of typical disturbances. Chebeir et al. (2019) proposed control structures with the implementation of composition controllers in a direct or cascade arrangement, while Luyben (2013) considered inferential composition control through temperature controllers and direct composition controllers. Both contributions consider the presence of composition analyzers in the plant but neglect the typical delay associated with composition measurements and measurement noise.

The presented work first focuses on the optimization of product quality control for the demethanizer column in the NGL recovery plant without the use of composition analyzers. To maintain product specifications, different indirect composition control strategies were developed to mitigate the effects of these disturbances while enhancing the plant's energy efficiency. However, due to the lack of a biunivocal relationship between temperature and composition, indirect control of the compositions does not guarantee the respect of the desired product purities in multicomponent columns. Thus, to overcome the need for concentration measures and without composition analyzers to achieve the best control performances, deep learning techniques were applied, considering historical measurement data easily available in industrial plants for the implementation of software sensors able to predict the evolution of process variables that are difficult to measure over time. Information on all the process variables can be obtained utilizing process simulators, although the related calculation time makes it impractical to use the simulated model to optimize, monitor and control a real industrial plant. However, the simulator allows the collection of large amounts of process data that can be used to develop a data-driven digital surrogate with much shorter computational times. The combined use of commercial simulators and emerging machine learning techniques in conjunction with process knowledge makes it possible to attainment of a surrogate model with which design control, management, and optimization strategies. The final goal of the study thus aims to present a novel approach for the development of a multicomponent distillation

column digital twin which approximates the real dynamics of the column and that could be used for improving the efficiency of the NGL recovery process.

1.2. List of Pubblications and Presentation in conferences

Some of the topics in the present Thesis led to the development of the following contribution:

- Mandis, M., Baratti, R., Chebeir, J.A., Tronci, S., Romagnoli, J.A. A Demethanizer column Digital twin with non-conventional LSTM neural networks arrangement. (2023). (Presented and accepted to the 33rd European Symposium on Computer Aided Process Engineering (ESCAPE33));

- Mandis, M., Chebeir, J.A., Romagnoli, J.A., Baratti, R., Tronci, S. Effect of the demethanizer improved control strategy on the separation train for the NGL separation process. (2022) IFAC-PapersOnLine, 55 (7), pp. 889-894. DOI: 10.1016/j.ifacol.2022.07.557;

- Mandis, M., Chebeir, J.A., Tronci, S., Baratti, R., Romagnoli, J.A. Control of a natural gas liquid recovery plant in a GSP unit under feed and composition disturbances. (2021) IFAC-PapersOnLine, 54 (3), pp. 182-187. DOI: 10.1016/j.ifacol.2021.08.239;

- Tronci, S., Chebeir, J.A., Mandis, M., Baratti, R., Romagnoli, J.A. Control Strategies for Natural Gas Liquids Recovery Plants. (2020) Computer Aided Chemical Engineering, 48, pp. 1291-1296. DOI: 10.1016/B978-0-12-823377-1.50216-0;

- Mandis, M., Baratti, R., Chebeir, J., Tronci, S., Romagnoli, J.A. Performance assessment of control strategies with application to NGL separation units. (2022) Journal of Natural Gas Science and Engineering, 106, art. no. 104763. DOI: 10.1016/j.jngse.2022.104763;

- Mandis, M., Chebeir, J.A., Baratti, R., Romagnoli, J.A., Tronci, S. Machine learning for monitoring and control of NGL recovery plants. (2021) Chemical Engineering Transactions, 86, pp. 997-1002. DOI: 10.3303/CET2186167;

- Mandis, M., Baratti, R., Chebeir, J.A., Mandis, M., Tronci, S., Romagnoli, J.A. Comparison of non-conventional neural network architectures for the realization of a Demethanizer column Digital. (2023). (Manuscript under preparation).

Works presented in national and international conferences:

- Dynamic simulation and control of NGL recovery plant, GRICU 2022 National Conference, 3 - 6 July 2022, Ischia (Italy);
- Control strategies for NGL recovery plants, ESCAPE 30 European Symposium on Computer Aided Process Engineering, 31st Aug – 1st Sep 2020, Milan (Italy);
- Control of a natural gas liquid recovery plant in a GSP unit under feed and composition disturbances, 11th IFAC International Symposium on Advanced Control of Chemical Processes, 13 -16 June 2021, Venice (Italy);
- Effect of the demethanizer improved control strategy on the separation train for the NGL separation process, 13th IFAC Symposium on Dynamics and Control of Process Systems (DYCOPS), 14 - 17 June 2022, Busan (Republic of Korea).

1.3. State of the art

The NGL fractionation process will be addressed in this research work by considering the use of several distillation columns for the separation of the light components contained in the original mixture. Distillation columns are designed to carry out unit operations where due to the establishment of a liquid-vapor equilibrium a given stream is separated into two or more products to meet specified purity levels of key components. The goal of the control and estimation problems in the distillation column concerns the achievement of the desired product quality under the presence of non-eliminable process disturbances with the minimum waste of energy. Here an overview of the most related control and estimation literature for multicomponent distillation columns will be presented. Also, a brief discussion of the use of neural networks in the field of industrial processes is reported.

1.3.1. Control of multicomponent distillation columns

The control of product quality indices in distillation columns allows the achievement of high product quality as well as reducing processing time and operating costs (X. Zhu & Ji, 2022). To obtain an offset-free product quality control under the effect of inlet disturbances in presence of changes in operating conditions, the use of composition analyzers for the implementation of composition controllers is required. This type of control strategy is the simplest in terms of construction, but it also has several negative aspects. Indeed, such analyzers present several disadvantages such as significant costs of purchasing and

maintenance, reliability problems, and measurement delays. Due to these unfavourable aspects, the use of direct composition controllers may be inadequate for online composition control. An alternative to direct control is the indirect control of composition through temperature measurements (Hori & Skogestad, 2007). In industry, column product quality control is typically addressed through temperature controllers employing available temperature measurements. This type of control is commonly realized with PI feedback controllers, the most widely employed control system in industrial distillation columns. In binary distillation columns, a biunivocal relation between temperature and composition subsists, which is not true for multicomponent columns where multiple compositions are involved in the equilibrium calculation, leading to the existence of multiple solutions related to the same considered temperature. The use of temperature controllers in multi-component columns can however provide good disturbance rejection in indirect product quality control if a proper location for the temperature sensor is selected. Thus, essential in cases of multi-component columns is the choice of the temperature sensor location. Different criteria have been employed to select the best temperature sensor location for multicomponent columns where non-key components can strongly influence the temperature. Luyben (2005) and Hori & Skogestad (2007) suggested that locations close to the bottom, the top, and the feed stages should be avoided. Rademaker et al. (1975) suggested that sensors should be located where the temperature gradient is the largest and non-key compositions are almost constant. Another selection criterion that highlights the variations of the temperature gradient due to the variations in the key and non-key component concentrations is given by the temperature gradient with a per-component contribution diagram analysis (Frau, 2011). The lack of informative temperature measurements on key component composition variations in a column section makes it impractically the installation of temperature controllers for dual-end control. In this case, only single-end control structures can be implemented for the quality control of distillate or residue. The remaining degree of freedom is fulfilled with the implementation of a ratio controller to limit the composition offset in the other product.

The analysis of the dynamics and the control of the NGL recovery process employing cryogenic distillation technology has been investigated in the contributions of Luyben (2013c, 2013a) and Chebeir et al. (2019). In the works of Luyben, the dynamic control of a demethanizer column with side reboilers is studied by comparing the effects of inferential composition control through temperature controllers and direct composition controllers.

Chebeir et al. examined the process dynamics of different NGL recovery processes in presence of typical disturbances. The work proposed a control structure that comprises the implementation of composition controllers in a direct or cascade arrangement. Despite both works comprising the presence of composition analyzers in the plant, the presence of delay, typically occurring with these measurement devices, was neglected not allowing a more realistic analysis of the use of composition controllers in the plant.

On the other hand, the use of indirect composition controls, employing temperature controllers, despite being widely used in industry, may not be the best control strategy to guarantee product specifications as it cannot guarantee the respect of product quality but only the limitation of the disturbance effects. For this reason, new solutions have been explored to avoid the use of composition analyzers, while achieving optimal product quality control.

1.3.2. Estimation in multicomponent distillation columns

In distillation columns, the targets of the estimation problem are generally represented by product composition, due to disadvantages related to the use of composition analyzers and their high cost. To optimally control the process production targets without incorporating composition analyzers, one possibility is the use of inferential control through real-time composition estimations. The estimation of process variables can be also necessary for process monitoring purposes. The development of composition estimators is usually realized by secondary measurements, such as temperatures or others easily available variables. Two main classes of estimators can be developed: input-output data-driven estimators and model-based estimators. The first class requires training data in input to detect the relationship between input and output considered. Algorithms used for estimation in distillation columns include singular value decomposition (SVD) (Yu & Luyben, 1987), partial component regression (PCR) (Al Kalbani & Zhang, 2023), artificial neural network (ANN) (Chetouani, 2007) modelling, partial least square (PLS) regression (Mejdell & Skogestad, 1991; Zamprogna et al., 2005). The model-based estimators benefit from the incorporation of the process model in their definition, which leads to the realization of estimators robust to changes in operating conditions. State estimation of multicomponent distillation columns was first addressed by Joseph & Brosilow (1978), using for composition estimation a linear combination of temperature and flow measurements. The most employed estimation algorithm for dynamic and nonlinear systems

in process engineering is the Extended Kalman Filter (EKF) (Kalman, 1960). A discrete EKF was employed for binary and multicomponent batch distillation columns form Oisiovici & Cruz (2000). Another estimator comparable with EKF which benefits from a systematic and simple tuning procedure (Frau, 2011) is the Geometric Estimator (GE) (Alvarez & López, 1999). A nonlinear geometric observer for composition estimation in a pilot-plant binary distillation column was developed by Tronci et al. (2005). A key issue in composition observers for distillation columns is the number and location of temperature measurements. In this work this issue has not to be considered as the realization of the estimators was conducted using data made available by the process simulator.

1.3.3. Neural Networks applied to chemical process modeling

As mentioned in the previous paragraph, ANNs are advanced tools that can be used for the realization of data-driven models in the industrial field. Commonly used methods include principal component regression, partial least squares, and artificial neural networks (ANNs) (Ge, 2017). ANNs have outstanding performance in apprehending the behavior and variables correlation in nonlinear physical systems and are known as universal approximators with the ability to learn and represent any complex input-output relationship (Lu et al., 2021). Thanks to these characteristics, ANNs are a powerful tool nevertheless, despite being theorized since the 1940s (McCulloch & Pitts, 1943), only recently it has become possible to take full advantage of its capabilities thanks to the possibility of access to the huge amount of information that can be acquired and exchanged in real-time with the rise of the so-called big data era in conjunction with modern advances in computational technology (Tao et al., 2016). Due to their simple structure and fast learning rate, a type of ANN widely used to model time series problems (Zhang et al., 2015) is given by feedforward neural networks (FNNs). However, their use allows the detection of only static correlations between inputs and outputs disregarding temporal dependencies, which is essential to obtain an adequate estimation when addressing the problem of time series modelling. Recurrent neural networks (RNNs) (Elman, 1990) were developed to address time-dependent problems. Due to the introduction of a recurrent loop and a cell memory, RNNs can determine and store temporal dependencies even between events occurring far in time. Among the various RNNs types developed over time, one of the most useful when addressing with long time dependency is the Long-Short Term Memory network (LSTM) (Hochreiter & Schmidhuber, 1997), designed to overcome the

problem of the vanishing gradient. LSTM networks have been applied to different nature problems in chemical engineering including fault diagnosis (Pang et al., 2022; Wang et al., 2022), process optimization (Zhu et al., 2020), soft sensors (Ke et al., 2017; Yuan et al., 2020), in particular soft sensors for product monitoring in distillation columns (Ferreira et al., 2022; Rosyadi et al., 2023; Singh et al., 2005) and digital twin realization for plant monitoring, and control (Qu et al., 2020; X. Zhu & Ji, 2022). In particular, the use of LSTM networks for the development of digital surrogate models is of great interest in various fields of study, including the process industry. Indeed, a digital twin (Grieves, 2015) consists of a virtual model of whole plants or individual units which is interconnected with the actual equipment with which it exchanges information in real-time, and it can predict their dynamic evolution over time. For this reason, a digital surrogate can provide a useful tool for performance monitoring, predictive asset maintenance, production optimization and advanced process control.

Chapter 2

NGL Recovery Industry

This chapter presents an overview of natural gas and NGL characterization, as well as a summary of their principal uses. Also, the world's main basins and the most common technologies used for NGL fractionation are reported.

2.1. Natural Gas characterization

Among the energy sources of fossil origin, natural gas, from an environmental point of view, is the cleanest, it is mainly used as a fuel as an alternative to the more traditional oil and coal. Indeed, natural gas is a clean-burning fossil fuel and is the least carbon-intensive fossil fuel. When burned, it produces lower emissions of sulfur dioxide, nitrogen oxides, and particulate matter compared to coal and oil. This makes it an attractive alternative for power generation and industrial use and one of the main uses of natural gas is as a fuel for heating and electricity generation.

2.1.1. Characteristics and Composition

Natural gas is a gas mixture colorless, odorless, and tasteless, as well as non-toxic and non-corrosive. The characteristics and composition of this gas can vary depending on its source, but in general, it is mainly composed of methane, typically 85-90% of the total composition (*Natural Gas - Composition and Properties of Natural Gas | Britannica*, s.d.), and small amounts of other hydrocarbons such as ethane, propane, and butane, as well as impurities such as water vapor and carbon dioxide. The amount of these impurities can vary depending on the source. For example, natural gas from shale formations can have higher levels of impurities compared to gas from conventional reservoirs. The presence of the hydrocarbon fraction of C2+, known as NGL, is an additional source of profit: the heavier hydrocarbon compounds are separated, liquefied, and used as raw materials for other production processes. The extraction of the hydrocarbon fraction of C2+ is also used as a technique for fuel conditioning and dew point control of the mixture to avoid the formation of liquid inside the pipelines that can cause slowdowns in the flow and give problems to measuring instruments (Kidnay et al., 2011).

2.1.2. Usage and Market price

One of the main uses of natural gas is as a fuel for heating in residential and commercial buildings, and for power generation since it is relatively cheap and produces lower emissions of pollutants compared to coal and oil. The use of natural gas to produce energy is not a recent practice (Kidnay et al., 2011), but this has increased in the last decades due to the so-called "shale gas revolution" (Caporin & Fontini, 2017) derived from technological advances in

extraction methods, including hydraulic fracturing and horizontal drilling. The technological advancement in fracking methods has bringing to access to huge volumes of gas trapped in shale formations (Feng et al., 2021). This has led to an increase in the quantities of Natural gas available and a consequent decrease in its selling price, which dropped to less than 30% of its previous highs (Brigida, 2014; Caporin & Fontini, 2017; Feng et al., 2021; Luyben, 2013c). The increasing employment of Natural gas is also driven by the new awareness for planet preservation which increased the focus on renewable energy sources, subjected to fluctuations related to the nature of the source of energy. Natural gas in this context can be seen as an integrative source, whose availability is comparable to that of coal and oil, but with a reduced environmental impact. Also, natural gas is used as a feedstock in the production of chemicals, fertilizers, and hydrogen. In recent years, the use of natural gas in transportation has also been increasing, with compressed natural gas (CNG) and liquefied natural gas (LNG) being used as fuel for vehicles . The price of natural gas is determined by a variety of factors, including supply and demand factors, such as changes in production levels, changes in consumption patterns, the availability of alternative energy sources, the price of competing fuels such as oil and coal and weather conditions. The price can also be affected by government policies and regulations.

2.1.3. World main basins

Natural gas is formed over millions of years from the remains of plants and animals, and is found in underground reservoirs. Some of the main natural gas basins in the world include (*The world's biggest natural gas reserves*, s.d.):

- Persian Gulf: This region is home to some of the largest natural gas reserves in the world. Iran holds the world's second biggest natural gas reserves mostly located offshore while Qatar, the world's largest exporter of liquefied natural gas (LNG), holds the third largest natural gas reserves;
- North Sea: it is located between the United Kingdom, Norway, Denmark, Germany, the Netherlands, and Belgium;
- Russia is one of the largest natural gas producers in the world and has the world's largest natural gas reserves which account for about a quarter of the world's total proven gas reserves. The main natural gas basins in Russia are located in Siberia.

- The United States, the world's largest producer and consumer of natural gas, has the fifth larger natural gas reserves, with the largest natural gas basins located in the Gulf of Mexico, the Rocky Mountains, and the Appalachian Basin;
- Middle East: it is a major natural gas producing region, significant reserves are located in Iraq, Oman, Saudi Arabia and the United Arab Emirates (UAE);
- Asia-Pacific: Turkmenistan holds the world's fourth largest natural gas reserves, while countries such as Australia, Indonesia, and Malaysia have significant reserves;
- Africa: Natural gas reserves are found in several countries in Africa, such as Algeria, Egypt, and Nigeria.

Natural gas exploration and production is a constantly evolving industry and new basins are being discovered and developed all over the world. The extraction of natural gas from a basin can be done through conventional and unconventional methods. Conventional natural gas extraction involves underground reservoirs drilling and pumping the gas to the surface. Unconventional natural gas extraction methods, such as hydraulic fracturing involve injecting water, sand, and chemicals into the ground to release the gas from shale rock formations.

2.2. NGL characterization

NGLs are a clean, low-cost energy source consisting of the hydrocarbon fractions of ethane, propane, butane and heavier hydrocarbons contained in Natural gas. They are separated from the natural gas stream during the processing of natural gas and can be used as a fuel source or as feedstock for the petrochemical industry. These compounds have a higher selling price than raw gas, justifying the construction and implementation of separation plants for their recovery.

2.2.1. Usage and Market price

NGLs have a variety of uses, including as a fuel source and as a feedstock for the petrochemical industry. The main uses of NGL can be summarized as follows:

- Ethane is used as a feedstock for the production of ethylene, which is used in the production of plastics, such as polyethylene and polyvinyl chloride;
- Propane is used as a fuel for heating and cooking in residential and commercial buildings, as well as for powering vehicles. It is also used as a feedstock for the

production of propylene, which is used in the production of plastics, such as polypropylene;

- Butane is used as a fuel for heating and cooking in residential and commercial buildings, as well as a component in the manufacturing of gasoline;
- Pentanes are used as a feedstock for the petrochemical industry and as a component in the manufacturing of gasoline;
- Natural gasoline, a mixture of different hydrocarbons, including pentanes and heavier molecules, is used as a component in the manufacturing of gasoline.

The demand and prices of NGLs are influenced by a variety of factors including geopolitical events, the price of crude oil, weather conditions, and competition from other energy sources. In addition, the prices of specific NGLs can also be influenced by their specific use and the availability of alternative feedstocks. The prices of NGLs can also vary depending on the location and method of transportation. Also, the profitability of the recovery process is impacted by the value of ethane as a liquid. Due to the difficulty of liquefying ethane compared to the other NGLs, it is the most energy-intensive and expensive to separate from raw gas (Ratner, 2018). When ethane's liquid value is high, maximizing its recovery leads to greater income. However, when ethane as a liquid has a low value, selling the ethane in residue gas provides greater income. While the value of liquid propane has almost always been higher than its value of gas (Pitman et al., 1998).

2.2.2. Most common recovery technologies

The fact that NGLs have normally a significantly higher value as products marketable separately than raw gas (Mokhatab et al., 2015) justifies the studies concerning plants and separation processes for their recovery. In the literature, several works in which different processes for the recovery of NGL are presented have been carried out by Manning & Thompson (1991), Mehrpooya et al. (2010), Kidnay et al. (2011), Chebbi et al. 2010, Getu et al. (2013), Park et al. (2015) and Kherbeck & Chebbi (2015). Several common technologies are used to recover NGLs from natural gas. Some of the most common include:

- Cryogenic processing: This method uses extremely low temperatures to separate NGLs from natural gas. This process allows NGLs to separate and condense into a liquid form;

- Absorption: This method uses a liquid absorbent, such as propane or ethane, to separate NGLs from natural gas. The natural gas is passed through a tower containing the absorbent, where the NGLs are absorbed into the liquid. The NGLs are then separated from the absorbent and recovered;
- Adsorption: This method uses a solid adsorbent, such as activated carbon, to separate NGLs from natural gas. The natural gas is passed through a tower containing the adsorbent, where the NGLs are adsorbed onto the solid. The NGLs are then separated from the adsorbent and recovered;
- Membrane separation: This method uses a semi-permeable membrane to separate NGLs from natural gas. The natural gas is passed through the membrane, which allows the NGLs to pass through but not the natural gas;
- Distillation: This method uses a distillation column to separate NGLs from natural gas. The natural gas is heated, causing the NGLs to be liquefied and separate from the natural gas.

The choice of recovery technology will depend on the specific characteristics of the natural gas, the desired recovery rate, and the cost of the equipment. Cryogenic processing and distillation are the most common methods for NGL recovery in natural gas processing plants, with the ability to recover the product at high purities (Olsen et al., 2012). This process involves the use of a train of distillation columns, the first distillation column of the train, the demethanizer, is the heart of the separation process. For this reason, various process modifications have been studied to enhance the separation occurring in this unit. Different process schemes were developed, one of the first proposed and most common industrial schemes is the conventional turboexpander process. In this scheme, the necessary refrigeration for cryogenic distillation is supplied using the pressure jump between the inlet stream and the nominal conditions inside the column utilizing a turbo-expander (Campbell & Wilkinson, 1981). Starting from this process scheme, with plant modifications and energy integrations operated to improve separation performance and reduce and minimize the energy demand required by the process (Wilkinson & Hudson, 1992), new process schemes have been realized. Among the most used are the Gas Subcooled Process (GSP) which uses the split-vapor concept to obtain column reflux and the Cold Residue Recycling Process (CRR) where, thanks to the addition of a cryogenic compressor, a part of the distillate is returned to the column as reflux, increasing in both cases the ethane recovery (Kherbeck & Chebbi, 2015).

Monitoring and control for NGL recovery plant

2.3. Conclusion of the Chapter

Natural gas is one of the cleanest fossil fuels and is primarily used as an alternative to oil and coal. It is a mixture of main methane and small amounts of other hydrocarbons, impurities such as water vapor and carbon dioxide. Natural gas is seen as an integrative energy source, with a lower environmental impact compared to coal and oil and is increasing in popularity due to the shale gas revolution and a greater focus on renewable energy sources. The main uses of natural gas include heating and electricity generation, as well as a feedstock for chemical production, fertilizers, and hydrogen. The price of natural gas is determined by various factors such as supply and demand, the availability of alternative energy sources, the price of competing fuels, and government policies and regulations. The extraction of NGLs from natural gas is an additional source of profit and is used as well for fuel conditioning and dew point control. The most common recovery technologies include cryogenic distillation, absorption, and adsorption. NGLs are a clean, low-cost energy source consisting of natural gas heavier hydrocarbon fractions and have a variety of uses such as being a fuel source or feedstock for the petrochemical industry. Ethane is used in the production of plastics, propane is used for heating and as a fuel, butane is used for heating and gasoline manufacturing, and pentanes and natural gasoline are used as feedstock for the petrochemical industry. The demand and prices of NGLs are influenced by various factors such as geopolitical events, crude oil prices, and competition from other energy sources.

Chapter 3

NGL Recovery Process

This chapter illustrates the NGL recovery process plant schemes simulated and used as a case study in the presented research work, as well as the operating condition considered and the selected process specifications required. In addition, a description of the design procedure used for the deethanizer, depropanizer and debutanizer columns is given.

3.1. NGL Recovery process simulation

The separation of NGLs is carried out through a fractionation unit consisting of a train of distillation columns in which first a cryogenic distillation for methane separation takes place. Subsequently, ethane, propane and butanes are separated using several distillation columns in a direct sequence arrangement. The NGL separation process was modelled and simulated through the Aspen HYSYS® process simulator, using the thermodynamic package given by the Peng-Robinson equations of state (EOS). The input data for the various simulations are based on realistic operating conditions (Chebeir et al., 2019). Natural gas is fed to the system with a flowrate of 4980 kmol/h at an inlet pressure and temperature of 5818 kPa and 35°C respectively, assuming that typical contaminants such as carbon dioxide, sulphuric acid, oils, and hydrates have been previously removed from the raw gas (Bassani et al., 2020; Nakhjiri et al., 2020). The composition of the gas is characterised by a low content of heavy hydrocarbons and is shown in Table 3.1.

Table 3.1: Nominal feed composition (Chebbi et al., 2010)

Components	Mol fractions
Nitrogen	0.01
Methane	0.93
Ethane	0.03
Propane	0.015
Butanes	0.009
Pentanes	0.003
Hexanes	0.003
%C_{2+}	6

3.2. Methane separation unit

Three plant schemes widely used in industry for the methane separation unit were considered:

- Conventional process;
- Gas subcooled process (GSP);
- Cold residue recycle (CRR).

The plants considered differ in the strategies used to optimize separation in the demethanizer, in terms of enhancing ethane recovery and energy efficiency.

3.2.1. Conventional Process scheme

The conventional scheme is depicted in Figure 3.1 together with the control loops necessary for the stability of the system. In this scheme, the main equipment of this separation system is a demethanizer column (T-100) of 30 stages with a reboiler (E-103) and no condenser. In this thesis the column trays are numbered from top to bottom, thus the number 1 will indicate the column top tray. The feed flow is pre-cooled through a heat exchanger (E-100) and a chiller (E-101). The chiller is intended to mimic a refrigeration system with an external refrigeration cycle. The precooled gas is sent to a first flash tank (TK-100) in which the condensed liquid is separated. The outgoing steam is sent to a further exchanger (E-102) to cool and condense the remaining hydrocarbons, which are separated from the gas by a second flash tank (TK-101). The gas exiting the flash tank (TK-101) is depressurised through a turbo-expander (TE-100) obtaining a gas-liquid flow supplied to the second stage of the demethanizer column. The liquid leaving the bottom of the separators is expanded, to meet the pressure required for column operations, with Joule-Thompson valves (JTV-100 and JTV-101) and fed into the column at the 8^{th} and 26^{th} stages. Once the hydrocarbon fraction of methane has been separated by the demethanizer, the NGL product is sent to the next columns of the separation train for heavier hydrocarbon separation and single commercialization. The sale gas leaving the top of the column goes through two heat exchangers (E-100 and E-102) as cold fluid and is then recompressed in the turboexpander TE-100 and compressor K-101. An important variable for ethane recovery is given by the flash tank (TK-100) temperature which depends on the conditions achieved in the chiller used to precool the feed. The specifications required by the

separation process were the achievement of an ethane recovery of 84% and a methane composition of 1 mol% at the bottom of the demethanizer column.

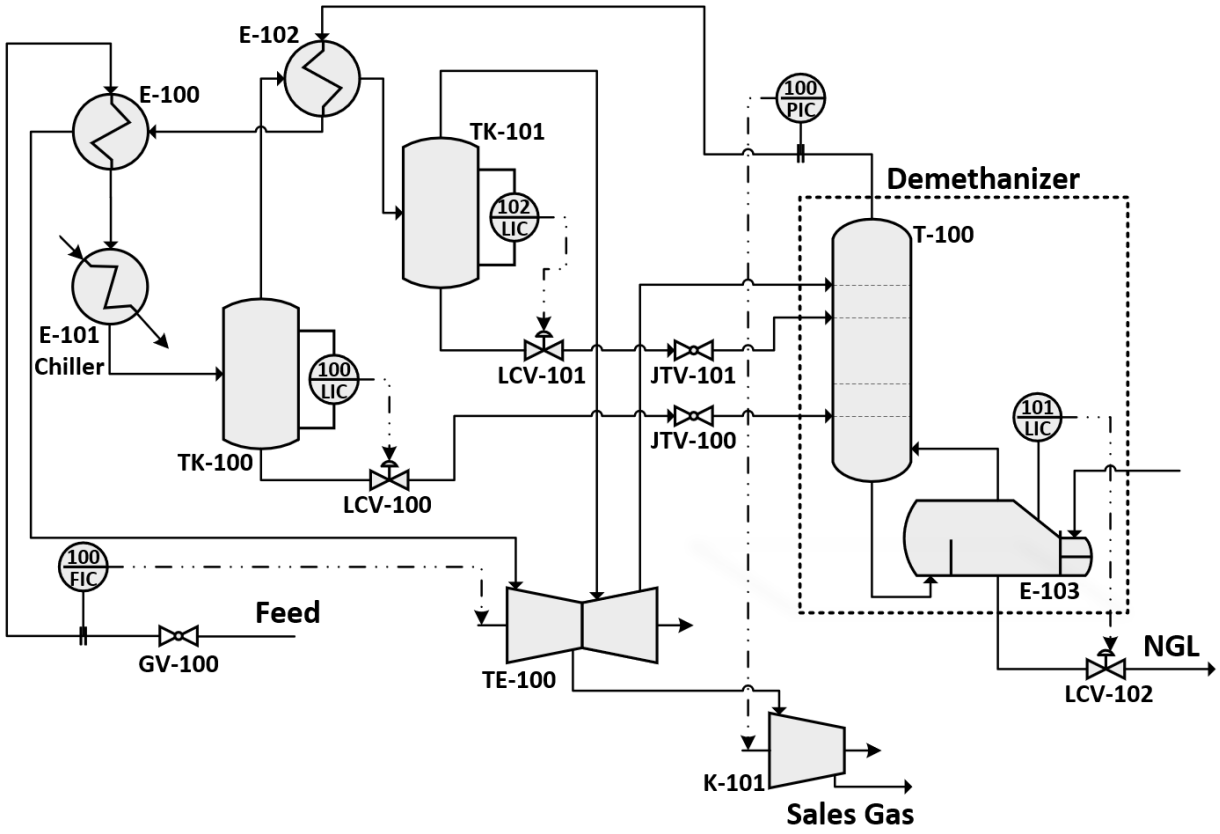

Figure 3.1: Conventional separation unit with stability control loops.

3.2.2. GSP Process scheme

A schematic representation of the GSP separation unit is depicted in Figure 3.2 together with the stability control loops. The main part of the separation unit consists of a 30 stage demethanizer column (T-100) with no condenser and a reboiler (E-103). As for the conventional unit, the feed gas goes through a two-stage cooling process constituted by a heat exchanger (E-100) and a chiller (E-101). The precooled raw gas is then fed to the flash tank (TK-100) placed upstream of the column. By applying the “vapor split” concept, the vapor and liquid streams leaving the flash tank are split into two liquid and vapor streams. This “vapor split” concept is a unique feature of the GSP scheme, and it is critical to increasing energy efficiency (Pitman et al., 1998). Out of the two gas streams, one is sent to the heat exchanger E-102 for additional refrigeration, expanded by a Joule-Thompson valve (JTV-100) and fed to the top of the column to provide a liquid with low content of heavy components that acts as

reflux. The presence of cool liquids at the top of the column contacts and rectifies the vapors exiting the turboexpander allowing ethane and heavier hydrocarbons to be recovered. The remaining gas flow is decompressed in the turboexpander (TE-100) to meet the required column pressure and fed at the 8th column stage. The condensed stream leaving the flash tank is depressurized by a Joule-Thompson valve (JTV-100) and fed to the 26th stage of the column. Again, the bottom product of the demethanizer column is sent to the fractionator train while the gas leaving the top of the column is used as the cold fluid in the two heat exchangers (E-100 and E-102) and then recompressed for its commercialization. Also in this case, the unit production goal was to reach 84% ethane recovery and a 1 mol% methane impurity level at the bottom of the demethanizer column.

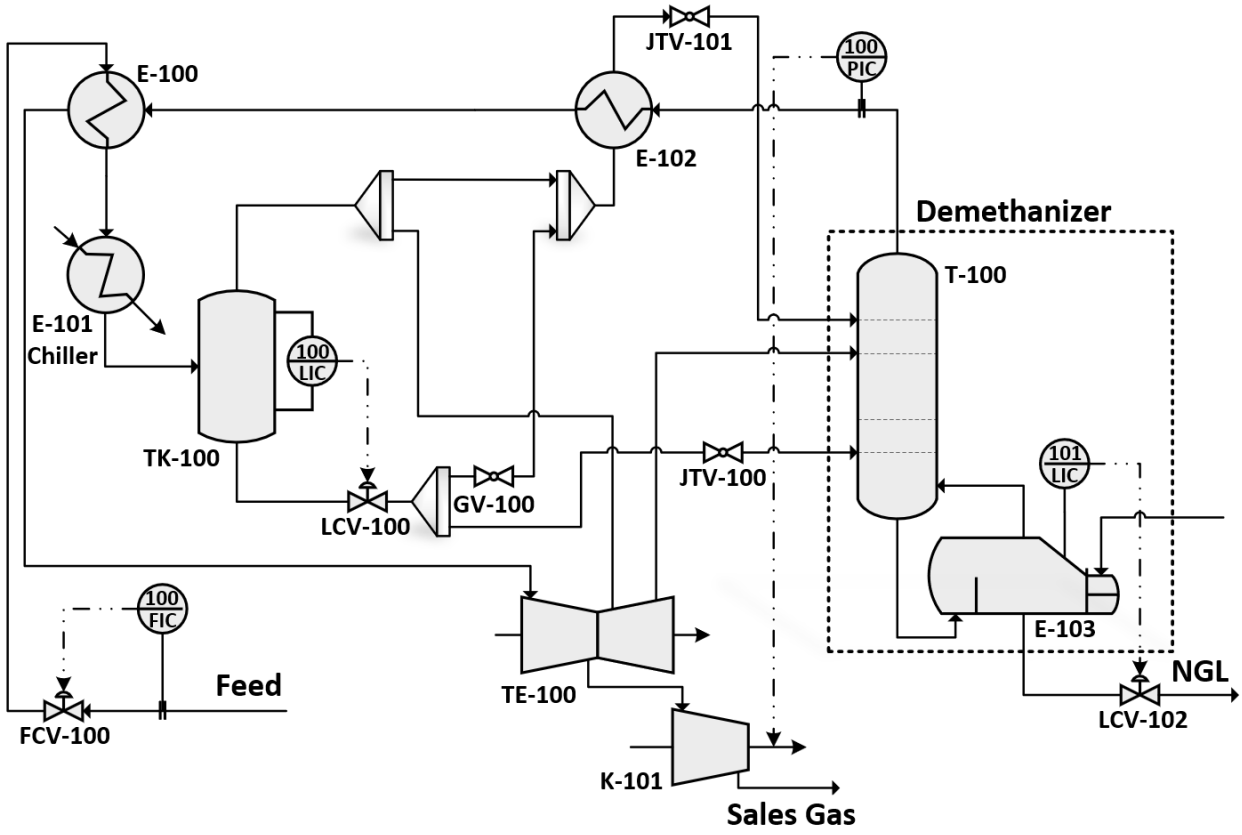

Figure 3.2: GSP separation unit with stability control loops.

3.2.3. CRR Process scheme

The CRR process scheme and the related stability control loops are depicted in Figure 3.3. This process represents an evolved version of the GSP scheme with the main goal of improving the economics of the NGL recovery process through a higher ethane recovery and a lower energy

demand (Hudson et al., 2003). The main difference of this process structure when compared to other schemes resides in the incorporation of a reflux stream to improve the rectifying section so that only a negligible amount of ethane and heavier components escaped from the column overhead. Again, the main part of the separation unit is the demethanizer column (T-100), which consists of a 30 stages distillation column with a reboiler (E-103) and no condenser. To provide column reflux, the top product is split into two streams. A cryogenic compressor (K-102) is used to boost one of those streams to a slightly higher pressure so that the nearly pure methane stream can then be condensed by the flashed split-vapor stream (Pitman et al., 1998) used as the cold fluid in the heat exchanger (E-104). The reflux of nearly pure methane is sent to the top of the demethanizer as a reflux stream. The other stream is used to precool the feed as cold fluid in the two heat exchangers (E-100 and E-102), this is then pressurized in the turboexpander TE-100 and compressor K-101 and stoked for selling. The desired specifications of the demethanizer separation are an ethane recovery of 84% and a methane impurity level of 1 mol% in the bottom product.

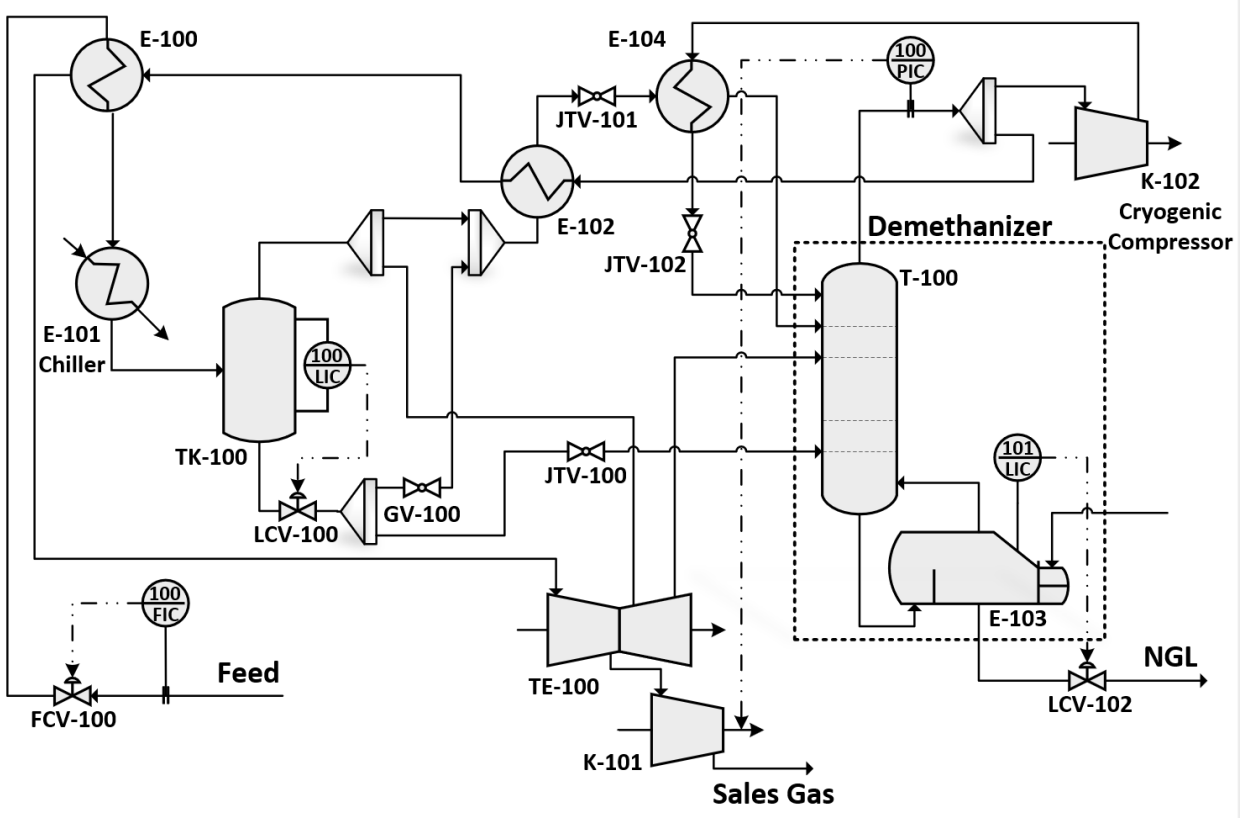

Figure 3.3: CRR separation unit with stability control loops.

3.3. Deethanizer column

After the demethanizer, the following column of the separation train is the deethanizer (T-101), which is a 30 stages distillation column with a reboiler (E-106) and a condenser (E-105). A schematic representation of this column is given in Figure 3.4 along with the other columns of the separation train and the corresponding stability control loops. The column is fed at the 12th tray with the liquid stream leaving the bottom of the demethanizer column. The feed conditions were a flowrate of 277 kmol/h, a temperature of -5.1°C and a pressure of 2459 kPa. The column removes the propane from the mixture and produces an ethane product of high purity in the distillate. The production targets required for the deethanizer separation are the maintenance of an impurity of propane of 1 mol% in the top product, and an ethane concentration of 0.34 mol% in the bottom product, these values were chosen following the process specification used in the work of Luyben (2013a).

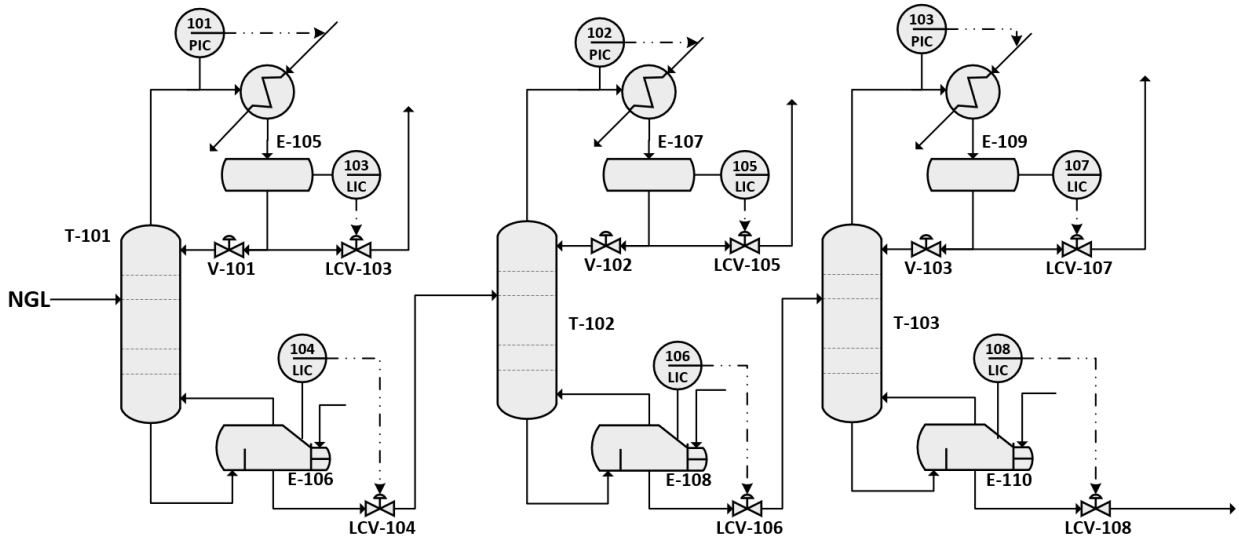

Figure 3.4:Distillation train comprehending the deethanizer column (T-101), the depropanizer column (T-102), the debutanizer column (T-103) with stability control loops.

3.4. Depropanizer column

The depropanizer (T-102) is constituted by a 46 stages distillation column with a reboiler (E-108) and a condenser (E-107). The feed is represented by the liquid stream leaving the bottom of the deethanizer column, which is introduced at the 19th tray. The feed conditions were an inlet flowrate of 148 kmol/h, a temperature of 83.5°C and a pressure of 1760 kPa. The column produces a propane product of high purity as distillate. The specifications required in this unit are for the column top product a value of 0.6 mol% in the sum of the concentrations of i-butane

and n-butane; for the column bottom product a propane concentration of 0.1 mol%. Those values for the depropanizer product specification were taken from Luyben (2013a).

3.5. Debutanizer column

The debutanizer (T-103) is a 35 stages distillation column with a reboiler (E-110) and a condenser (E-109). This column is responsible for the removal of the butane fraction from the remaining mixture outcoming the bottom of the depropanizer. This liquid stream is fed at the 18^{th} tray with the feed conditions of a flowrate of 74 kmol/h, a temperature of 78.5°C and a pressure of 608 kPa. The product targets required for the separation are an impurity of i-pentane of 0.2 mol% in the column top product and an impurity of n-butane of 0.2 mol% in the bottom product (Luyben, 2013a).

3.6. Separation Train Design

During this research work, the columns of the separation train following the demethanizer column were designed and simulated by using the Aspen HYSYS® process simulator. The design specifications for the deethanizer, depropanizer, and debutanizer columns, are represented by the top and bottom impurity levels of key components, as well as the operating pressure of the various columns. The operating pressures for the deethanizer and depropanizer columns are chosen following the data reported in the work of Luyben (2013a), while the operating pressure of the debutanizer column was chosen so that cooling tower water could be used as a coolant in the condenser. The columns were firstly designed using the Aspen HYSYS® simulation in stationary mode, in which the properties of the mixtures are also calculated using the Peng-Robinson equations of state (EOS). For the design, the required purity targets for the top and bottom products were inserted as column specifications. In this way, the simulation modifies the flow ratios in the column by varying the condenser and reboiler duties, until convergence (if physically achievable) to the desired concentration values.

3.6.1. Selection of Reflux Ratio and Number of Plates

Having set the desired purities, the number of column stages was increased until the minimum reflux ratio was found. The values obtained were multiplied by a typical multiplication value of 1.3, resulting in the actual reflux ratio. The number of stages was determined by selecting

the number of stages that would guarantee the reflux ratio closest to the desired one, still considering the active specifications of the desired product quality. The number of column trays was then recalculated considering a separation efficiency of 75%. The choice of the feed plate was then made based on economic considerations, in particular the plate that could guarantee the lowest energy consumption considering reboiler and condenser duty was selected. The values of the reflux ratio, the number of plates and the feed plate position of the different columns are shown in Table 3.2.

Table 3.2: Design specifications selected for deethanizer, depropanizer and debutanizer columns

	Deethanizer	**Depropanizer**	**Debutanizer**
Light Key component	ethane	propane	n-butane
Heavy Key component	propane	butanes	i-pentane
Nominal reflux ratio	1.125	2.533	1.554
Number of trays	30	46	35
Pressure drop [kPa]	0.62	0.61	0.6
Feed tray	12°	19°	18°

3.6.2. Column diameter and hold-up calculation

The column diameters were designed using the automatic function available in the internals section of the Aspen HYSYS® simulator. The volumes of the reflux drum and the reboiler were obtained by considering a 5 min of liquid holdup when the vessel is 50% full as commonly used heuristics (Luyben, 2013b). The volume calculation for the reboilers was performed considering an inlet liquid flowrate equal to the liquid flowrate exiting the last tray of the corresponding column. While for the volume calculation for the reflux drums, an outlet flowrate equal to the sum of the reflux and distillate flowrates was considered. The values obtained for the column diameters and the corresponding reboiler and reflux drum volumes are shown in Table 3.4.

Table 3.3: Column diameters and volumes selected for deethanizer, depropanizer and debutanizer columns

	Deethanizer	**Depropanizer**	**Debutanizer**
Diameter [m]	2.2	2.1	1.7
Reflux drum Volume [m^3]	4.15	4.31	2.14
Reboiler Volume [m^3]	8.42	5.30	2.10

3.7. Conclusion of the Chapter

The NGL recovery process was modelled and simulated through the Aspen HYSYS® process simulator using Peng-Robinson equations of state considering a row gas with a low-content liquid. Three widely used plant schemes in the industry involving cryogenic distillation for methane separation were considered: the conventional, gas subcooled process (GSP), and cold residue recycle (CRR). The goal of the demethanizer separation was an ethane recovery of 84% and a methane composition of 1% at the bottom of the demethanizer column. The subsequent distillation columns of the train, the deethanizer column, the depropanizer column, and the debutanizer column were described and designed for the achievement of the required purity specification. The deethanizer desired product quality considers an impurity of propane of 1 mol% in the top product and an ethane concentration of 0.34 mol% in the bottom product. In the depropanizer, the specification regarded a sum of the concentrations of i-butane and n-butane value of 0.6 mol% in the top product and for the bottom product a propane concentration of 0.1 mol%. The debutanizer desired product quality concerned an impurity of i-pentane of 0.2 mol% in the top product and an impurity of n-butane of 0.2 mol% in the bottom product.

Chapter 4

Steady state analysis

In this chapter, the steady state temperature and composition column profiles have been analyzed giving insight into the separation operations and understanding the internal behavior of the distillation columns of the plant. Furthermore, the influence of the composition variations on the column temperature gradient for the four columns has been studied by performing a temperature analysis with per component contribution analysis.

4.1. Temperature profile analysis

To understand the thermal behavior of the column and obtain valuable information about the column's performance, in steady state conditions, the temperature column profiles of the demethanizer, deethanizer, depropanizer and debutanizer columns, were recorded and analyzed. The distribution of temperature, which is linked to pressure and composition in each tray as a result of the thermodynamic equilibrium established between the liquid and vapor phases, is a tool that allows the determination of the column's appropriate functioning.

The temperature column profiles obtained for the demethanizer column of the conventional and GSP recovery unit are reported in Figure 4.1 and Figure 4.2. Concerning the CRR configuration, the profiles obtained are not reported as very similar to the ones obtained for the GSP.

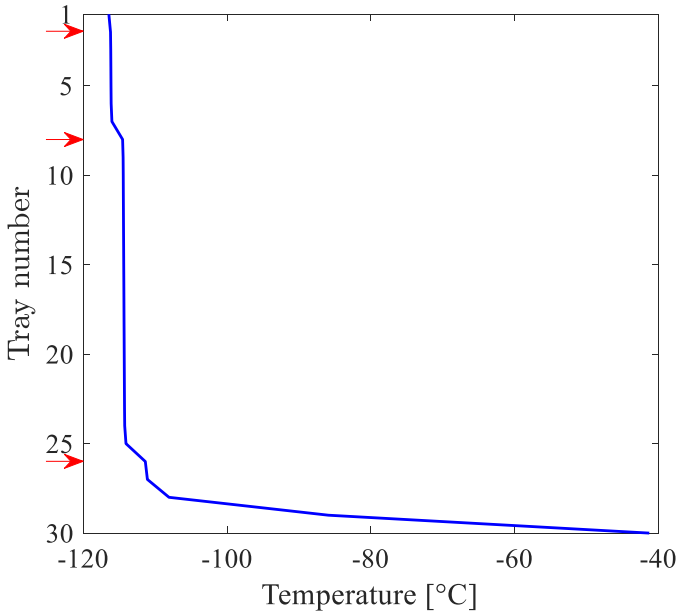

Figure 4.1: Conventional separation unit: Demethanizer temperature column profile. The red arrows indicate the position of the feed trays.

The column temperature profile (Figure 4.1) obtained under nominal steady state conditions for the demethanizer located in the conventional unit shows to be practically flat across the enrichment section of the column, only a variation of about 4°C is observed in correspondence of the 8th tray where one of the three column feeds is located. Most of the temperature variations are localized in the stripping section of the column. This is due to the presence of the feed at the 26th tray and the presence of methane above its critical temperature of -82.6 °C, this last

part of the column is the region where most of the separation in the key components takes place.

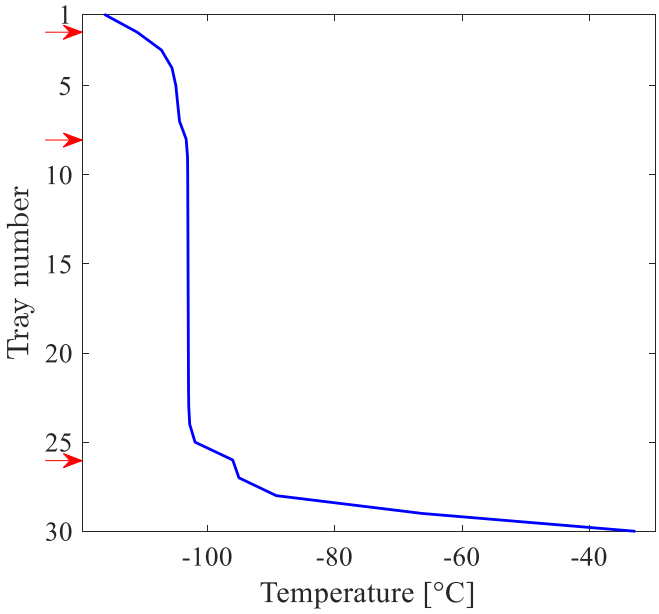

Figure 4.2: GSP separation unit: Demethanizer temperature column profile. The red arrows indicate the position of the feed trays.

The column temperature profiles obtained for the demethanizer column in the GSP unit are shown in Figure 4.2. Here the column temperature gradient depicts a higher variability compared to the one obtained with the conventional scheme. In the first stages of the rectifying section, a temperature gradient of approximately 10°C can be observed. From this point on, the profile remains almost flat until the 26th tray, where the feed plate is located. Also, in this case, a drastic temperature increase can be seen in the last plates of the column due to the supercritical conditions of the methane fraction present. This analysis makes it possible to observe that the modifications introduced for the GSP scheme led to a more distributed separation along the column, with an enhancement on the separation operations localized in the first few trays of the enrichment section, as evidenced by the temperature gradient observed. The same results were found in the analysis of the CRR column temperature profiles. The same trend is registered in correspondence of the stripping section of the column, the temperature profile in the main part of the column is flat. Thus, it is possible to infer that the variability in concentration profiles is located near the top and especially in the last few stages of the column.

The steady state temperature column profiles obtained for the remaining distillation columns of the separation train are shown in Figure 4.3.

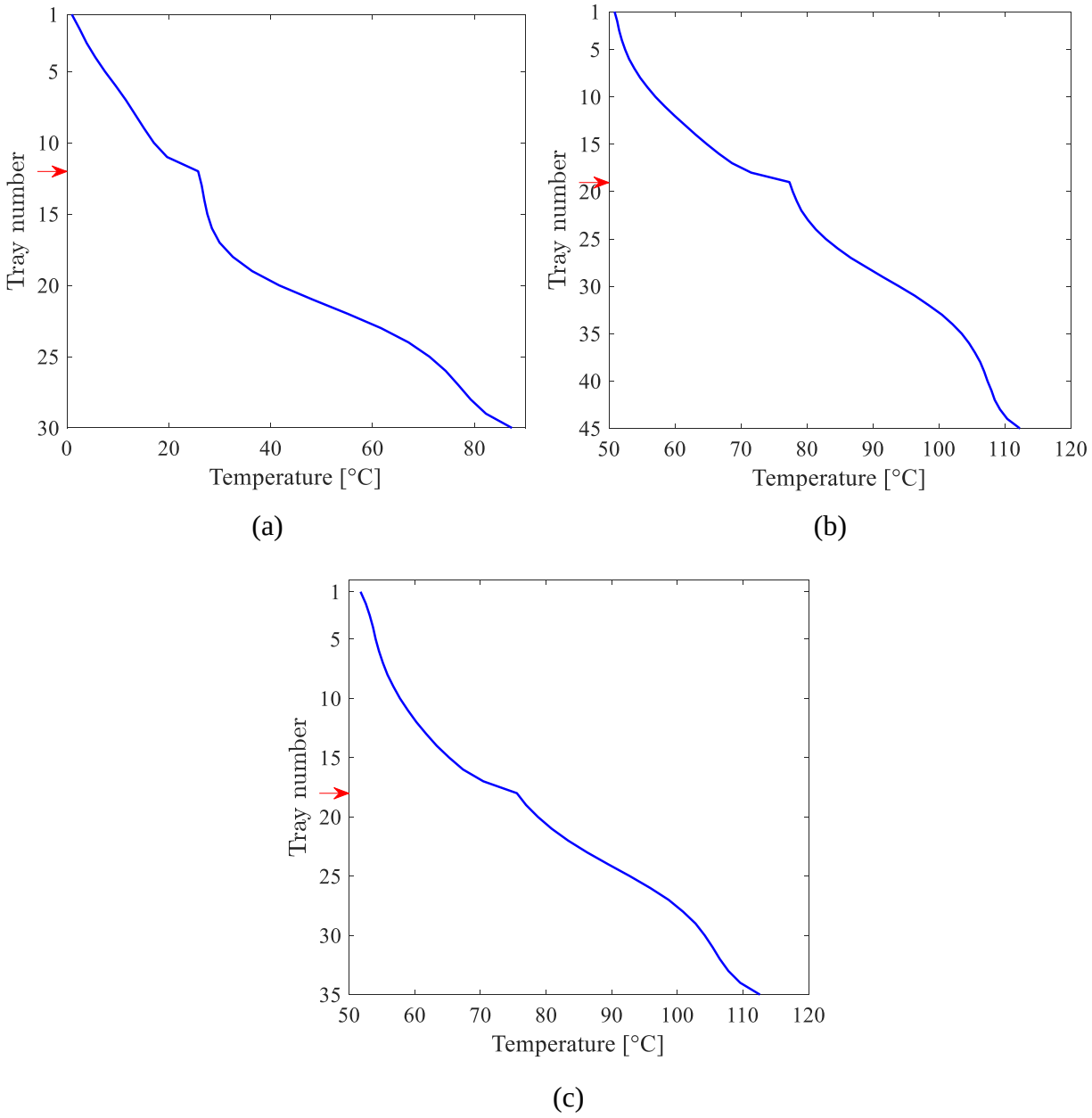

Figure 4.3 Deethanizer temperature column profile (a), Depropanizer temperature column profile (b), Debutanizer temperature column profile (c). The red arrow indicates the position of the feed tray.

The temperature profiles obtained for deethanizer (Figure 4.3a), depropanizer (Figure 4.3b) and debutanizer (Figure 4.3c) depict similar results. As it is possible to observe, the three profiles show a distributed variability across the column, highlighting the fact that the separation of the components occurs more continuously along the entire columns. However, it is possible to observe that in correspondence with the column enrichment sections, the gradient obtained for the temperature profiles is less pronounced, with a higher gradient occurring

around the feed plates. The area of the three columns where the most rapid temperature changes are located is registered around the 21st and 24th tray for the deethanizer column, around the 22nd and the 27th for the depropanizer column and around the 27th and the 32nd tray for the debutanizer column.

4.2. Composition profile analysis

When dealing with multi-component separation, as there is no univocal relationship between temperature and concentration, it is necessary to study the composition profiles within the column. This section analyses the column composition profiles obtained by the Aspen HYSYS® simulations in steady state conditions for the distillation columns considered. First, an analysis of the composition profiles across the columns implemented in the different separation schemes considered was conducted. To visualize the results obtained, the composition profiles along the demethanizer column of the Conventional unit and the GSP unit are shown in Figure 4.4 and Figure 4.5 respectively.

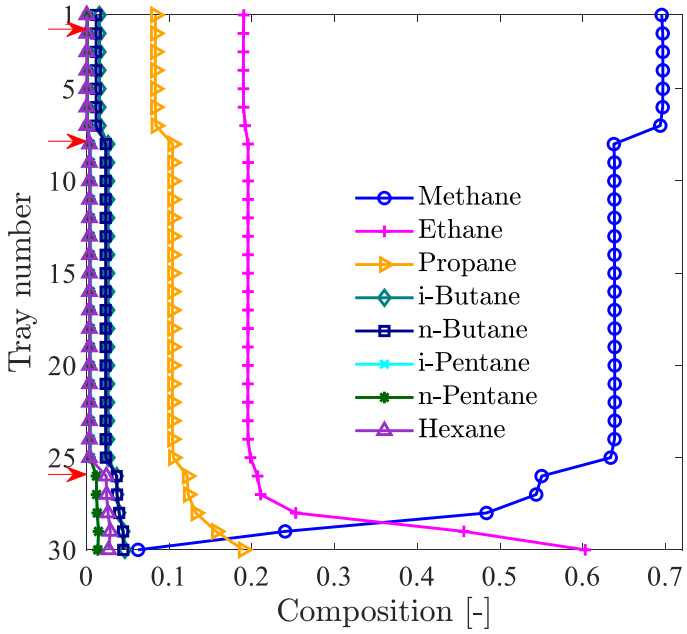

Figure 4.4: Conventional separation unit: Components composition column profile. The red arrows indicate the position of the feed trays.

The analysis of column composition profiles confirms the observations made from analyzing column temperature profiles in both the demethanizer columns of conventional and GSP schemes. It is noteworthy that in the conventional unit, the drop in methane composition is concentrated in the last few trays, starting from the 26th tray down to the tray just above the

reboiler. In contrast, the graph of the column concentration profiles obtained for the GSP unit shows significant variations in the composition profiles of both the first trays of the enrichment section and the last trays of the stripping section. The composition profiles remain relatively flat in the middle part of the column. Similar results are obtained for the composition column profiles in the CRR unit to those obtained with the GSP separation scheme. The decrease in methane composition and increase of other components principally take place at the end of the stripping section. The opposite occurs in the enrichment section while in the middle part of the column, there are almost no variations.

The steady state column composition profiles obtained for the deethanizer, depropanizer and debutanizer columns are reported in Figure 4.6.

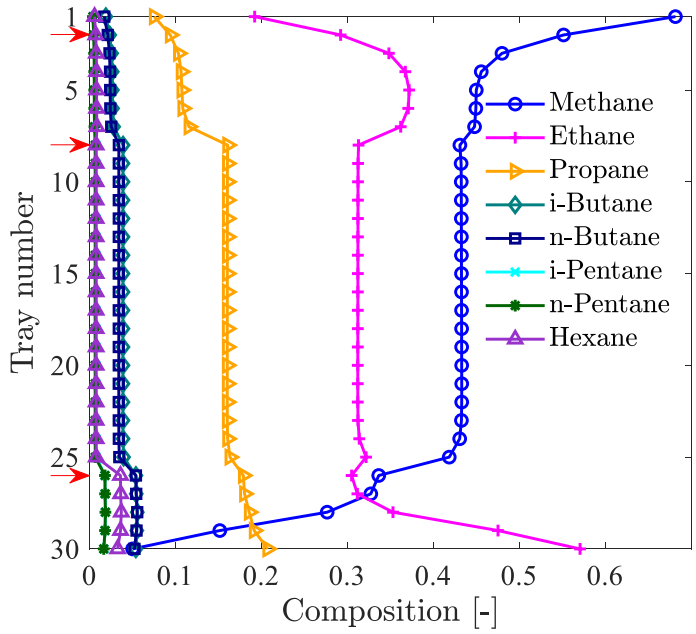

Figure 4.5: GSP separation unit: Components composition column profile. The red arrows indicate the position of the feed trays.

In line with what was obtained for the column temperature profiles of the distillation columns in the separation train, Figure 4.6 depicts a distributed variability in the composition profiles of key components along the columns. The drops in concentration of the light-key components—ethane in the deethanizer (Figure 4.6a), propane in the depropanizer (Figure 4.6b), n-butane in the debutanizer (Figure 4.6c)—are distributed homogeneously from the top of the column to the last tray above the reboiler. The same remark can be made for the increasing concentration of the columns' heavy-key components—propane in the deethanizer (Figure 4.6a), sun of butanes in the depropanizer (Figure 4.6b), i-pentane in the debutanizer

(Figure 4.6c)—which display quite uniform behaviors proceeding from the bottom to the top of the column. Nevertheless, it can be seen in Figure 4.6 that the profiles obtained for non-key components also undergo significant variations throughout the column, thus largely influencing the temperature gradients in the column.

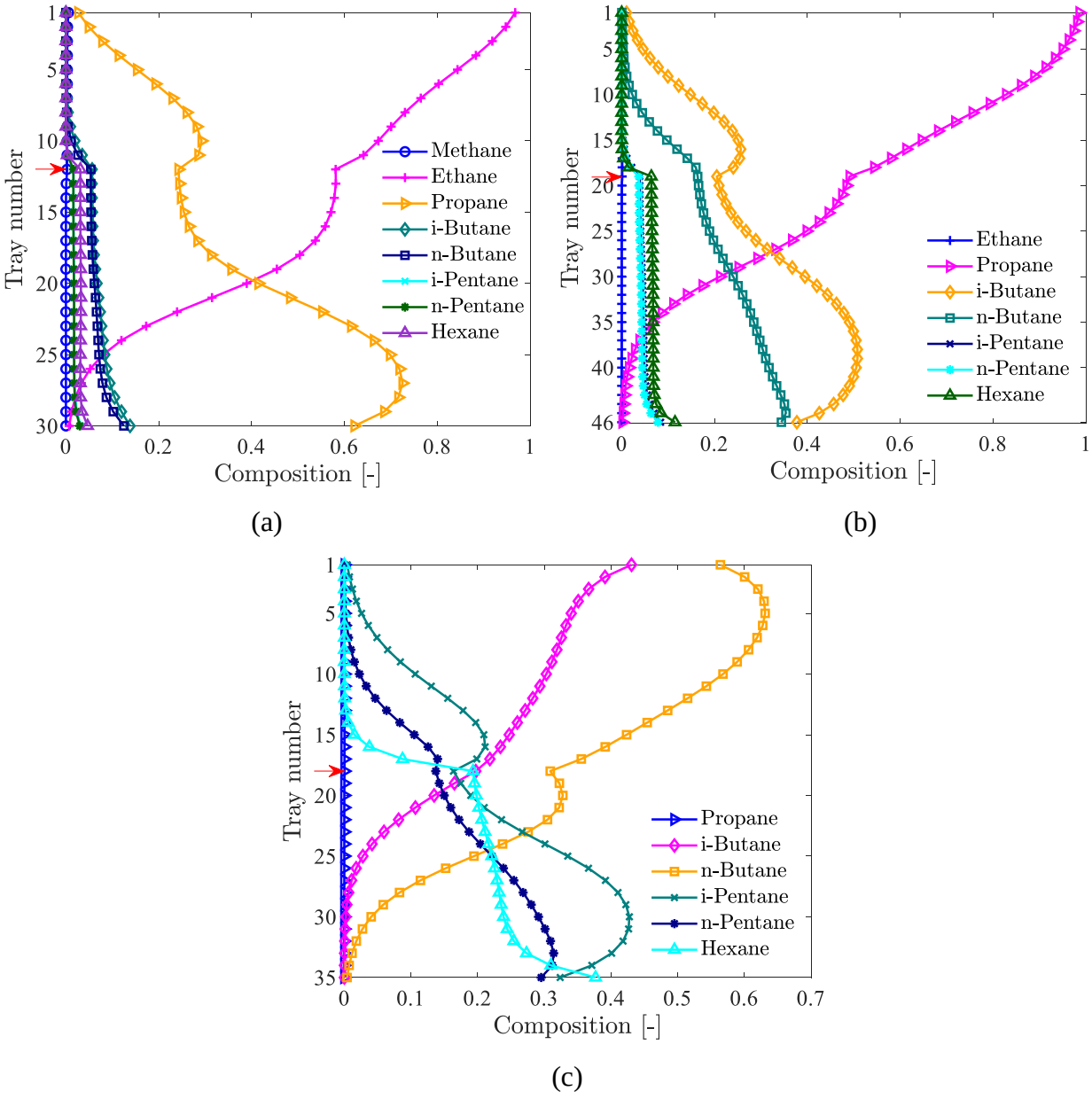

Figure 4.6: Deethanizer composition column profiles (a); Depropanizer composition column profiles (b); Debutanizer composition column profiles (c). The red arrow indicates the position of the feed tray.

4.3. Per component temperature gradient contribution analysis

As mentioned above, the analysis of temperature gradients is necessary because, as this quantity is easily and usually measured in columns, it can be used to control or monitor separation operations. Since there is a bi-univocal correspondence between temperature and composition in a bicomponent distillation column, product quality control is usually achieved with indirect concentration controllers utilizing column temperature controllers. This biunivocal bond is no longer present in multicomponent distillation columns, where the same temperature may be associated with a different composition in a considered tray. For this reason, alongside the examination of temperature gradients, it is also necessary to study the influences of component variations on the temperature gradient. In a multicomponent column, the best position to place a temperature sensor is in the section where the sensitivity of temperature to composition changes is higher. To establish a better position of the temperature sensors to control the tray temperature in the considered columns and to relate the influence of components variation on the temperature gradient inside the column the analysis of the temperature gradient with a per-component contribution diagram (Porru et al., 2013) has been performed. In the analysis, the bubble point calculation was performed with data taken from the Aspen Properties® simulator and assuming an ideal behavior for the components inside the column.

4.3.1. Demethanizer column

The effects of the component compositions change on the temperature profile in the demethanizer column of the considered separation units have been evaluated with the use of the temperature gradient with per-component contribution diagram analysis. The results obtained for the demethanizer columns in the conventional and GSP separation unit are reported in Figure 4.7 and Figure 4.8 respectively, along with the methane composition gradient in the columns.

The temperature gradient with the per-component contribution diagram obtained for the conventional unit is depicted in Figure 4.7a. Here the bars show the contributions of the various components to the actual temperature gradient, indicated by the black line. As it is possible to visualize the analysis conducted is useful for obtaining a qualitative measure of the components' influence on the temperature gradient. Indeed, although the magnitude of the

gradients obtained does not reflect the actual recorded values of the temperature gradient in the column, the trends obtained are congruent with the actual one. The deviations obtained are due to the presence of methane under supercritical conditions. This required an approximate calculation of Henry's constant for the mixture when calculating the bubble point function.

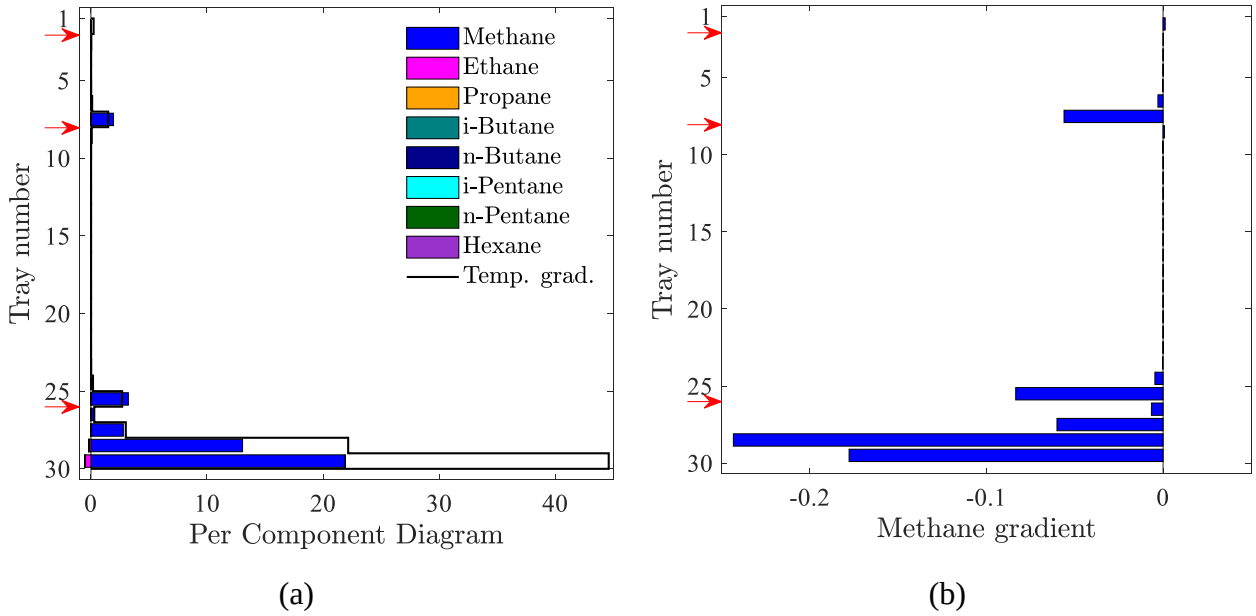

Figure 4.7: Conventional unit demethanizer per component diagram (a) and methane composition column gradient (b). The red arrows indicate the position of the feed trays.

Analyzing the bar graph obtained, it is evident that the temperature variation depends mostly on the methane variation inside the column. The peaks around the 8th and the 26th trays depend on the methane concentration increase due to the multiple feeds to the column. In the last trays, we can observe that the contribution of this component to the temperature gradient becomes very high. After the 29th stage, this component is over the critical temperature. Its presence is due to the solubility in the liquid mixture. This fact has two effects on tray temperature: its presence has a negative contribution due to the reduction of the perceived pressure, but the magnitude of the methane concentration drop brings to the significant increment of the heavy components fraction that leads to the high increase of temperature.

The best position for the sensor must be as far as possible from the feeds that have a significant influence on the temperature profile and from the last tray. Based on this consideration, the choice of tray location for the sensor is between the 27th and the 29th plate. Considering that there is no maximum on the temperature gradient and the variation is almost entirely due to the methane variations, an adjunctive analysis was conducted to establish which of these plates,

was related to the higher variability in methane concentration. The result of this investigation is depicted in Figure 4.7b. Here it is observable that between trays 28-29, the methane has the concentration drop, the most appropriate location for the sensor was thus selected on the 28th tray which is the furthest from the end of the column.

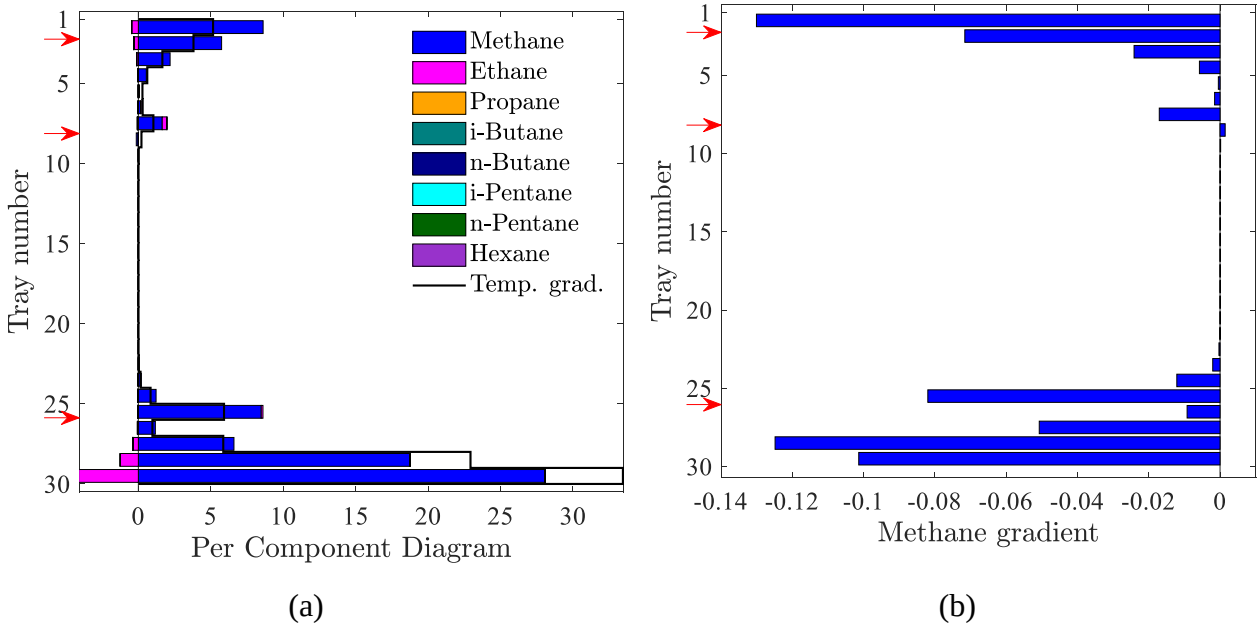

Figure 4.8: GSP unit demethaizer per component diagram (a) and methane composition column gradient (b). The red arrows indicate the position of the feed trays.

In Figure 4.8a, the temperature gradient with the per-component contribution diagram obtained for the GSP unit is reported. It is possible to notice some differences from the diagram obtained for the conventional scheme. Even though also in this case the component that most influences the temperature gradient is again methane, it is evident that the ethane variations in the last part of the column depletion section also affect the temperature variations. Along with the peaks obtained around the positions of the feeds at the 8th and 26th trays, the temperature gradient in the trays immediately below the column head is also mainly due to methane variations. In this region, a minor contribution is also given by ethane variations. Again, in the last trays, due to the supercritical conditions of methane, the variations of this component lead to an extremely high increase in the temperature gradient. For this reason, no peak is observed in the temperature gradient obtained and the choice of the tray in which to locate the thermocouples is again made by analyzing the methane gradient in the column, thus the component whose variations most influence the temperature gradient. The methane gradient along the demethanizer of the GSP scheme is depicted in Figure 4.8b. Here it can be noticed in the stripping section of the column that the highest methane variation is again located between the

28th and 29th trays. With the need to distance the sensor location from locations that may affect temperature gradients, such as feed trays and column ends, the choice of sensor placement once again landed on the 28th tray. Again, similar results were obtained with the CRR separation unit for which the same temperature sensor location was selected.

4.3.2. Deethanizer column

To highlight temperature variations caused by changes in key component concentrations in the deethanizer column and also consider the effects on the temperature gradient of non-key components, a temperature gradient analysis was performed using component contribution diagrams. The resulting diagrams are shown in Figure 4.9.

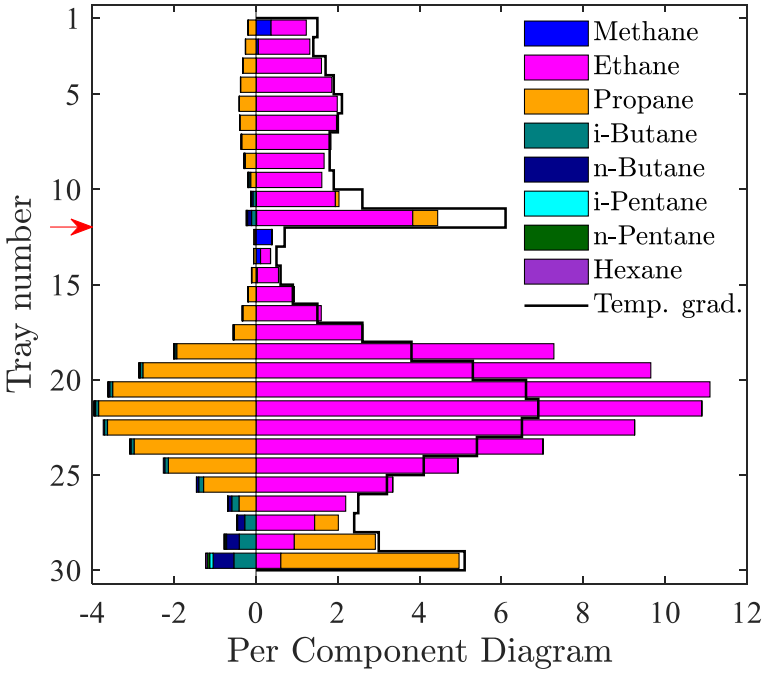

Figure 4.9: Deethanizer per component diagram. The red arrow indicates the position of the feed tray.

In the diagram in Figure 4.9 except for the temperature variation around the feed plate, located in the 12th tray, the per-component analysis can describe the influence of composition variations in the temperature gradient inside the column. As it is possible to visualize, in the rectifying section the variations of the heavy key component (propane) produce a negligible impact on the temperature profile. According to this result, the placement of a thermocouple in this section would be ineffective, as the detected temperature variations would be less informative about propane variations in this part of the column. Therefore, also the implementation of a temperature controller to maintain the propane concentration in the top

product is not recommended. Only a reflux ratio controller may be implemented to mitigate the effect of feed disturbances on the heavy-key component in the top product. On the other hand, in the stripping section light key component (ethane) variations have a high impact on the temperature profile, reaching a peak located in the 21st tray. The most appropriate location for the sensor was thus selected on this tray.

4.3.3. Depropanizer column

The per-component contribution diagram obtained for the depropanizer column to examine the influence on the column temperature gradient due to the variation in key and non-key components is displayed in Figure 4.10.

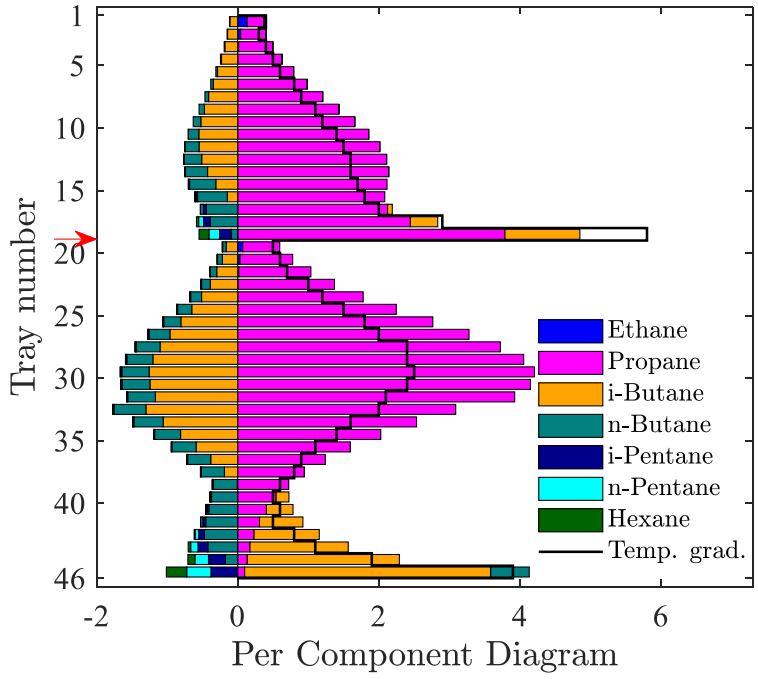

Figure 4.10: Depropanizer per component diagram. The red arrow indicates the position of the feed tray.

As depicted in Figure 4.10, in the rectifying section of the depropanizer the influence of the sum of i-butane and n-butane variation leads to a region of trays (from the 10th to the 13th) where the temperature gradient is practically constant. As result, also in this case the process would not be beneficial from the installation of a thermocouple in this column section as it would not give significant information about the changes in the heavy key components. By observing the region of the graph corresponding to the stripping section of the column, it is possible to notice that the effect of the light key component (propane) variations, has a high

influence on the column temperature gradient. This influence is highest around the 30th, thus this was selected as the most appropriate location for the temperature sensor placement.

4.3.4. Debutanizer column

Figure 4.11 depict the results of the per-component temperature gradient analysis conducted on the debutanizer column to link the changes in the column temperature gradient with the component concentrations gradients along the column.

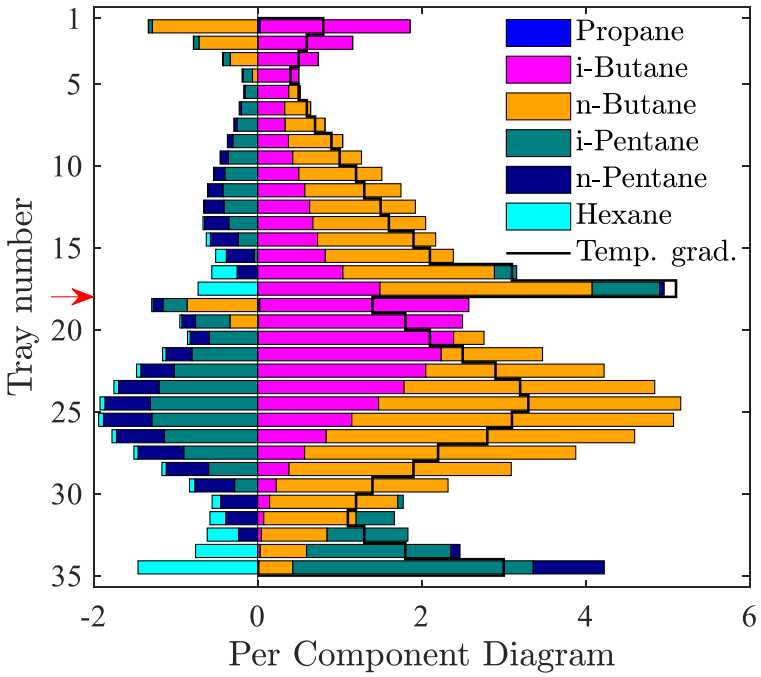

Figure 4.11: Debutanizer per component diagram. The red arrow indicates the position of the feed tray.

The per-component analysis conducted on the debutanizer columns (Figure 4.11) yielded analogue results. In the rectifying section of the column, the variations in the heavy key component (i-pentane) have a small effect on the temperature gradient. Thus, also in this case the placement of a thermocouple in this section would be ineffective, and only a reflux ratio controller may be implemented to mitigate the effect of feed disturbances on the heavy-key component in the top product. In contrast, in the stripping section of the debutanizer, changes in the light key component (n-butane) had a large effect on the temperature gradient. As a result, the best position for the thermocouple would be the tray where the influence of this component on the temperature gradient is higher, thus the 26th tray.

4.4. Conclusion of the Chapter

The analysis of the temperature and composition profiles of the distillation columns considered in the case study has been conducted for a better column operation understanding. The results showed that the modifications in the GSP scheme led to a more distributed separation along the demethanizer column, compared to the conventional separation unit, for which the column temperature profiles appear almost flat except in the last stages above the reboiler. As opposed, the temperature profiles for the other columns depicted temperature variability distributed across the columns, highlighting the fact that the separation of the components occurs along the entire column. The analysis of the composition profiles confirms what was inferred from the temperature profiles. Indeed, in the GSP scheme, the separation of key components also occurs in the first tray of the demethanizer column, while the separation occurs regularly throughout the subsequent columns of the separation train. The analysis of temperature gradients is crucial for controlling and monitoring distillation operations in columns, especially in multicomponent columns where variations of components need to be examined for their impact on the temperature gradient. In this chapter, a temperature gradient per-component contribution diagram analysis was conducted to determine the best location for the temperature sensors and to study the impact of variations in key and non-key component concentrations on the temperature gradient of all the columns considered in the case study. The results for the demethanizer columns of conventional and GSP separation units show that the temperature variation depends mostly on the methane variation and the 28th tray resulted in the most appropriate location for the thermocouple positioning. The results obtained for the remaining columns of the train showed that variations in heavy key components had little effect on the rectifying section temperature gradient for all three columns. Therefore, the placement of a thermocouple in this section would not be effective. As result, to mitigate the effect of feed disturbances on the heavy-key component in the top product the use of a reflux ratio controller was suggested. In contrast, it was observed that light key component variations have a high effect on the stripping section temperature gradient of the columns. Here the best position for the thermocouple was found to be on the 21^{st} tray for the deethanizer, in the 30^{th} tray for the depropanizer and 26^{th} tray for the debutanizer.

Chapter 5

NGL recovery process Control

This chapter focuses on the control problem of the NGL extraction CRR process under typical disturbances, with the goal of first, maximizing the recovery of ethane and minimizing methane impurity levels in the bottom of the demethanizer, and second, meeting the required product purity in the other distillation column of the train. Different control structures by the knowledge of online temperature measurements were considered including firstly direct temperature control and cascade control schemes. These configurations have been analyzed to determine their response in the presence of typical disturbances and their ability to achieve the main control objectives. The results obtained were then compared with the action of a hybrid cascade control that uses offline and delayed concentration measurements to update the controller setpoint at each sampling period. The last part of the chapter analyzes the effect on product quality control in the separation train using the control strategy defined for the demethanizer column under feed flowrate disturbances.

5.1. Control structures

The fractionation of NGL is an energy-demanding process, often conducted with a separation train that includes cryogenic distillation columns. The demethanizer column is the critical unit of the separation plant as the methane separation requires a cryogenic separation and it provides the feed to the subsequent distillation train to improve the control strategy for the NGL recovery plants. Therefore, optimizing this process is crucial from an economic and environmental standpoint. The demethanizer unit quality control problem has been addressed, starting from the control structure proposed by Chebeir et al. (2019). The control system proposed was modified considering the possibility to attain the composition goals without the implementation of composition analyzers. Considering that the typical disturbances for the considered process are variations in the plant feed flowrate and composition, the disturbances applied to the plant were variations of 10% in the plant feed nominal value of 4980 $\frac{kmol}{h}$ (chosen following the feed changes used by Chebeir et al. (2019), and variations of 40% on the ethane inlet composition nominal value of 0.03, changing accordingly the composition of methane in the raw gas. The control strategies proposed for the demethanizer column quality control have been analyzed and compared with the typical control strategy used in real industrial plants. The comparison confronts the ability of the control structure developed on limiting the effect of the applied disturbances on the plant. The control solution showing the best performances is then implemented in the full plant to analyze its influence in the control of the product quality of the demethanizer, depropanizer and debutanizer columns for which only indirect composition controllers were considered.

5.1.1. Demethanizer column control strategies

To optimize the bottom product quality in the demethanizer column of the three considered separation units, different control strategies were compared with the main objective to achieve a methane composition of 1 mol% in the bottom product stream, while maintaining recovery of ethane at 84 %. Only the control loops developed for product quality control were addressed in this work, the other control loops implemented (depicted in Figure 3.1, Figure 3.2 and Figure 3.3 with the schematic representation of the three considered separation units) are described as follows.

In the CRR unit:

1) The inlet feed flowrate variations are realized by manipulating the opening of the valve FCV-100 upstream the flash tank TK-100.
2) The column pressure is controlled by manipulating the power of the compressor K-101 used to recompress the methane product stream.
3) The flash tank (TK-100) level is controlled by manipulating the liquid stream leaving the separator through the valve LCV-100.
4) The liquid level in the reboiler E-103 is controlled by manipulating the flow of the bottom product through the valve LCV-102.
5) The ratio between the gas feed streams to the column is controlled by manipulating the flow through the turbo expander TE-100.
6) The reflux ratio is controlled by manipulating the power to the cryogenic compressor.

In the GSP unit:

1) The inlet feed flowrate variations are realized by manipulating the opening of the valve FCV-100 upstream the flash tank TK-100.
2) The column pressure is controlled by manipulating the power of the compressor K-101 used to recompress the methane product stream.
3) The flash tank (TK-100) level is controlled by manipulating the liquid stream leaving the separator through the valve LCV-100.
4) The liquid level in the reboiler E-103 is controlled by manipulating the flow of the bottom product through the valve LCV-102.
5) The ratio between the gas feed streams to the column is controlled by manipulating the flow through the expander TE-100.

In the conventional unit:

1) The inlet feed flowrate variations are realized by manipulating the power of the expander TE-100.
2) The column pressure is controlled by manipulating the power of the compressor K-101 used to recompress the methane product stream.

3) The levels of the flash tank TK-100 and flash tank TK-101 are controlled by manipulating the liquid streams leaving the separators through the valves LCV-102.

4) The liquid level in the reboiler E-103 is controlled by manipulating the flow of the bottom product through the valve LCV-102.

Indirect composition control through temperature control

To modify the control structure proposed by Chebeir et al. (2019), by realizing a control system without the use of composition analyzers, thus without the knowledge of composition measurements, the possibility of removing the ethane recovery controller and the methane impurity level controller was studied. Two indirect composition controllers have been realized thanks to the availability of online temperature measurements in the flash tank (TK-100) and the demethanizer column, this control structure will be referred to as CS1 and is schematize in Figure 5.1.

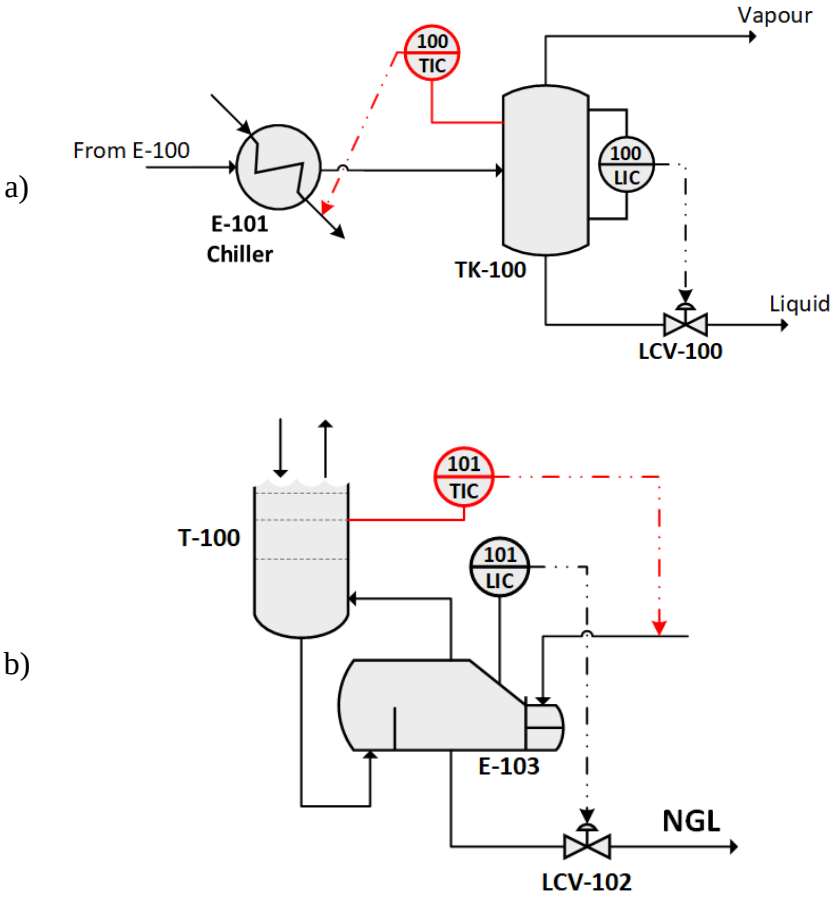

Figure 5.1: Demethanizer bottom product quality indirect control: direct flash-tank temperature control loop (a) and direct column tray temperature control loop (b) implemented in the CS1 control strategy.

In this control strategy, the first control loop is represented by the flash tank (TK-100) temperature control, as this variable is directly connected with the recovery of ethane, while the manipulated variable is given by the heat loss in the chiller E101. In the second control loop, the controlled variable is represented by the tray temperature at stage 28 related to the concentration of methane. This tray is chosen following the gradient temperature analysis performed and reported in the previous chapter. The manipulated variable is represented by the reboiler duty. This is a control structure widely used in the industry as it is associated with a reduced cost, due to the absence of composition analyzers. Furthermore, in a binary distillation column, direct temperature control is sufficient to obtain the desired product quality as the link between temperature and composition is biunivocal. This is not verified in the case of multicomponent columns, additionally, the last stages of the demethanizer column are associated with the higher variability in the column temperature gradient with variations around 60°C. This makes the bottom product quality control of the column more complicated and chooses a simple temperature controller insufficient for limiting disturbances entering the system requiring the design of new control strategies.

For a clearer reader understanding, the control structures presented in this subsection are summarized in Table 5.1, along with the control structures designed to improve the quality control of the demethanizer column bottom product that will be presented and described in the following subsections.

Table 5.1: Control structure developed for demethanizer column bottom product quality control

		CS1		**CS2**		**CS3**		**CS4**		**CS5**	
Manipulated variables	Chiller heat loss	✓		✓		✓		✓		✓	
	Column reboiler duty		✓		✓		✓		✓		✓
Controlled variables	Flash tank temperature	✓								✓	
	Pressure compensated temperature (PCT)			✓		✓		✓			
	Column tray temperature		✓		✓		✓		✓		✓
	Approximated ratio flow						✓		✓		
	Methane composition								✓		✓

Improvements in Ethane recovery indirect control

Since the indirect control of ethane recovery, thus the control of the flash tank temperature is located upstream of the column, this was the first control loop addressed in the work. The improvement of the ethane recovery indirect control scheme was realized starting from the analysis and knowledge of the plant operation in the considered schemes. In the GSP and CRR schemes, the inlet flowrate variations are realized by manipulating the pipeline's pressure through the valve FCV-100 upstream of the flash tank TK-100 (see Figures 3.2-3.3), while in the conventional process scheme, the flowrate variations are performed by changing the pipeline's pressure by manipulating the action of the turboexpander (equipment TE-100 in Figure 3.1). This implies that changes in the feed gas flowrate affect the pressure variations in the flash tank TK-100. With the flash tank (TK-100) temperature held constant by the control action, flash tank (TK-100) pressure changes affect the thermodynamic equilibrium resulting in changes in the separator outflow composition. Since the outflow of the flash tank (TK-100) represents the feeds of the demethanizer column this implies that variation in the column feed composition occurs influencing the ethane recovery. With the purpose of improving the flash tank (TK-100) direct temperature control, and consequently ethane recovery, a pressure compensator is placed in this unit and a new control variable has been considered within the loop instead of the separator temperature. This new variable is represented by a fictitious temperature, calculated on basis of Antoine's law. This is a pressure compensated temperature (PCT) given the Equation 5.1 (Brambilla, 2014):

$$PCT = T^m - C \ln \frac{P}{P^{rif}} \qquad 5.1)$$

Where T^m is the flash tank (TK-100) temperature, P is the flash tank pressure; P^{rif} is the flash tank pressure nominal value and C is the compensation coefficient obtained from temperature data recorded during the imposition of pressure variations at constant composition with the Aspen HYSYS®.

The resulting control strategy in which the process variable is given by the flash tank (TK-100) PCT, schematize in Figure 5.2, will be referred to as CS2. By compensating for the pressure changes in the flash tank (TK-100), it is possible to link the temperature variations to the flash tank pressure changes and mitigate the resulting concentration disturbances. The setpoint selected for the TIC-102 corresponds to the direct control of the flash tank (TK-100) temperature setpoint, as the PCT only acts in the presence of pressure variations and under

nominal conditions, this fictitious variable coincides with the actual temperature. The use of a PCT control instead of temperature control is addressed to overcome the pressure changes induced in the flash tank (TK-100) by inlet flowrate variations to the plant, thus this is an important aspect when feed flow disturbances are present.

Improvements in Methane impurity level control

The implementation of the pressure compensator in the flash tank (TK-100) has a positive influence also in the control of the methane impurity level in the bottom of the demethanizer column. To further enhance this improvement different control strategies were developed to mitigate the effect of the disturbances in presence of both feed and composition variations and at the same time obtain a fast control action.

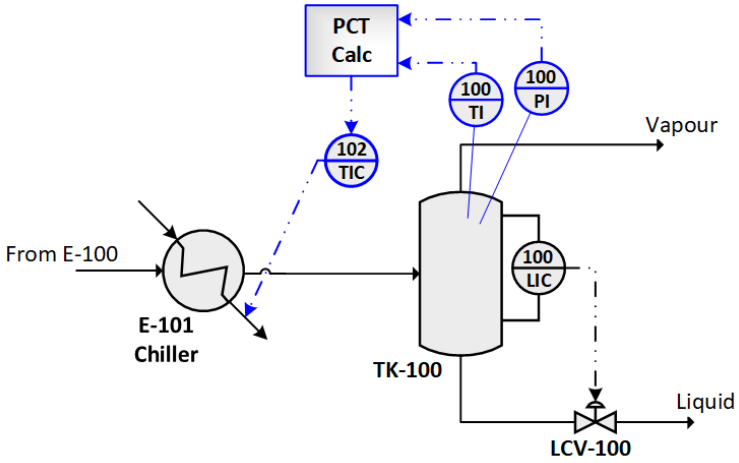

Figure 5.2: Inferential PCT control loop implemented in the CS2 control strategy for the indirect control of ethane recovery.

Approximate boilup to bottom product ratio flow control

Considering that maintaining constant ratios between internal and external column flows ensures constant product composition, to limit the effects of inlet feed disturbances, the introduction of a ratio controller at the bottom of the demethanizer column has been evaluated. Thus, the possibility to control the ratio between the vapor leaving the reboiler and the column bottom product has been investigated. For the realization of this control loop, there is thus the necessity of bottom product flow and boilup flow measures, and the latter is not generally measured in real plants. To overcome this drawback, assuming to have only common measurement data available in real industrial plants, it is possible to substitute the boilup measure with an estimation. Since not enough information was available for boilup calculations

a boilup approximation is obtained by the process information available and based on a balance around the reboiler, as expressed by:

$$\lambda V + c_p(T_B - T_L)(V + B) = Q \qquad 5.2)$$

Here, B is the bottom product stream; V is the actual boilup; Q is the reboiler duty; λ is the latent heat of vaporization of the mixture; c_p is the specific heat capacity at constant pressure; T_B and T_L are the temperature of the stream B and the temperature of the liquid stream entering the reboiler, respectively. Considering different values of inlet flowrate, the open-loop response of V, B, T_L, and T_B are registered by using the model testing function of Aspen HYSYS® on the reboiler duty with an amplitude of 2%. These data are used to perform a multi-linear regression considering the following regression model:

$$\hat{V} = p_0 + p_1 B + p_2 T_B + p_3 T_L \qquad 5.3)$$

where $\hat{V}$ is the boilup estimation. The regressors considered are the registered data of B, T_L, and T_B while $p_i, i = 0, \dots 3$ are the model parameters. The reboiler duty is not considered in the regression since it is the manipulated variable that depends on the control action. The boilup estimation was implemented in a flow controller, where the setpoint was obtained by multiplying the desired bottom product ratio by the bottom product measure.

Two loops cascade control

Considering that temperature control is necessary for feed composition changes (Shinskey, 1996), to speed up the responses obtained by the direct column tray temperature controller the estimated boilup to bottom product ratio flow controller has been implemented in a cascade controller with the temperature controller. The resulting control structure, referred to as CS3, is a cascade control configuration in which the primary controller is a temperature controller that gives the setpoint to the ratio flow controller between the approximate boilup flowrate and bottom product stream, which in turn manipulates the reboiler duty (Figure 5.3). This control structure considers the use of PCT as the process variable for ethane recovery indirect control.

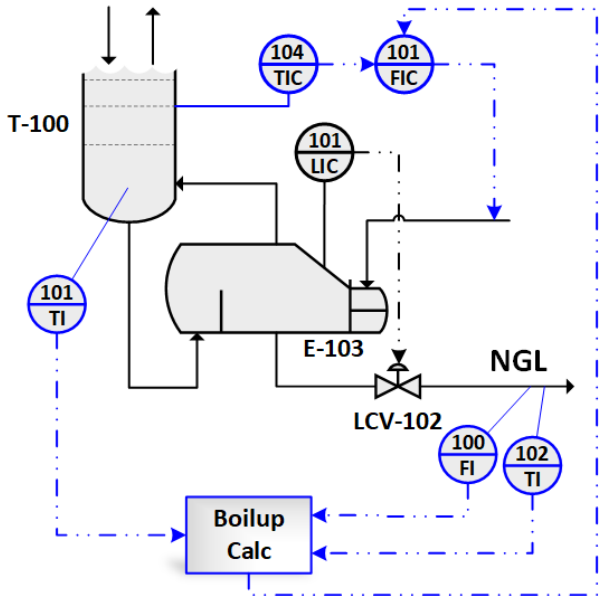

Figure 5.3: Cascade control scheme with boil-up approximation implemented in the CS3 control strategy for the indirect control of methane impurity level in the demethanizer bottom product.

Three loops cascade control

The presented CS3 control strategy may be useful to reject the disturbances derived from variations in the inlet feed to the plant. However, in presence of column inlet composition disturbances, it is not sufficient. As observed previously, in the NGL separation process considered, inlet feed disturbances, causing flash tank (TK-100) pressure and thus thermodynamic equilibrium variation in the flash tank, turns into collateral column inlet composition disturbances. The influence of these composition disturbances on the demethanizer product quality is limited but not eliminated by the PCT control. This means that the CS3 control will significantly reduce the steady state offset in the presence of inlet feed variations, nevertheless it won't be able to eliminate it. A possible solution that allows the elimination of the methane composition offset is represented by the introduction of a composition analyzer in the plant and thus a composition controller. The analyzer is assumed to analyse the product composition of all the distillation units downstream of the demethanizer present in the column of the train which is a common practice in industrial plants. For this reason, a sampling time of 30 minutes has been assumed, considering the time needed by the measuring apparatus to complete a measuring cycle in the entire plant, and a measurement delay of 10 minutes related to the measurement time for this type of mixture. This implies that only discrete and delayed methane measurements are available for the methane composition controller which is added in cascade with the cascade configuration of CS3. In particular, the

discrete methane composition controller acts only at every delayed sampling time to adjust the temperature controller setpoint. The three loops cascade control scheme is illustrated in Figure 5.4b. The resulting control structure will be referred to as CS4. To compare the performances of the CS4 structure with the control strategies proposed by Luyben (2013b, 2013a) and Chebeir et al. (2019), the use of the gas chromatograph is considered and implemented in the CS1 control structure. The new control structure referred to as CS5 is obtained with the realization of a cascade control structure where the master control is given by the composition controller and the slave was the column tray temperature controller of CS1 configuration (Figure 5.4a). Again, CS5 considers the knowledge of delayed and discontinuous composition measurements resulting from the typical delay of online analysers, which were not considered in the above-mentioned contributions.

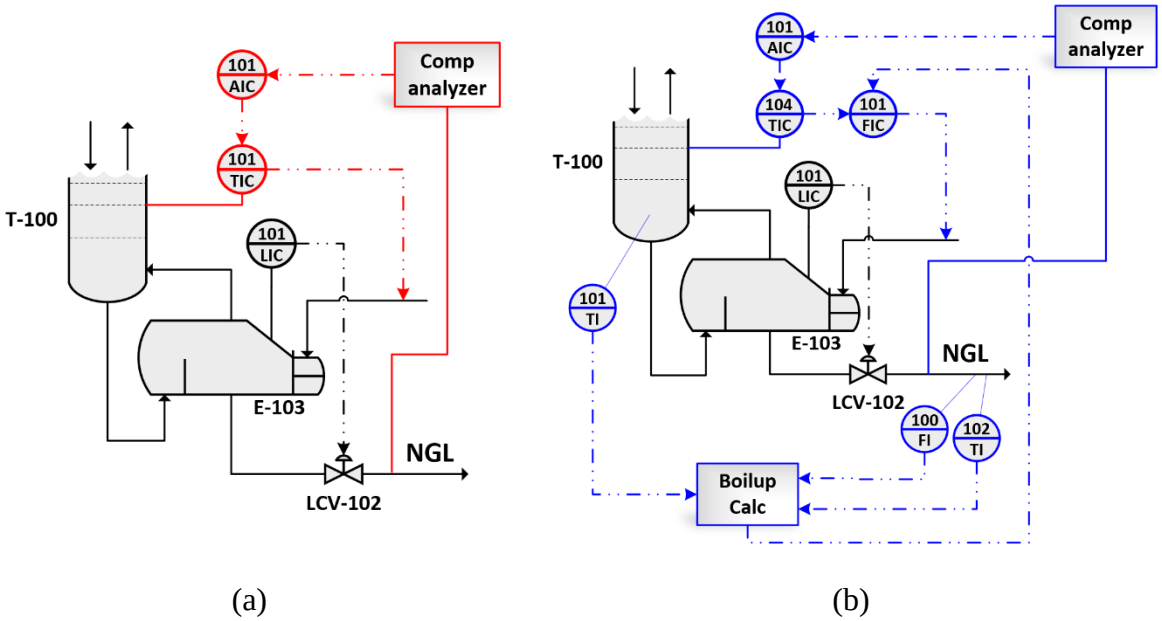

(a) (b)

Figure 5.4: Direct methane impurity level control: two loops cascade control scheme with the composition controller as the primary loop and the direct column tray temperature controller as the secondary, implemented in the CS5 control strategy (a).; three loops cascade control scheme with boil-up approximation implemented in the CS4 control strategies (b).

Demethanizer product quality control tuning parameters

The tuning of the control loops employed in the five control structures developed for the bottom product quality control of the demethanizer, summarized in Table 5.1, was conducted through step test model identification. The responses of process variable and controller output were registered by using the model testing function of Aspen HYSYS®. The model identification was conducted utilizing the System Identification Tool available in the MATLAB® System Identification Toolbox (The MathWorks Inc, 2019). After the identification, the tuning

parameters were obtained by applying the IMC approximate model rules (Rivera et al., 1986). The tuning parameters obtained for the different structures with the three considered separation units are reported in Table 5.2- Table 5.4.

Table 5.2: Conventional separation unit: control structures tuning parameters

Controlled variables	Control structures	K_c	τ_I[min]
Flash tank (TK-100) temperature	CS1 - CS2	1.5	5
Column (T-100) tray temperature	CS1 - CS2 - CS5	1.95	17.30
	CS3 - CS4	10.70	4.05
Approximated ratio flow	CS3 - CS4	0.56	14.30
Methane composition	CS4	0.30	9
	CS5	0.18	9

Table 5.3: GSP separation unit: control structures tuning parameters

Controlled variables	Control structures	K_c	τ_I[min]
Flash tank (TK-100) temperature	CS1 - CS2	1.5	5
Column (T-100) tray temperature	CS1 - CS2 - CS5	1.6	13.8
	CS3 - CS4	10.4	10.5
Approximated ratio flow	CS3 - CS4	0.75	12.5
Methane composition	CS4	0.30	9
	CS5	0.18	9

Table 5.4: CRR separation unit: control structures tuning parameters

Controlled variables	Control structures	K_c	τ_I[min]
Flash tank (TK-100) temperature	CS1 - CS2	1.5	5
Column (T-100) tray temperature	CS1 - CS2 - CS5	1.55	13.8
	CS3 - CS4	9.72	10.5
Approximated ratio flow	CS3 - CS4	0.78	12.3
Methane composition	CS4	0.30	9
	CS5	0.18	9

5.1.2. Deethanizer column control structure

In the deethanizer column, responsible for separating the ethane from the stream leaving the demethanizer, the control strategy aims to maintain the process specification concerning a propane concentration at 1 mol% in the top product and impurity of ethane at the value of 0.34 mol% in the bottom product. To reach the desired quality in the bottom product the indirect control of ethane composition in the column bottom product was realized by controlling the temperature of the 21st tray and manipulating the reboiler duty. The location of the temperature sensor in the column is chosen following the deethanizer gradient temperature analysis performed and reported in the previous chapter. The remaining control loops implemented in the plant are indicated as follows:

1) The column pressure is controlled by manipulating the duty to the condenser E-105.
1) The level of liquid in the reflux drum is controlled by manipulating the flow of the distilled product through the valves LCV-103.
2) The liquid level in the reboiler E-106 is controlled by manipulating the flow of the bottom product through the valves LCV-104.
3) The composition of the impurity in the top is controlled with a ratio flow controller between the reflux stream and the distillate, which manipulates the reflux stream valve V-101.

5.1.3. Depropanizer column control structure

The depropanizer column is used for the propane separation from the bottom product of the deethanizer column, with the control objectives of maintaining the process specification concerning impurity level values of 0.6 mol% for the sum of the concentrations of isobutane and n-butane in the top product, and 0.1 mol% for the propane concentration in the bottom product. To keep the desired propane impurity in the bottom product an indirect composition controller was realized by controlling the temperature of the 30th tray and manipulating the reboiler duty. Also in this case, the location for the temperature sensor in the column was selected considering the gradient temperature analysis reported in the previous chapter. The remaining control loops implemented in the plant are indicated as follows:

2) The column pressure is controlled by manipulating the duty to the condenser E-107.
3) The level of liquid in the reflux drum is controlled by manipulating distillate flow through the valves LCV-105.
4) The liquid level in the reboiler E-108 is controlled by manipulating the flow of the bottom product through the valves LCV-106.
5) The composition of the impurity at the top product is indirectly controlled with a ratio flow controller between the reflux stream and the distillate, which manipulates the reflux stream valve V-102.

5.1.4. Debutanizer column control structure

The purpose of the debutanizer column is the separation of iso-butane and n-butane from the remaining heavier hydrocarbon mixture. The control goal consists in holding constant the impurity of iso-pentane of 0.2 mol% in the top product and the impurity of n-butane of 0.2 mol% in the bottom product. To maintain the concentration impurity target in the column bottom product, the n-butane composition is indirectly controlled by controlling the temperature of the 26th tray by manipulating the reboiler duty. Again, the tray in which locate the temperature sensor was selected considering the gradient temperature analysis reported in the previous chapter. The remaining control loops implemented in the plant are indicated as follows:

1) The column pressure is controlled by manipulating the duty to the condenser E-109.

2) The level of liquid in the reflux drum is controlled by manipulating the distillate flow through the valves LCV-107.

3) The liquid level in the reboiler E-110 is controlled by manipulating the flow of the bottom product through the valves LCV-108.

6) The composition of the impurity of the top product is controlled with a ratio flow controller between the reflux stream and the distillate, which manipulates the reflux stream valve V-103.

5.2. Evaluation of the control structures performances

In this section, the dynamic responses obtained with the Aspen HYSYS® simulations, considering ramp changes over 30 minutes in the feed flowrate and step changes in the inlet ethane composition, have been analyzed. Figure 5.5 and Figure 5.6 depict the disturbance applied respectively in the inlet feed to the plant and the ethane inlet composition to the plant, for which realization the inlet methane composition was changed accordingly.

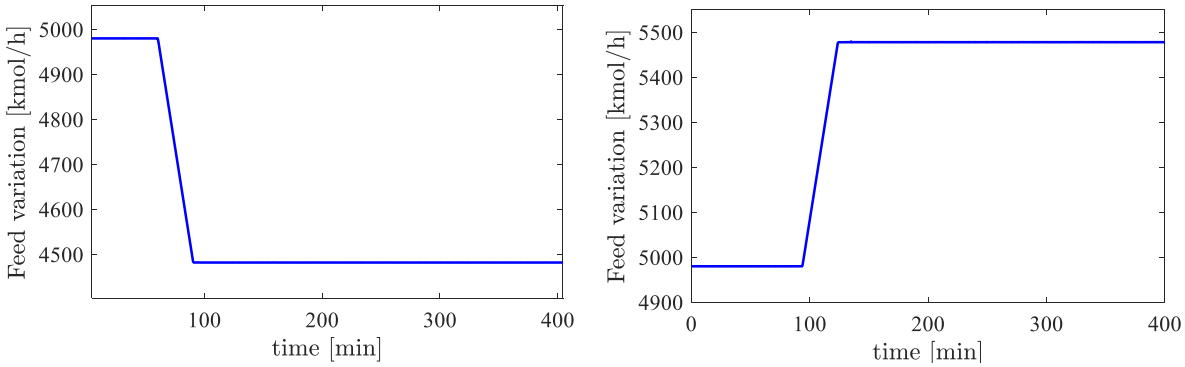

Figure 5.5: Decreasing and increasing ramp variations over 30 minutes of 10% amplitude in the plant feed flowrate nominal value of 4980 $\frac{kmol}{h}$, considered as inlet feed flowrate disturbances in the NGL recovery process.

Firstly, the ability of the control structure of disturbances rejection is evaluated considering the control goal of keeping an ethane recovery of 84% and a methane composition of 1 mol% in the bottom of the demethanizer column. Subsequently, the effect of the proposed indirect composition control configuration on the separation operations of the subsequent columns of the train was evaluated in presence of flow disturbances only.

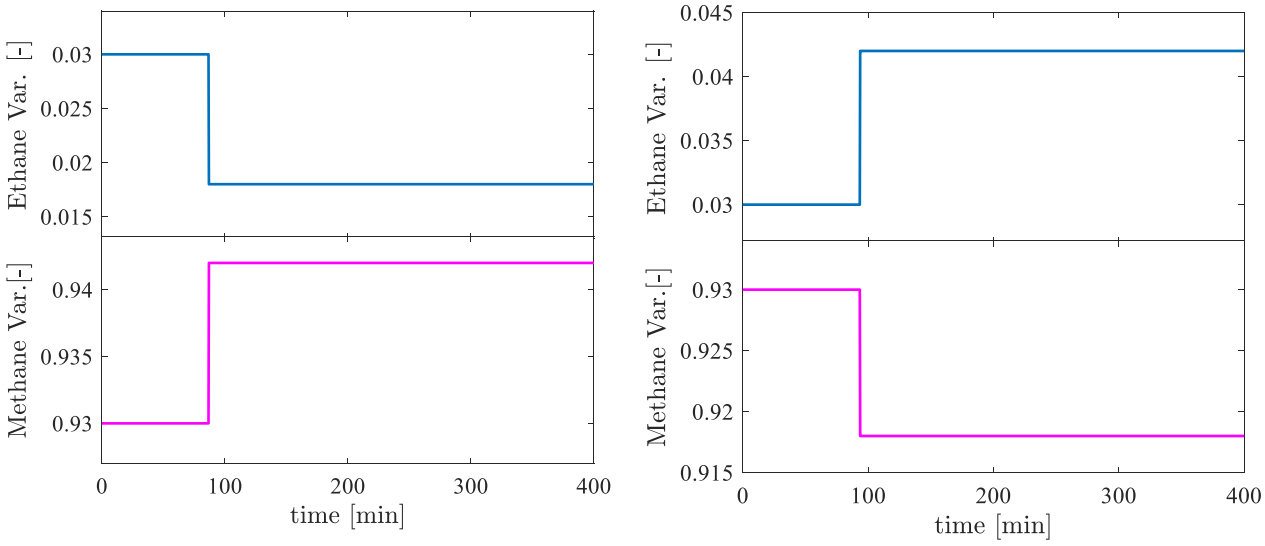

Figure 5.6: Decreasing and increasing step variations of 40% amplitude in the plant ethane inlet composition and methane inlet composition variation in accordance, considered as inlet composition disturbances in the NGL recovery process.

5.2.1. Demethanizer control structures performances

Indirect composition control through temperature control

The results obtained with the implementation of the flash temperature controller for the ethane recovery indirect control and of the column tray temperature control for the methane impurity level indirect control, thus the CS1 configuration, in the three considered separation schemes are depicted in Figure 5.7-Figure 5.10.

In Figure 5.7 and Figure 5.8 the responses obtained to the applied disturbance in the inlet feed of 10% to the three plant schemes are depicted. Figure 5.7 shows the results obtained for the indirect control of ethane recovery (Figure 5.7a) and methane impurity level (Figure 5.7c) corresponding to a decreasing variation in the feed flowrate while Figure 5.8 shows the results obtained by increasing the flowrate to the plant of the same percentage (Figure 5.8a and Figure 5.8c respectively). As it is possible to visualize, in both cases the implementation of the CS1 control configuration is not able to guarantee the required product specifications in the considered separation units. Larger ethane recovery offsets at the new steady state condition are obtained with GSP and CRR process schemes compared to the conventional, with a higher initial variation in the GSP in which the CS1 also present a slower speed of response and a higher initial deviation. High new steady state methane composition offsets are obtained with all the process schemes considered, confirming that this basic control configuration is not the

best control choice for the separation processes under examination, and it is inadequate for efficiently rejecting feed flowrate disturbances entering the system.

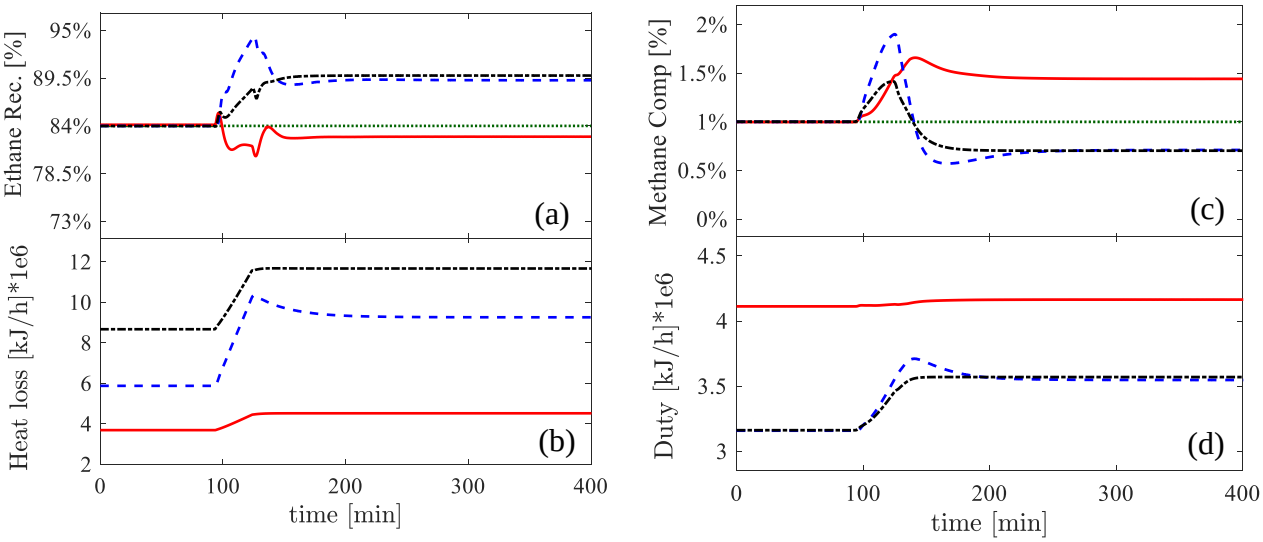

Figure 5.7: Responses obtained for the conventional unit (continuous red lines), GSP unit (dashed blue lines), and CRR recovery unit (dash-dotted black lines) by the CS1 scheme under the presence of a 10% decrease in the plant feed flowrate nominal value. The green dotted lines depict the control target values.

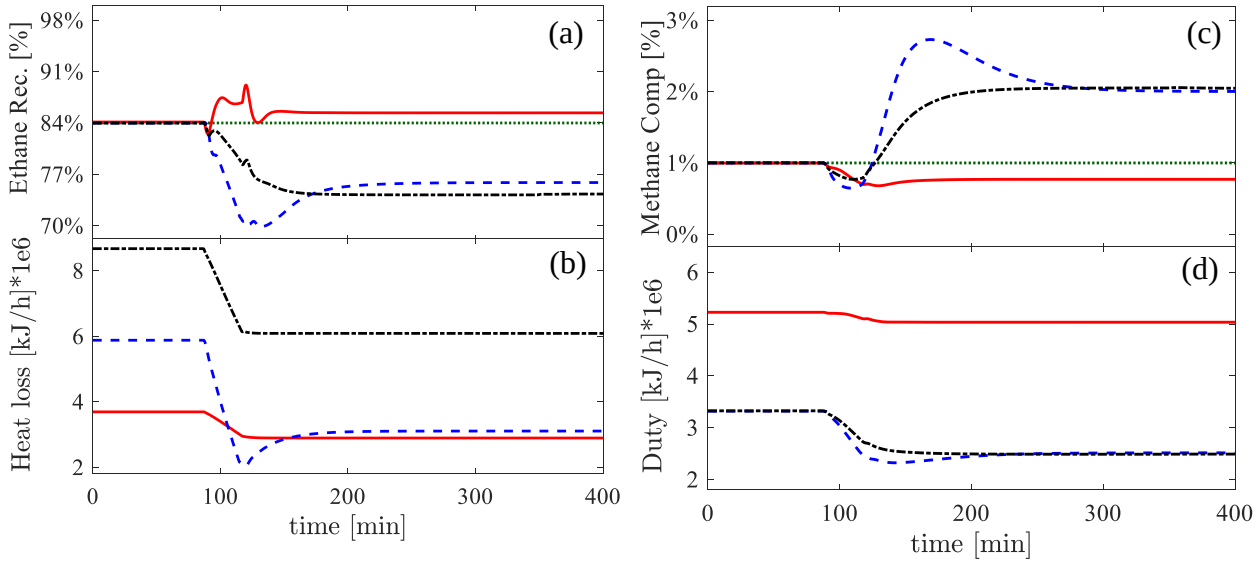

Figure 5.8: : Responses obtained for the conventional unit (continuous red lines), GSP unit (dashed blue lines), and CRR recovery unit (dash-dotted black lines) by the CS1 scheme under the presence of a 10% increase in the plant feed flowrate. The green dotted lines depict the control target values.

To have a complete view of the performances obtainable with the CS1 configuration, also the action of this control structure under the effect of the composition disturbances considered has been examined. Figure 5.9 and Figure 5.10 depict the responses obtained by the three separation schemes to the applied disturbance in the inlet ethane composition of 40%.

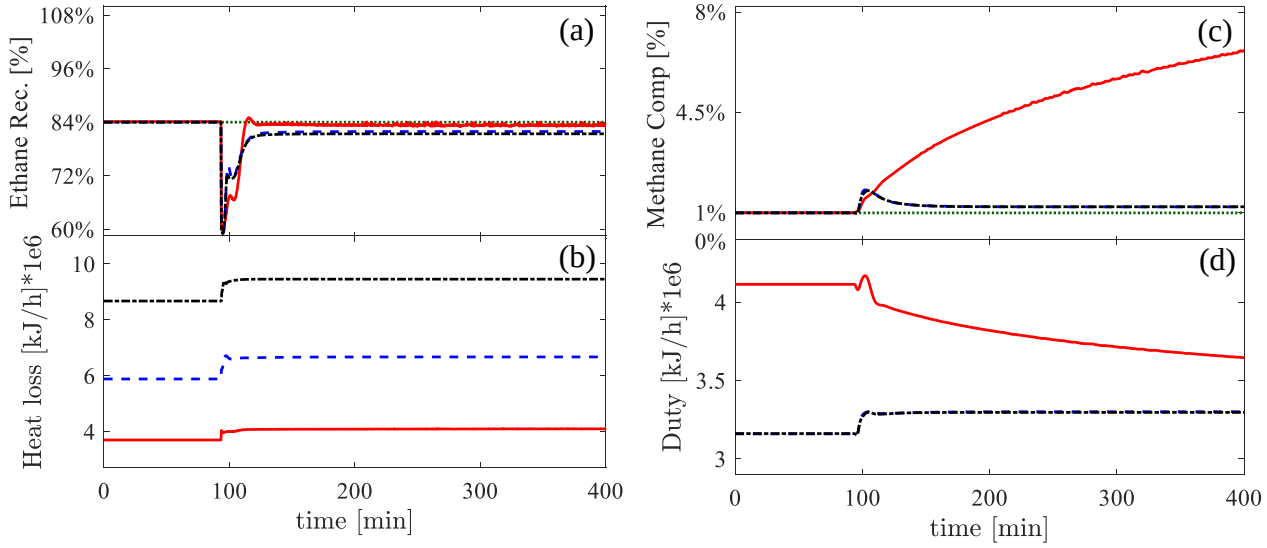

Figure 5.9: Responses obtained for the conventional unit (continuous red lines), GSP unit (dashed blue lines), and CRR recovery unit (dash-dotted black lines) by the CS1 scheme under the presence of a 40% decreasing in the ethane inlet composition of the raw gas. The green dotted lines depict the control target values.

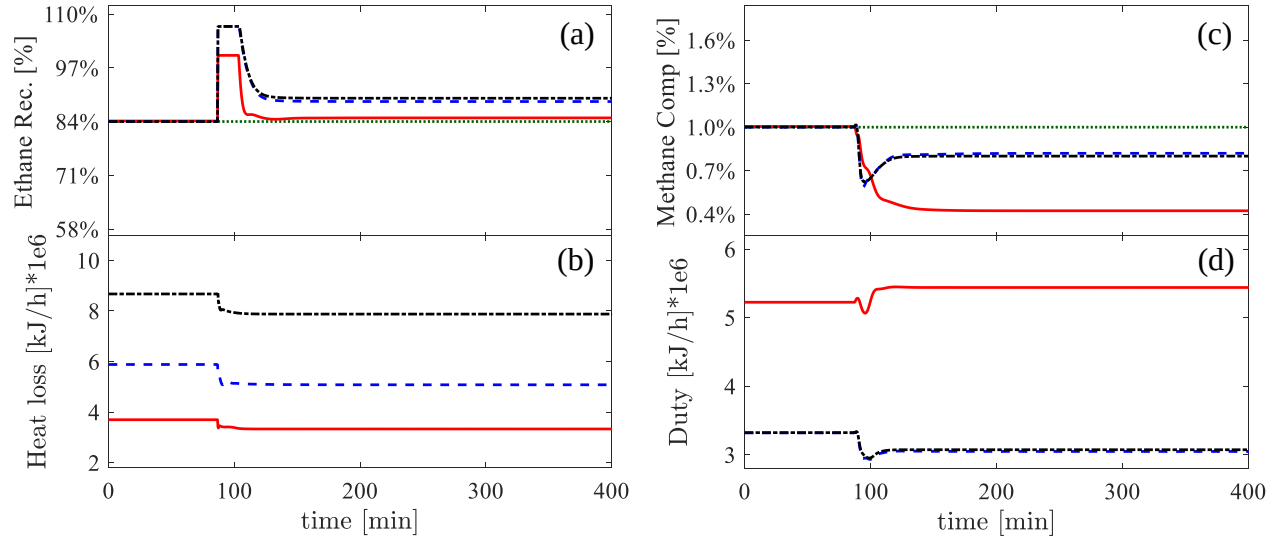

Figure 5.10: Responses obtained for the conventional unit (continuous red lines), GSP unit (dashed blue lines), and CRR recovery unit (dash-dotted black lines) by the CS1 scheme under the presence of a 40% increase in the plant inlet ethane composition. The green dotted lines depict the control target values.

Figure 5.9 shows the results obtained for the indirect control of ethane recovery (Figure 5.9a) and methane impurity level (Figure 5.9c) corresponding to a decreasing variation in the ethane inlet composition while Figure 5.10 shows the results obtained with a decreasing variation of the same amplitude in the ethane inlet composition to the plant for the ethane recovery and the methane concentration (Figure 5.10a and Figure 5.10c respectively).

Analysing the profiles obtained for ethane recovery under the two considered variations in the ethane inlet composition produces in the three schemes a very high initial variation. In both cases, after about half an hour the profiles approach the new steady state values with offsets of around 5.6% with the CRR unit, 4.9% with the GSP and 0.9% with the conventional unit in presence of the decreasing variation in the ethane inlet composition and of around 2.6% with the CRR unit, 2.1% with the GSP and 0.5% with the conventional unit in presence of the increasing inlet ethane composition. Considering the results obtained for the indirect control of methane composition in the bottom of the demethanizer column also in this case the CS1 control scheme is not able to meet the methane impurity level specification. In particular, very high offsets are registered for the conventional separation schemes, for a decreasing variation of 40% in the ethane inlet composition, with a value of 0.58%, while a deviation of 5.6% is registered after 5 hours from the application of the increasing ethane inlet composition disturbance. After this time, as it is possible to visualize from Figure 5.9c, the methane composition profile has not reached the new steady state conditions yet.

Pressure compensated control

As stated, the feed flow variations induce pressure variations in the flash tank (TK-100), in which the temperature is kept constant by the temperature controller of CS1. To limit the impact of these pressure variations on the recovery of ethane, the control of the temperature compensated in pressure on the flash tank has been evaluated. The results obtained with the applications of the CS1 control schemes are compared with the modification proposed in the CS2 control structure, the direct PCT control in the flash tank (TK-100) and shown in Figure 5.11 and Figure 5.12. For sake of brevity, only the results obtained with the GSP control scheme are reported since as depicted in Figure 5.7a and Figure 5.8a the CS1 control showed the worst performances: although the offset obtained is slightly lower than the one obtained with the CRR process scheme, in the GSP the action of the CS1 configuration shows a lower speed of response and a higher initial variation.

The right panel of Figure 5.11 depicts the comparison of the transient profiles obtained under a 10% decreasing variation in the inlet feed to the plant with the CS1 and CS2 control structures. In Figure 5.11a the temperature transient profiles are depicted, here it is possible to visualize that both the control structures under comparison can bring the process variables to the setpoint value after approximately 80 min with the CS2 and 95 min with the CS1. The profile obtained with the temperature actual flash tank (TK-100) temperature, indicated by the

dash-dotted cyan line with the CS2 and with the dashed red line with CS1 displays different behaviors, indeed with the use of the PCT the actual flash tank temperature varies following the flash tank pressure variations.

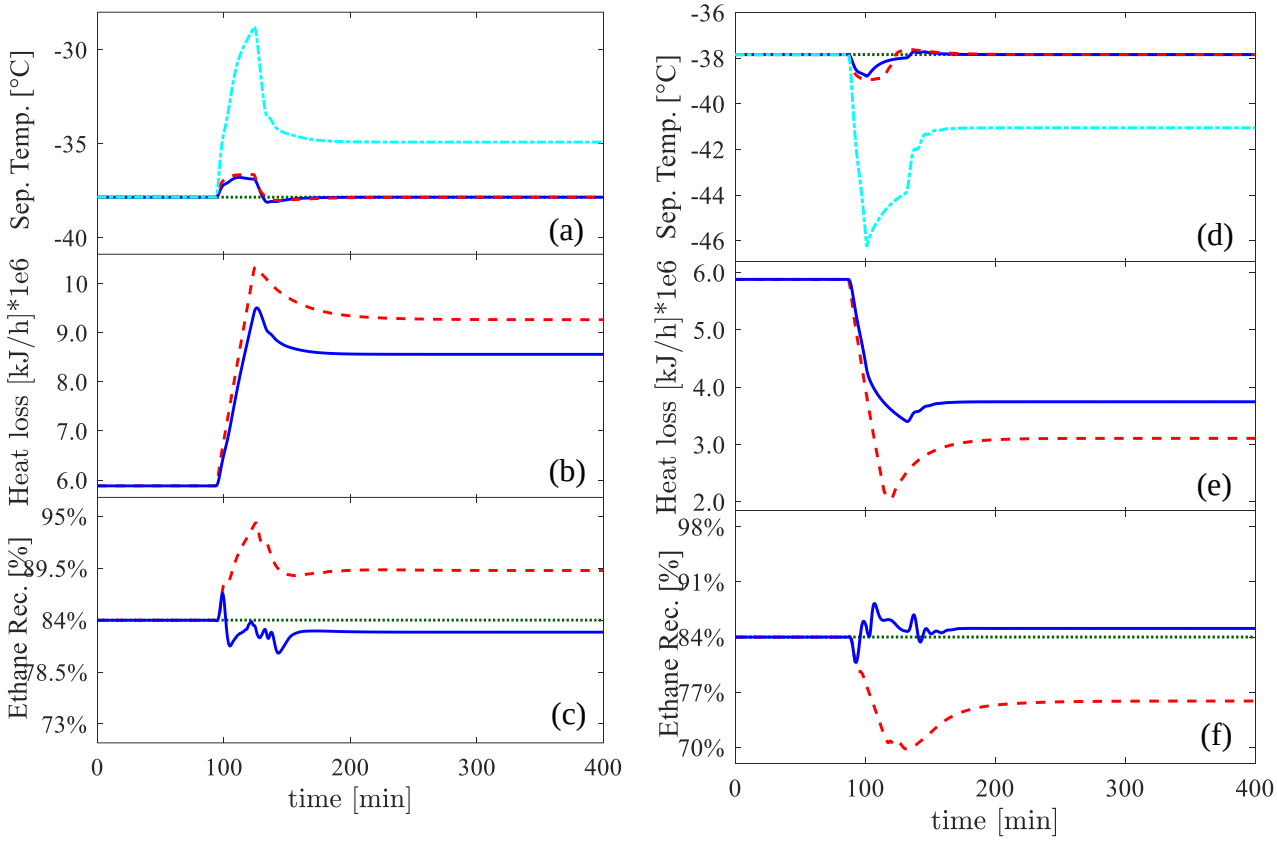

Figure 5.11: Responses obtained for the demethanizer column of the GSP unit by the CS1 scheme (dashed red lines) and the CS2 scheme (continuous blue lines) for a 10% decrease in the plant feed flowrate (left panel graphs) and increasing of the same amplitude in the nominal feed to the plant (right panel graphs). The green dotted lines depict the control targets and setpoint values.

Figure 5.11b depicts the action of the manipulated variable, the chiller heat loss. As shown with the implementation of the CS2 the manipulated variable has a lower initial variation and a lower variability at the new steady state conditions. Thus, with the use of the CS2 scheme, not only the flash tank (TK-100) temperature compensates for the flash tank pressure variations, but this control structure is associated with more energy-efficient operations. Figure 5.11c depicts the transient profiles of ethane recovery, the reported results show that none of the two control structures can meet the ethane recovery specification. The new steady state values for the ethane recovery are 76% with the CS1, and 85% with the CS2 scheme. Nevertheless, the ethane recovery profile obtained with PCT control shows a lower initial deviation, a faster speed of response and a lower offset at the new steady states, demonstrating that concentration disturbances due to the feed variations are reduced and thanks to the implementation of the PCT control, even without an ethane composition controller, it was

possible to drastically reduce the new steady state offset. Analogue results are obtained with an increase of 10% in the feed flowrate, shown in the left panel of Figure 5.11. As depicted in Figure 5.11e also in this case with the CS2 control the manipulated variable shows a lower variability, allowing better control of ethane recovery with less refrigerant consumption. As it is possible to visualize in Figure 5.11f, using the separator temperature controller, thus with the CS1 configuration, also under the increasing variation of inlet flowrate, the process is not able to maintain the recovery target, reaching the new steady state value of 89.2% with an offset of 5.2%. On the other hand, with the PCT control, the new steady state offset is reduced to the value of 1.3%, bringing the ethane recovery to the value of 82.7%.

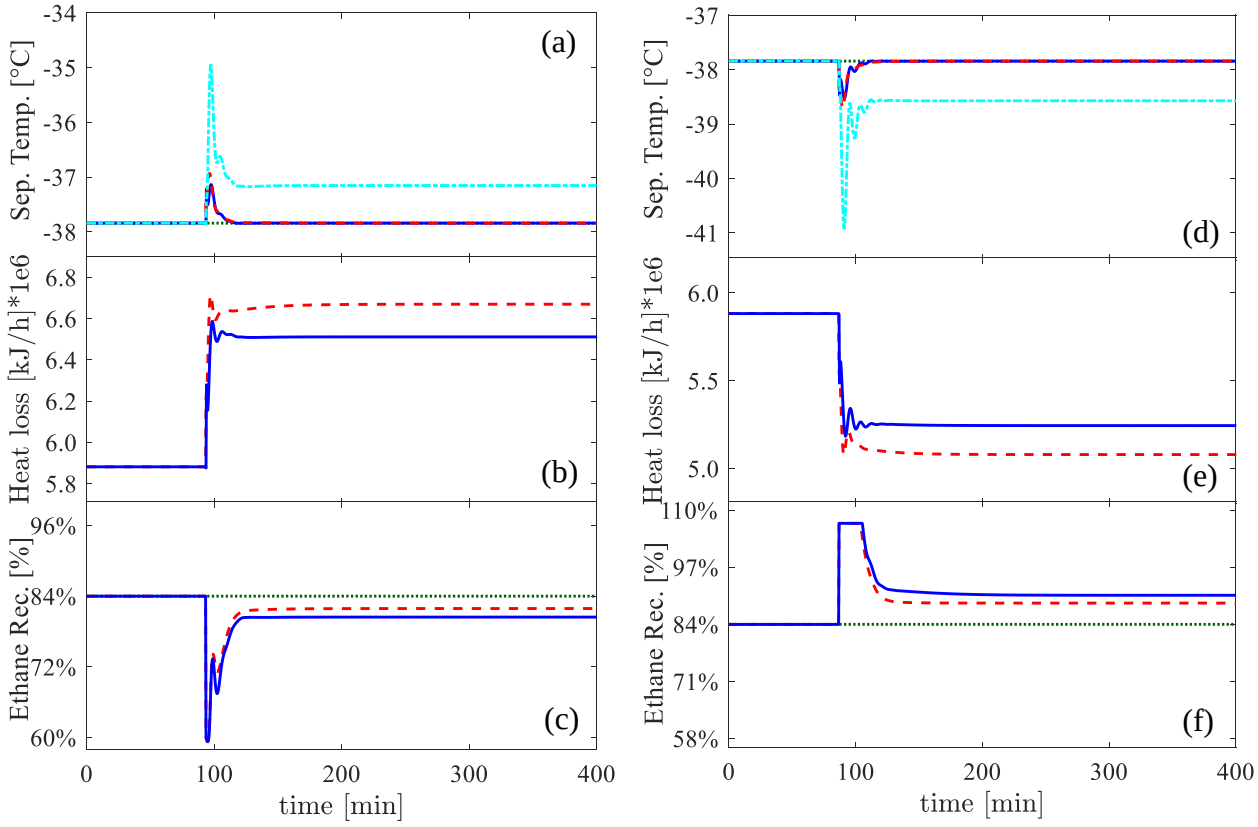

Figure 5.12: Responses obtained for the demethanizer column of the GSP unit by the CS1 scheme (dashed red lines) and the CS2 scheme (continuous blue lines) for a for a 40% increasing (left panel graphs) and for a 40% decreasing of the ethane inlet composition to the plant (right panel graphs). The green dotted lines depict the control targets and setpoint values.

Figure 5.12 displayed the transient profiles obtained by using the CS1 and the CS2 control structure in the GSP scheme, under the imposition of the 40% increase variation (left panel) and decrease variation (right panel) in the ethane inlet composition. In presence of both the applied disturbances, the same results are obtained. As it is possible to visualize in Figure 5.12a and Figure 5.12d, depicting the flash tank (TK-100) temperature profiles, both the control structures keep the process variable at the desired setpoint value. Here when controlling the

PCT in the flash tank (TK-100) the new steady state value of the actual flash tank temperature differs by around 1°C from the nominal conditions. In Figure 5.12b and Figure 5.12e, the profiles obtained for the manipulated variables depict a lower variability as well in case of feed disturbances to the plant. By looking at the ethane recovery behaviours displayed in Figure 5.12c and Figure 5.12f, it is possible to observe that also in this case the two control strategies are unable to reach the desired ethane recovery value. The controlled variables reach the steady state value of 80.4% with the CS2 and value of 81.9% with the CS1 control under the increasing variation in the considered disturbance and a new steady state value of 90.6% with the CS2 and 88.8% with CS1 control with the decreasing variation. Hence, the improvement obtained in case of feed disturbances is not registered in case of variations in inlet ethane concentration. Nevertheless, the distance between the value obtained with the PCT control is 1.5%, with a final offset of 3.6% for the increasing variation, and 1.8% with a final offset of 6.6% for the decreasing variation.

Overall, with pressure compensation temperature control, it is possible to obtain faster responses to the application of flowrate and ethane input concentration disturbances. With feed disturbances, the offset values of ethane recovery are drastically reduced. This improvement is not observed in the other case since the pressure compensator was developed without considering input composition variations. However, the distance of the new steady state values obtained in comparison with the direct temperature control is not excessively large. This is since minor pressure variations compared to the ones associated with inlet flowrate disturbances, are still present in the flash tank (TK-100) due to the composition changes and are responsible for the deviations registered in the new steady state value of the actual flash tank temperature with the PCT control.

Effect of Pressure compensated control on methane impurity level control

After having observed the improvements obtained with the use of the PCT control over the ethane recovery indirect control, the influence of its implementation on the methane impurity level indirect control is evaluated. With this purpose, the performances of the CS1 and CS2 on the methane composition impurity control in the demethanizer column of the Conventional unit are depicted in Figure 5.13 and Figure 5.14 respectively under the presence of both inlet feed and composition disturbances. This process scheme was chosen considering that for the conventional separation unit the CS1 depicts the worse performances under the presence of the

composition disturbances (Figure 5.9c and Figure 5.10c) and the increasing variation in the inlet flowrate to the plant (Figure 5.7c).

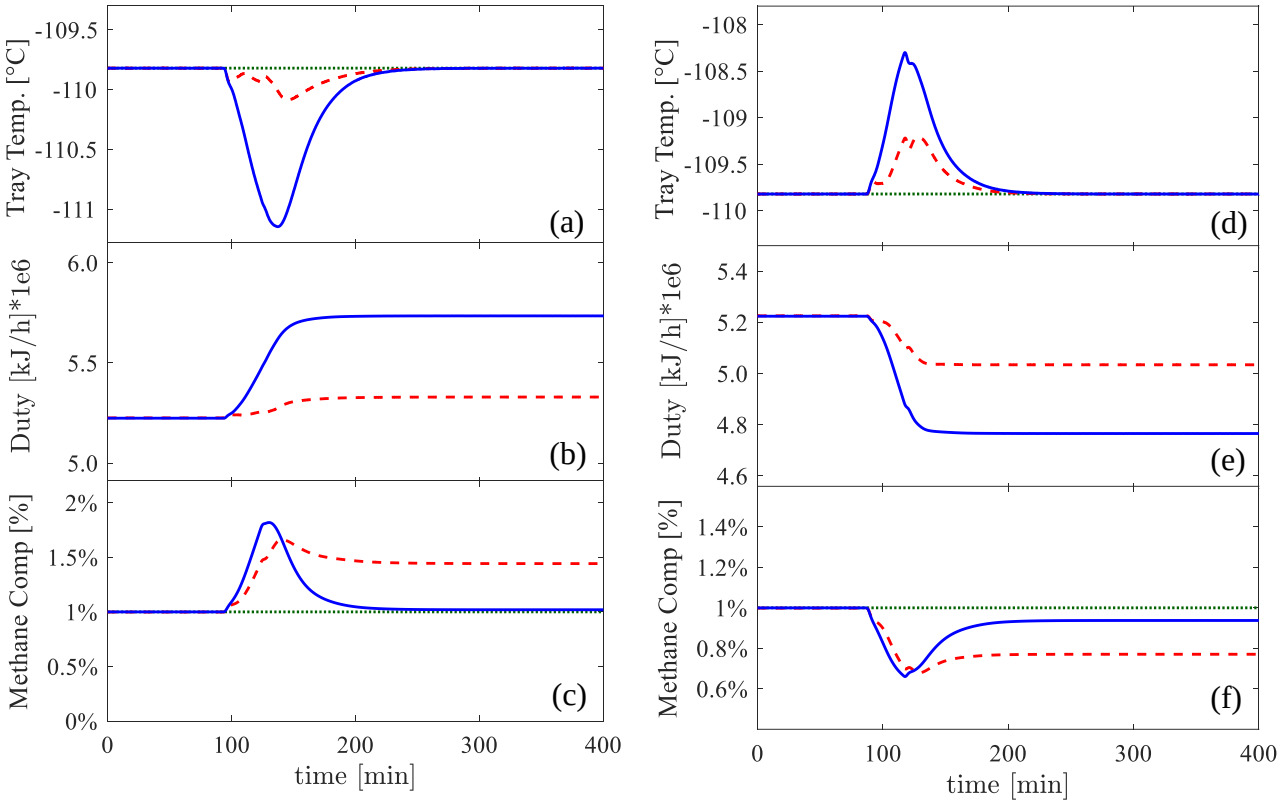

Figure 5.13: Responses obtained for the demethanizer column of the conventional unit by the CS1 scheme (dashed red lines) and the CS2 scheme (continuous blue lines) for a 10% decrease in the plant feed flowrate (left panel graphs) and increasing of the same amplitude in the nominal feed to the plant (right panel graphs). The green dotted lines depict the control targets and setpoint values.

In the left panel of Figure 5.13, the effect of the implementation of the CS2 scheme over the methane impurity level under a 10% increasing variation of the nominal value of the plant feed is depicted. Figure 5.13a displays the column 28th tray temperature profiles which are controlled by the direct temperature controller that manipulates the reboiler duty. Here under the action of both the compared control structures the temperature controller brings back the temperature to the setpoint value. A larger initial variation registered with the CS2 of 1.32°C, while the CS1 produce an initial variation lower than 0.30°C. By considering the manipulated variable which is depicted in Figure 5.13b, here with the use of the CS2 control the variability of the reboiler duty is higher than the one obtained with the CS1, with an increase of about 382.80%.

The same results are obtained under the effect of a decreasing variation in the feed to the plant and are depicted in the right panel of Figure 5.13. The influence of the PCT control brings a higher initial variation in the column tray temperature (Figure 5.13d) and a slower response. By looking at the manipulated variable (Figure 5.13e) also in this case it is registered a higher variability with the CS2 control with an increase compared to the CS1 value of about 141.40%. By considering the methane bottom impurity profiles (Figure 5.13f) even if the response obtained with the CS2 is slower, the obtained new steady state offset is reduced from the value of 0.23% with the CS1 to the value of 0.06% with the CS2.

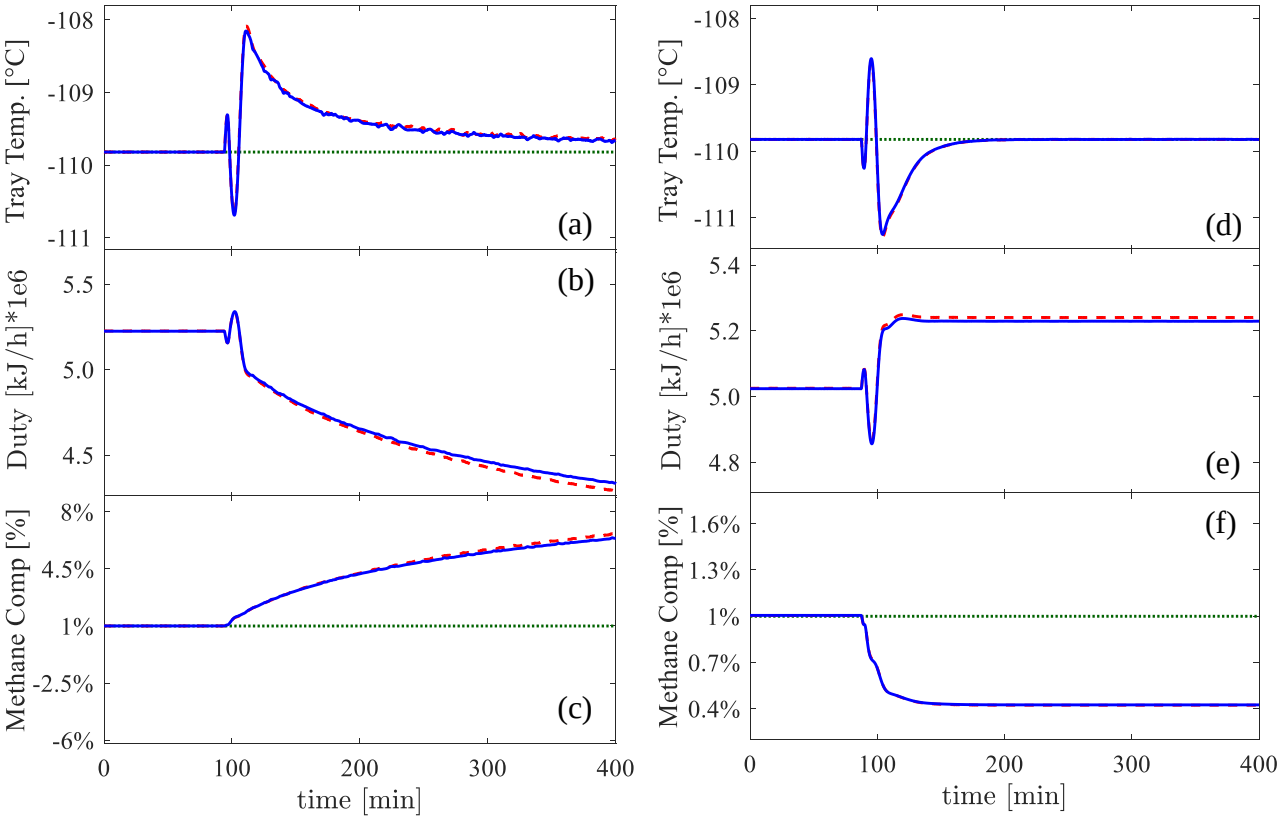

Figure 5.14: Responses obtained for the demethanizer column of the conventional unit by the CS1 scheme (dashed red lines) and the CS2 scheme (continuous blue lines) for a for a 40% increasing (left panel graphs) and for a 40% decreasing of the ethane inlet composition to the plant (right panel graphs). The green dotted lines depict the control targets and setpoint values.

The results obtained under the effect of a variation of 40% in the inlet ethane composition are shown in the panels of Figure 5.14. By looking at the results obtained under the increasing variation (left panel) and decreasing variation (right panel), in the conventional separation scheme the use of the PCT control over the methane impurity indirect control has no influence. The performances obtained are comparable probably because of the presence of the second flash tank (TK-100) in the conventional unit whose outlets supply the higher methane content to the column.

To obtain a quantitative comparison of CS1 and CS2 control performances, the Integral Absolute Error (IAE) of controlled and target variables has been calculated and Reported in Table 5.5 and Table 5.6.

Table 5.5: Integral Absolute Error (IAE) obtained for CS1 and CS2 under the considered decreasing variation in the plant inlet flowrate

		Conventional	**GSP**	**CRR**
Controlled outputs				
Tray Temperature	CS1	26.78	318.64	162.68
	CS2	64.03	107.46	127.14
Methane Concentration	CS1	0.77	3.51	2.86
	CS2	0.33	0.20	0.35
Ethane Recovery	CS1	6.70	37.70	22.44
	CS2	10.24	22.69	16.61
Flash Tank Temperature	CS1	5.11	29.42	29.58
PCT	CS2	1.78	3.89	1.20

Table 5.6: Integral Absolute Error (IAE) obtained for CS1 and CS2 under the considered decreasing variation in the plant inlet ethane composition

		Conventional	**GSP**	**CRR**
Controlled outputs				
Tray Temperature	CS1	42.03	78.73	75.23
	CS2	41.58	59.95	64.60
Methane Concentration	CS1	1.85	0.63	0.69
	CS2	1.84	0.98	1.07
Ethane Recovery	CS1	3.12	7.00	7.68
	CS2	3.31	5.28	5.43
Flash Tank Temperature	CS1	5.87	20.51	22.96
PCT	CS2	5.76	26.69	26.69

Table 5.5 report the IAE values for controlled and target variables obtained with the CS1 and CS2 under the decreasing ramp variation in the plant inlet flowrate nominal value. As it is

possible to visualize the results agree with what was found from the obtained profiles' qualitative analysis. In the GSP and CRR process schemes, the use of the CS2 control strategy leads to improved control performances concerning methane impurity (IAE reduction of 94,3% and 87,7% respectively) and ethane recovery (IAE reduction of 39.8% and 26,0% respectively) at the bottom of the demethanizer. Improved control performances are also observed for all the controlled variables. Concerning the conventional process scheme, the use of the CS2 control configuration leads to an improvement in methane impurity level (IAE reduction of 57,1%), while it is shown a negative effect on the recovery of ethane with an IAE increase of 52,8%, which is probably due to the influence of the flash tank (TK-102) present in the plant.
Table 5.6 shows the IAE values obtained with the CS1 and CS2 under the decreasing variation of the inlet ethane composition to the plant. As it is possible to notice the use of the CS2 control scheme instead of CS1 has no registered effects on the control performances associated with the conventional process scheme while exhibiting adverse effects on the performances related to the GSP and CRR schemes. Nevertheless, in those cases, the IAE values obtained for ethane recovery and methane impurity levels still appear to be lower than the ones obtained with the CS1 under feed disturbances.

Boilup to bottom product ratio control

Therefore, it was observed that the introduction of PCT control leads to a sensible reduction in the methane impurity levels obtained in the bottom of the demethanizer column in presence of feed flowrate disturbances. This improvement was however achieved at the expense of the control system's speed of response and the energy efficiency of the plant. To overcome this drawback, the introduction of an approximate boilup to bottom product ratio flow controller was tested. To compare the approximations obtained during the transient time, the action of the actual ratio controller, thus considering that the actual boilup measurement is known, and the approximated ratio controller has been tested considering a fixed setpoint determined based on an optimal analysis around the operative conditions. In this section the results obtained for the realization of the demethanizer boilup approximation for the three considered separation units are shown in Figure 5.15- Figure 5.18 under the imposition of the decreasing considered variation in the inlet feed and composition disturbances.

The tuning of the ratio control loops was conducted through step test model identification and using the IMC approximate model rules, as described above for model identification and control parameters tuning of the structures compared in the chapter. The tuning parameters

obtained for the two ratio flow controllers with the three considered separation units are reported in Table 5.7.

Table 5.7 Ideal and approximated ratio flow controller tuning parameters

Controllers	Unit	K_c	τi [min]
Ideal ratio flow	Conventional	0.54	12.3
	GSP	0.75	10.5
	CRR	0.75	10.5
Approximate ratio flow	Conventional	0.56	14.3
	GSP	0.75	12.5
	CRR	0.75	12.3

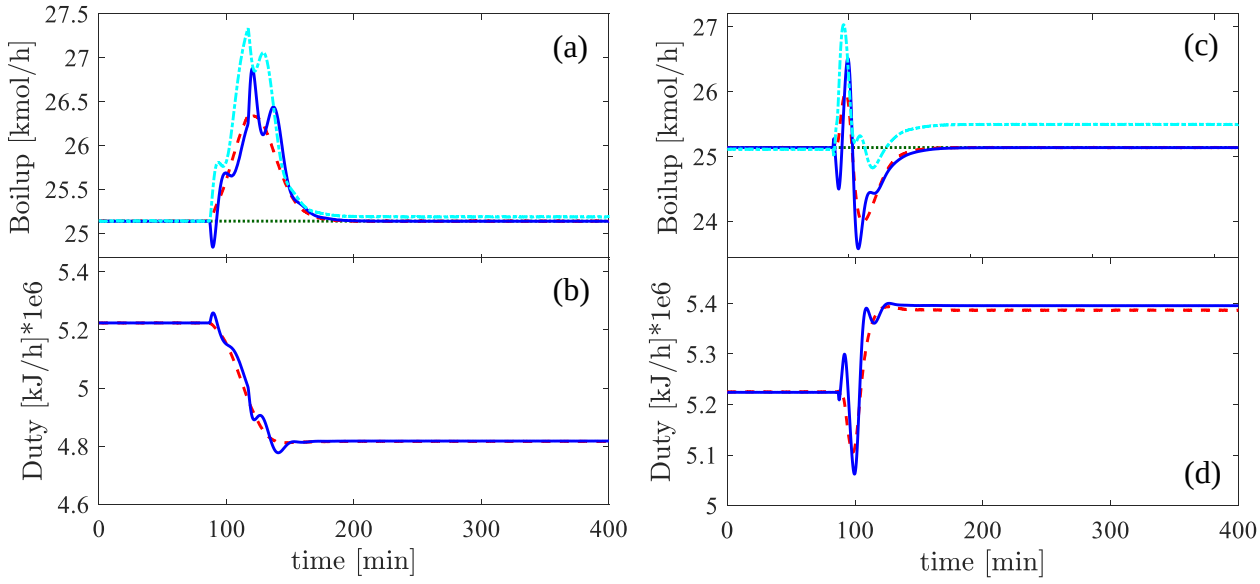

Figure 5.15: Responses obtained for the demethanizer column of the conventional unit by the ideal ratio flow controller (dashed red lines) and the approximated ratio flow controller (continuous blue lines) for a 10% decrease in the plant feed flowrate (left panel graphs) and for a 40% decrease in the ethane inlet composition to the plant (right panel graphs). The green dotted lines depict the setpoint values and the cyan dash dotted line depicts the actual boilup when the approximated boilup is controlled.

In the left panel of Figure 5.15, the comparison between the control of the actual boilup to bottom product ratio and the approximated ratio control in presence of a variation of 10% in the feed to the conventional recovery unit is depicted. As it is possible to observe in Figure 5.15a, under nominal conditions the boilup approximation and the corresponding real boilup measure (dash-dotted cyan line) are perfectly overlaid, after the imposition of the feed

disturbance the approximated boilup under the action of the control action depicts an initial inverse response of the duration of 6 min. After this period, it approximates the actual boilup trend with a maximum error of 1 $\frac{kmol}{h}$. Figure 5.15b depicts the action of the manipulated variable, the reboiler duty, which depicts a comparable behaviour for the actual and the approximated ratio controllers. The results obtained for the manipulated variable express the fact that, although there are detectable differences in the profiles of the actual boilup and its approximation, these are not sufficient to affect the control of the considered variable in the presence of the composition disturbance considered.

Similar results are obtained under the imposition of a decrease of 40% in the ethane inlet composition, as observable in the results reported in the right panel of Figure 5.15. In Figure 5.15c, it is possible to notice that the approximation fails to correctly represent the actual trend of the boilup in the transient time, and an offset of 0.36 $\frac{kmol}{h}$ is achieved. Nevertheless, the actual and the approximated profiles have a comparable speed of responses and by looking at the comparison of the manipulated variable actions depicted in Figure 5.15d even if the general transient trends depict a different behaviour, also in this case, the reboiler duty actions are overall comparable.

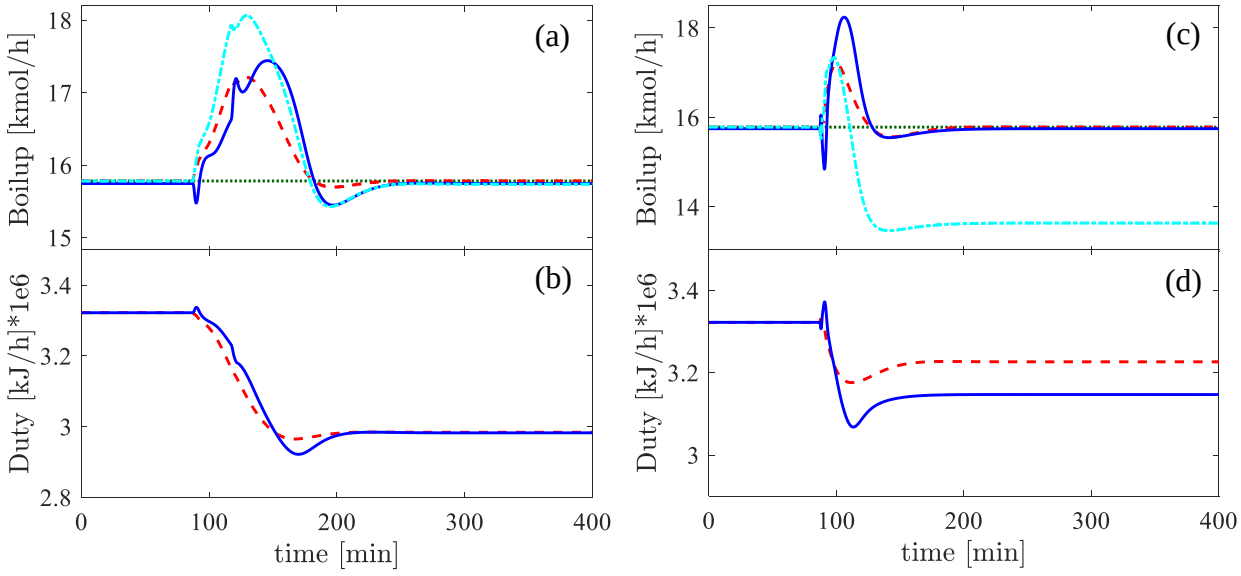

Figure 5.16: Responses obtained for the demethanizer column of the CRR unit by the ideal ratio flow controller (dashed red lines) and the approximated ratio flow controller (continuous blue lines) for a 10% decrease in the plant feed flowrate (left panel graphs) and for a 40% decrease in the ethane inlet composition to the plant (right panel graphs). The green dotted lines depict the setpoint values and the cyan dash dotted line depicts the actual boilup when the approximated boilup is controlled.

The comparison between the action of the approximated and the actual ratio flow controller for the CRR separation scheme under the action of a decreasing variation in the inlet plant flowrate

is depicted in the left panel of Figure 5.16. In Figure 5.16a, by comparing the action of the actual and approximate flow controllers it is possible to observe that also in this case the approximated boilup profile presents an inverse response in the first 5 min, and a lower initial deviation compared to the actual boilup profile (dash-dotted cyan line), with a maximum error of 1 $\frac{kmol}{h}$. After 90 min the approximation converges to the real profile with no significant deviation in the new steady state value. By comparing the action of the reboiler duty (Figure 5.16b) in the two cases, the manipulated variables present similar behaviours during the transient arriving at the same new steady state value. Overall, the approximation obtained results in a valid alternative to the actual boil-up as process variables for the ratio flow controller under the presence of inlet feed disturbances in the CRR scheme. The right panel of Figure 5.16 presents the results obtained with the CRR separation unit under the presence of the decreasing variation in the inlet ethane composition. Here the boilup profiles (Figure 5.16c) obtained through the action of the ratio flow controllers, present different behaviours. The approximation shows a higher deviation compared to the actual boilup with a final deviation in the new steady state of about 2 $\frac{kmol}{h}$. Nevertheless, the transient behaviours obtained for the approximated and actual boilup have a comparable speed of response. Considering the action of the manipulated variables depicted in Figure 5.16d, the action obtained with the approximation shows a higher variability with an increase at the new steady state of 2.5%. The approximation obtained for the CRR scheme does not provide a proper estimation of the actual boilup under ethane inlet composition variations. Considering that the estimation has a comparable speed of response with the actual boilup, the approximation obtained can still be useful as a secondary loop in a cascade arrangement, where the setpoint value changes following the action of the primary controller.

The results inherent to the boilup estimation in the GSP unit under the 10% decreasing variation in the feed plant nominal value are shown in the left panel of Figure 5.17. Here the boilup approximation obtained displays similar results to the ones obtained for the CRR separation unit. As observable in Figure 5.17a, the boilup approximation depicts a similar profile to that obtained for the actual profile, converging to the same value after about 95 min. Also, the manipulated actions obtained with the actual and the approximated ratio flow control are similar during the transient time and converge to the same value when the new steady state is reached. Considering the GSP results under the imposition of the considered ethane inlet composition decreasing variation, depicted in the right panel of Figure 5.17, also in this case

the performance obtained by the boilup approximation is similar to the ones obtained for the CRR separation unit. The boilup profiles are reported in Figure 5.17c, also in this case through the action of the ratio flow controller the approximated boilup profile presents a higher initial variation and a deviation of 1.8 $\frac{kmol}{h}$ from the actual profile in the new steady state conditions. Again, even if the boilup approximation shows to not be able to correctly estimate the actual boilup, with the action of the approximated ratio flow controller the two profiles have a comparable speed of response, suggesting the possibility to use the boilup approximation as the controlled variable in the secondary loop of a cascade control scheme.

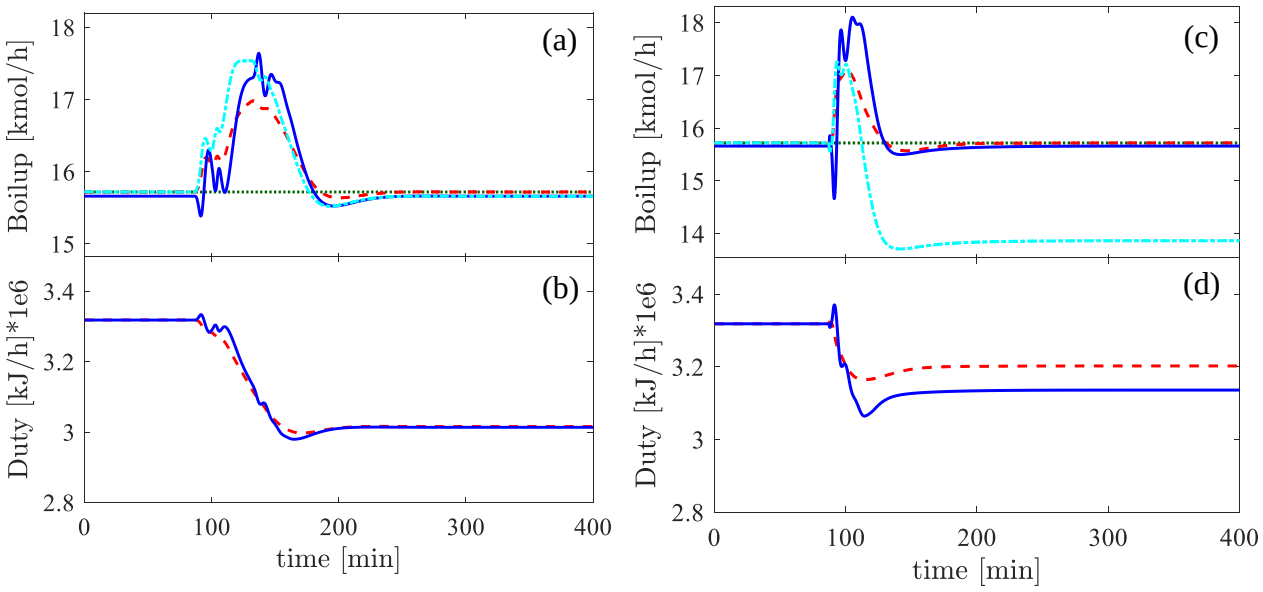

Figure 5.17: Responses obtained for the demethanizer column of the GSP unit by the ideal ratio flow controller (dashed red lines) and the approximated ratio flow controller (continuous blue lines) for a 10% decrease in the plant feed flowrate (left panel graphs) and for a 40% decrease in the ethane inlet composition to the plant (right panel graphs). The green dotted lines depict the setpoint values and the cyan dash dotted line depicts the actual boilup when the approximated boilup is controlled.

Two loops cascade control

As stated in the previous subsection the implementation of the ratio flow controller in the separation units is only able to reject the disturbances in the case of the presence of flow disturbances alone. As seen previously in the considered NGL separation units, the flow disturbances are always coupled with collateral composition disturbances. These are reduced using the pressure compensator and thus the control of the PCT in the flash tank (TK-100), but not removed. Also, the approximation obtained for the boilup fails to approximate the actual boilup in the presence of the composition disturbances considered, necessitating a master controller to adjust the shot of the ratio controller. For these reasons as well as to speed up the

action of the column tray temperature controller, the performances of the cascade arrangement in the CS3 are here compared with the basic CS1scheme. The results of this comparison for the three considered recovery units under the considered disturbances decreasing variation are depicted in Figure 5.18- Figure 5.20.

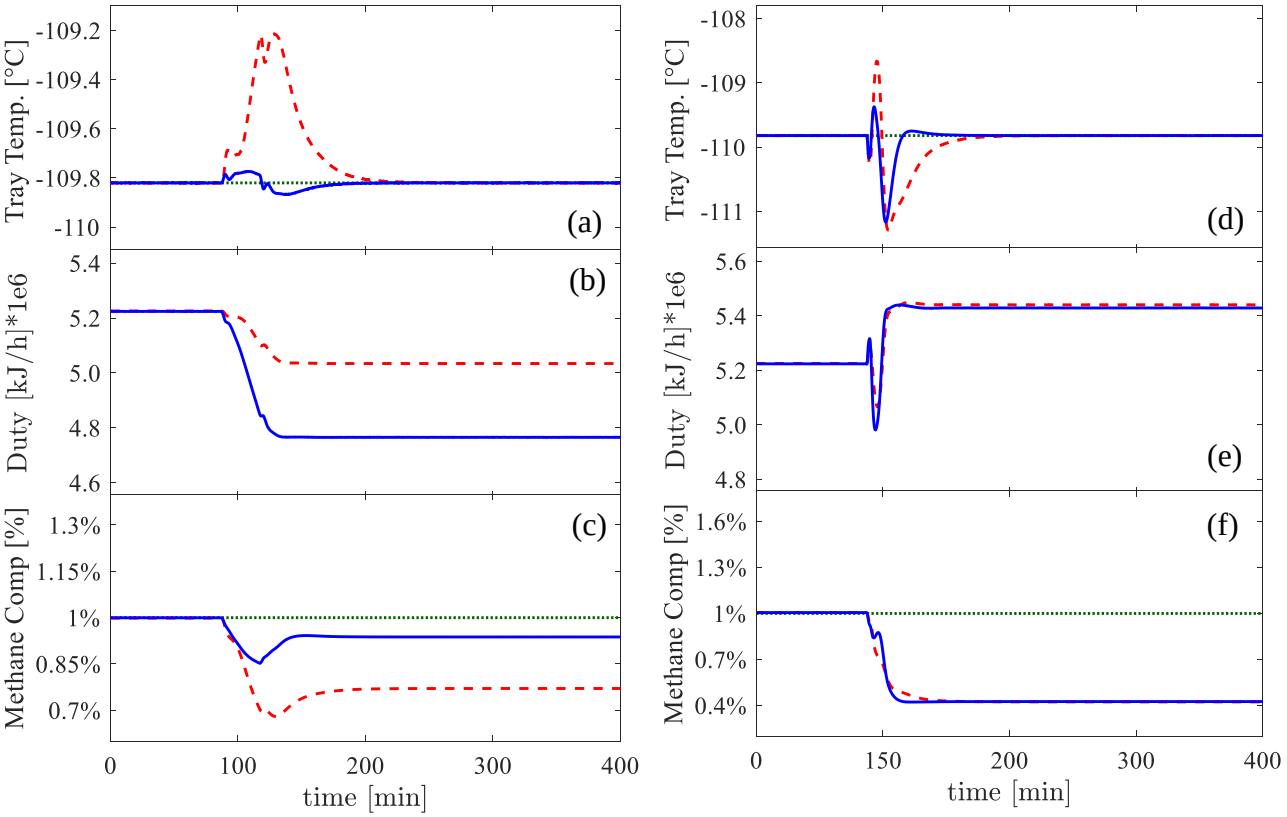

Figure 5.18: Responses obtained for the demethanizer column of the conventional unit by the CS1 scheme (dashed red lines) and the CS3 scheme (continuous blue lines) for a 10% decrease in the plant feed flowrate (left panel graphs) and for a 40% decrease in the ethane inlet composition to the plant (right panel graphs). The green dotted lines depict the control targets and setpoint values.

The results obtained for the conventional separation scheme under the decreasing disturbance in the inlet feed flowrate are reported in the left panel of Figure 5.18. In Figure 5.18a, the profiles obtained for the column tray temperature with the two compared control structures are shown. As it is possible to observe with the CS3 the process variable shows a lower initial variability and a faster response, with registered maximum variations lower than 0.1°C compared to the 0.6°C obtained with the CS1. Thus, CS3 allows a better disturbance rejection, but at the expense of energy efficiency, indeed, as observable in Figure 5.18b the reboiler duty exploits a higher variability with the CS3 scheme. In Figure 5.18c are depicted the profiles obtained for methane composition indirect control. As it is possible to observe, with the CS3 it is possible to obtain a profile with a lower initial variability, with a maximum distance from

the target of 0.32% for the CS1 and of 0.15% for the CS3 control strategy. Furthermore, the steady state offset is significantly reduced, a reduction of 78.40% is indeed registered through the employment of the CS3 strategy, which also depicts a higher speed of response, arriving at the new steady states around 40 min earlier.

In the right panel of Figure 5.18 are depicted the results obtained with the conventional process scheme under the imposition of the decreasing inlet ethane composition disturbance. By observing the tray column temperature profile (Figure 5.18d) also in this case the implementation of the CS3 control led to a better disturbance rejection. Indeed, it is possible to observe that the temperature profile obtained with this control structure displays a lower variability and a faster speed of response, confirming also the benefit deriving from the introduction of the approximated ratio flow controller. Nevertheless, by considering the methane composition profiles depicted in Figure 5.18f none of the compared control strategies can meet the requested methane impurity level at the bottom of the demethanizer, reaching a new steady state value of 0.43%, with an offset of 0.57%.

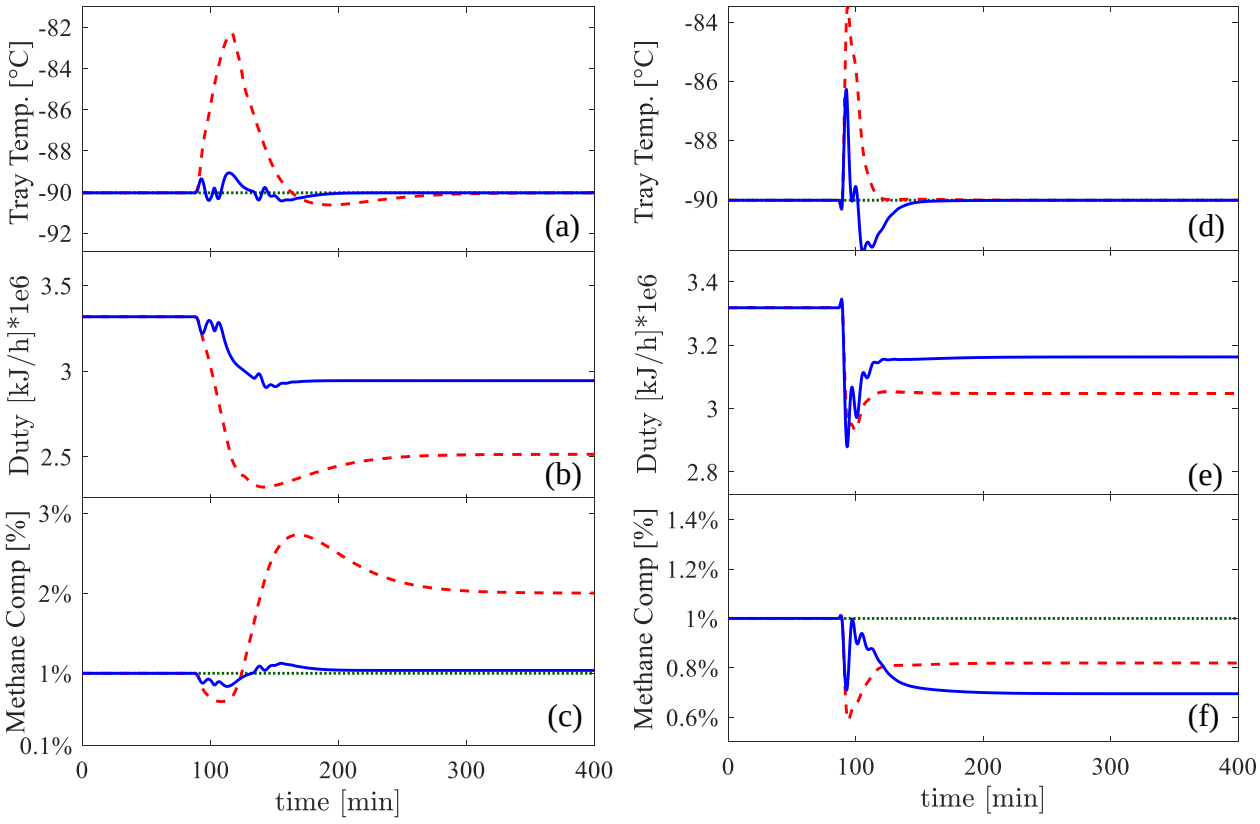

Figure 5.19: Responses obtained for the demethanizer column of the GSP unit by the CS1 scheme (dashed red lines) and the CS3 scheme (continuous blue lines) for a 10% decrease in the plant feed flowrate (left panel graphs) and for a 40% decrease in the ethane inlet composition to the plant (right panel graphs). The green dotted lines depict the control targets and setpoint values.

The dynamic evolution of the profiles obtained with the GSP separation unit under the considered decreasing inlet feed disturbances is depicted in the left panel of Figure 5.19. As it is possible to observe, the column tray temperature profiles (Figure 5.19a) with the CS3 configuration depict a lower initial variation (1°C compared with around 8°C of CS1) and a faster speed of response, arriving at the new steady state value around 70 min earlier. Figure 5.19b depicts the manipulated variable actions, and here, in contrast to what is observed for the conventional separation scheme, the responses obtained with the CS3 strategy show a lower variability, with a reduction in the new steady state condition of 53.5%. For what concern the results obtained for the methane impurity level indirect control, the correspondent profiles are depicted in Figure 5.19c. Here with CS1, the methane composition profiles depict higher deviations from the targets than what is registered for the conventional process with the same control scheme. With the CS3, the initial deviation from the target as well as the response time is reduced. Moreover, the offsets exhibit a reduction of 96.4%, with a final offset of about 0.04%.

In the right panel of Figure 5.19, the results obtained with the decreasing inlet ethane composition variation for the GSP separation unit are shown. Comparing the profiles obtained for the column tray temperature profiles (Figure 5.19d) with the CS3 the initial deviation from the setpoint value is reduced but a lower speed of response is registered. In Figure 5.19e are depicted the obtained manipulated variables profiles, and here with the CS3 control a lower variability is obtained, with a reduction of 42.7%. Nevertheless, by observing the methane composition profiles (Figure 5.19f) also in this case, none of the compared control strategies can bring back the methane impurity at the target value, with the CS3 structure showing the worse performances: lower speed of response and a higher offset at the new steady state conditions. An offset value of 0.18% is obtained with the CS1 scheme while an offset of 0.3% is obtained with the CS3.

The results obtained for the CRR separation scheme under the decrease of 10% of the plant feed are shown in the left panel of Figure 5.20. By observing the results obtained for the column temperature profiles (Figure 5.20a), accordingly to what was found for the conventional and the GSP recovery schemes, with the CS3 control configuration the initial variation is reduced, with a maximum deviation value of 0.7°C compared to the value of about 4°C obtained with the CS1. By looking at the reboiler duty profiles reported in Figure 5.20b, it is also observable that with the CS3 control, the manipulated variable has a lower variability, with a reduction of 47.7%, allowing the disturbance rejection with a lower power consumption. Nevertheless, also

in this case, even if the controllers bring the controlled variables at the setpoint value, none of the two configurations can keep the methane impurity (Figure 5.20c) at the desired target value. The implementation of the CS3 control strategy results in a lower deviation from the targets and smaller offsets, with a reduction of 91.4% compared to the steady state deviations achieved by CS1. Furthermore, the CS3 led to a faster response of the methane composition arriving at the new steady state conditions about 25 min earlier compared to the CS1.

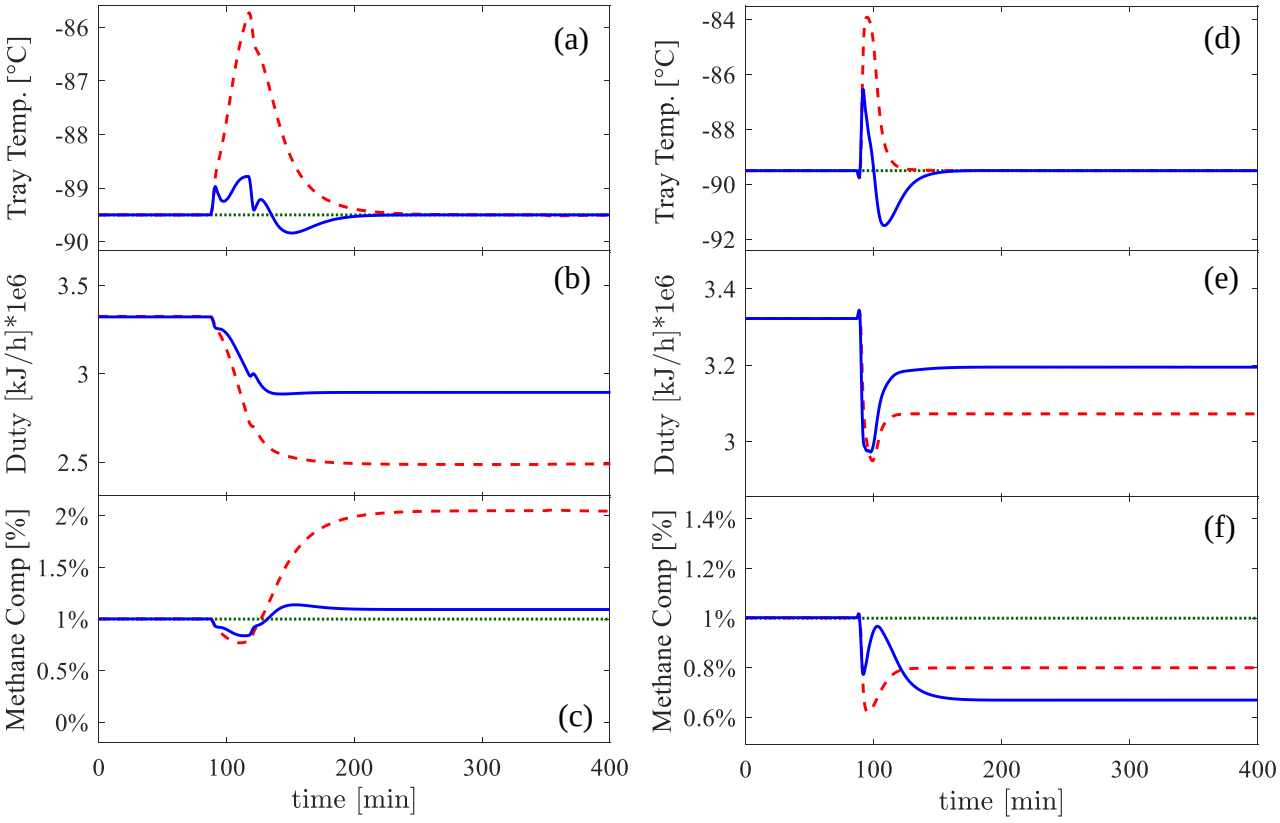

Figure 5.20: Responses obtained for the demethanizer column of the CRR unit by the CS1 scheme (dashed red lines) and the CS3 scheme (continuous blue lines) for a 10% decrease in the plant feed flowrate (left panel graphs) and for a 40% decrease in the ethane inlet composition to the plant (right panel graphs). The green dotted lines depict the control targets and setpoint values.

The results obtained with the CRR for a decreasing variation in the considered composition disturbances are reported in the right panel of Figure 5.20. The obtained results are similar to the ones obtained for the GSP unit under the same disturbances. With the action of the CS3 control the initial deviation of the column tray temperature (Figure 5.20d) is reduced from a value of around 6°C with the CS1 to a value of around 2°C with the CS3, although with this control strategy, a lower speed of response is registered. As well as for the GSP unit the obtained manipulated variable (Figure 5.20e) has a lower variability with a reduction of 48.9% with the CS3. By comparing the effects of the two control structures in the methane composition transient profiles (Figure 5.20f), neither configuration can eliminate the effect of

disturbance on the bottom product methane composition. None of the compared control strategies can meet the methane impurity requirements at the new steady state conditions, with the CS3 structure showing worse control performances.

From the comparison between the responses obtained with the CS3 and the CS1 control schemes for ramp changes in the inlet feed flowrate in all the considered separation schemes, it is possible to conclude that the approximate configuration has the best control performances. As expected, the implementation of the approximated ratio flow controller as a secondary loop in the cascade configuration improves the convergence speed of the control system. Indeed, this controller has the highest convergence velocity, contrary to CS2 whose response speed in the presence of input flow disturbances was lower than that obtained with CS1. By considering the effects of the CS3 control structure, thus the implementation of the PCT control in the flash tank (TK-100) and the cascade control of the demethanizer tray temperature, on the methane composition, the registered offset is drastically reduced but not eliminated, due to the presence of the collateral composition disturbance. Nevertheless, the registered improvements are not observed in presence of composition disturbances, where the offsets obtained with the CS1 control, under the considered inlet ethane variations, are even lower for the GSP and CRR separation schemes. To eliminate the offset still present in the case of input flow disturbances and to improve the control system performances in presence of input composition disturbances, it is, therefore, necessary to have information regarding the composition of methane in the demethanizer bottom product. With this purpose, the effect of introducing a composition analyzer in the plant was considered.

A quantitative comparison of CS1 and CS3 control performances is given by the calculation of the Integral Absolute Error (IAE). The IAE calculated values of controlled and target variables are reported in Table 5.8 and Table 5.9.

Table 5.8: Integral Absolute Error (IAE) obtained for CS1 and CS3 under the considered decreasing variation in the plant inlet flowrate.

		Conventional	**GSP**	**CRR**
Controlled outputs				
Tray Temperature	CS1	26.78	318.64	162.68
	CS3	2.78	30.73	30.11
Methane Concentration	CS1	0.77	3.51	2.86
	CS3	0.22	0.17	0.32

Table 5.8 reports the IAE values obtained with the CS1 and CS2 control structures for the three process schemes, under the decreasing ramp variation in the plant inlet flowrate nominal value. As it is possible to observe the use of the CS3 leads to improved performances in both the controlled variables and methane impurity levels in all the considered separation units. IAE reductions of 71.4%, 95,2% and 88.8% are obtained in the methane concentration respectively for the conventional, the GSP and the CRR units.

Table 5.9: Integral Absolute Error (IAE) obtained for CS1 and CS3 under the considered decreasing variation in the plant inlet ethane composition.

		Conventional	**GSP**	**CRR**
Controlled outputs				
Tray Temperature	CS1	42.03	78.73	75.23
	CS3	16.63	52.19	60.85
Methane Concentration	CS1	1.85	0.63	0.69
	CS3	1.85	0.93	1.01

The IAE results corresponding to the action of CS1 and CS3 under the decreasing variation of the inlet ethane composition are shown in Table 5.9. Here it is possible to observe that, even if the IAE of the controlled variable, the column tray temperature shows enhanced control performances with the CS3, depicting lower values of IAE, the IAE value obtained for methane impurity level shows no variation for the conventional unit and these are higher for GSP and CRR units. Again, the IAE values obtained for methane impurity under the considered composition disturbance remain lower than the ones obtained with the CS1 under feed disturbances, proving that, in any case, the use of CS3 is recommended and generally leads to better control performances.

Three loops cascade control results

As previously stated in the presence of both incoming flowrate disturbances and composition disturbances to eliminate the methane impurity level offset at the new steady state conditions, it is required to have information on the methane composition in the demethanizer bottom product. To test the performances obtained with the introduction of the composition analyser in the plant in this subsection the results of the comparison obtained with CS4 (the three loop cascade control) and CS5 (methane composition controller in cascade with the direct

temperature controller), both using discrete methane composition measurements as the process variable in the composition controllers, will be presented. The results of this comparison for the three considered separation schemes are depicted in Figure 5.21-Figure 5.23 under the imposition of the decreasing variation in the inlet feed and ethane composition disturbances.

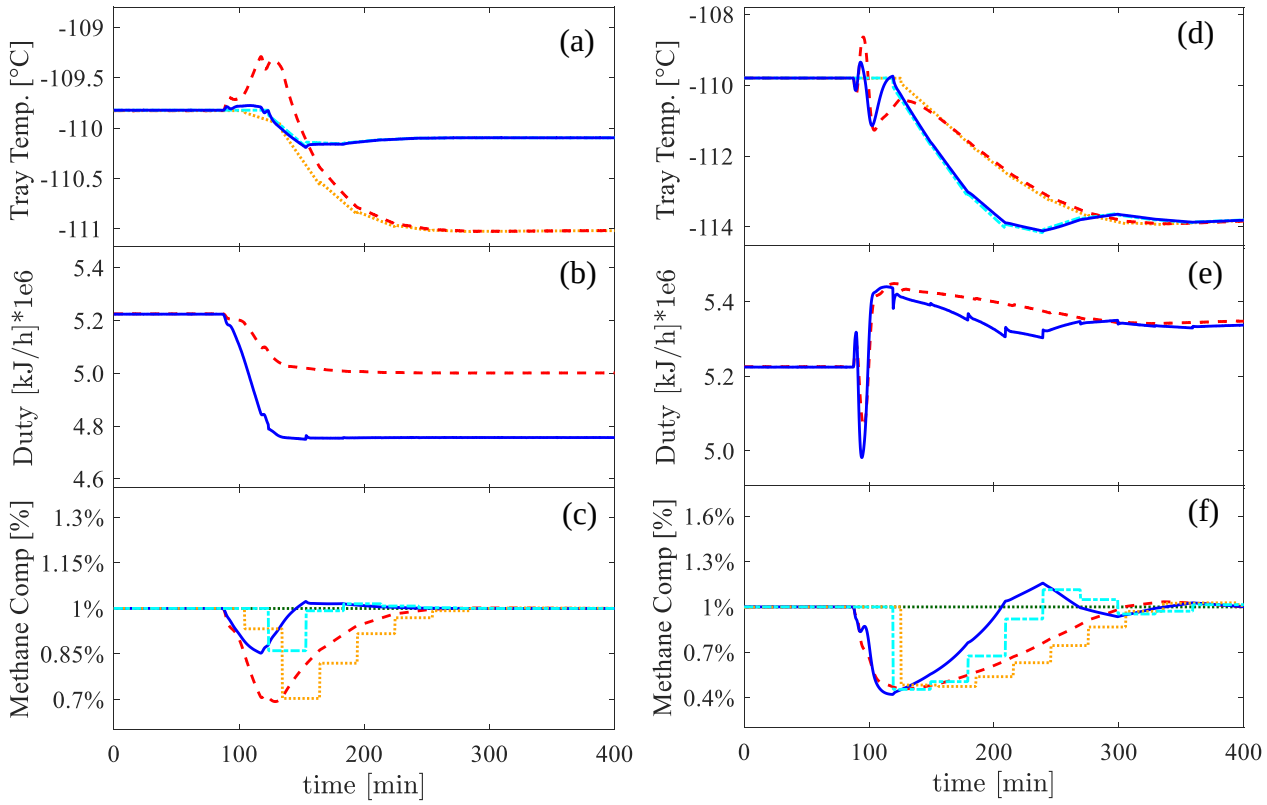

Figure 5.21: Responses obtained for the demethanizer column of the conventional unit by the CS5 scheme (dashed red lines) and the CS4 scheme (continuous blue lines) for a 10% decrease in the plant feed flowrate (left panel graphs) and for a 40% decrease in the ethane inlet composition to the plant (right panel graphs). The green dotted lines depict the control targets. The dash-dotted cyan and the dotted orange lines depict the tray temperature setpoint and the methane composition measurements respectively for the CS4 and CS5 control schemes.

The left panel of Figure 5.21 depicts the trajectories obtained with the CS4 and CS5 control schemes for the conventional recovery unit under the presence of the decreasing variation in the plant feed flowrate. Considering the column tray temperature profiles reported in Figure 5.21a, with the CS4 configuration the temperature can follow the corresponding setpoint without considerable deviations during the transient time, arriving at the new steady state value faster than the profile obtained with the CS5 control, for which a maximum deviation of about 0.5°C is registered. The improvement obtained with the CS4 control is achieved with higher power consumption as it is observable from the comparison of the manipulated variable actions (Figure 5.21b), for which the CS4 strategy led to a higher reboiler duty variability. Considering the responses obtained for the methane concentration, also in this case the CS4 depicts the best control performances, with reduced initial variability and a faster response. However, thanks

to the presence of the methane concentration controllers both the control strategies can meet the target specification in the new steady state conditions but the CS4 control relates to a better disturbance rejection.

The results obtained for the same unit under the decreasing variation of the ethane inlet composition are depicted in the right panel of Figure 5.21. With the use of the CS4 configuration the column tray temperature profile (Figure 5.21d), after 35 min from the application of the disturbance, is perfectly able to follow the related setpoint variable, 30 min earlier than the profile obtained with the CS5, and with a maximum variation registered of 1.2°C. By considering the manipulated variable (Figure 5.21e), with the two control structures, it depicts a comparable action, however, a higher initial deviation is registered with the CS4, which is also associated with lower variability. From the analysis of the profiles obtained for the methane composition (Figure 5.21f), it is possible to observe that with the CS4 control the methane composition depicts an oscillatory behaviour, that leads to a lower transient deviation from the setpoint value. The tuning of the composition controller is therefore more aggressive than the one used in CS5 and would require a detuning for a better control performance comparison.

Under the presence of the decreasing variation in the plant feed flowrate, similar results are obtained from the comparison of the CS4 and CS5 control structures in the GSP and CRR recovery units depicted respectively in the left panels of Figure 5.22 and Figure 5.23. As observed in Figure 5.22a and Figure 5.23a the tray temperature profiles obtained with the CS4 have a lower initial deviation converging in less time to the related setpoint variables, with a maximum deviation of 1°C with the GSP and 0.7°C with the CRR scheme. While the temperature profiles obtained with the CS5 depict a maximum deviation of 7.8°C with the GSP and 5.4°C with the CRR scheme, following the related setpoint variables after respectively 165 min and 175 min. in Figure 5.22b and Figure 5.23b depicts the action of the manipulated variables, which depict a lower variability and thus, a lower power consumption with the CS4 scheme. Further, by considering the profiles obtained for methane concentration (Figure 5.22c and Figure 5.23c) with the CS4 not only it is possible to obtain a faster control speed of response, but the deviation from the setpoint value during the transient is drastically reduced, with a reduction respectively of 88.9% and 77.8% in the maximum deviation obtained with the GSP and CRR schemes.

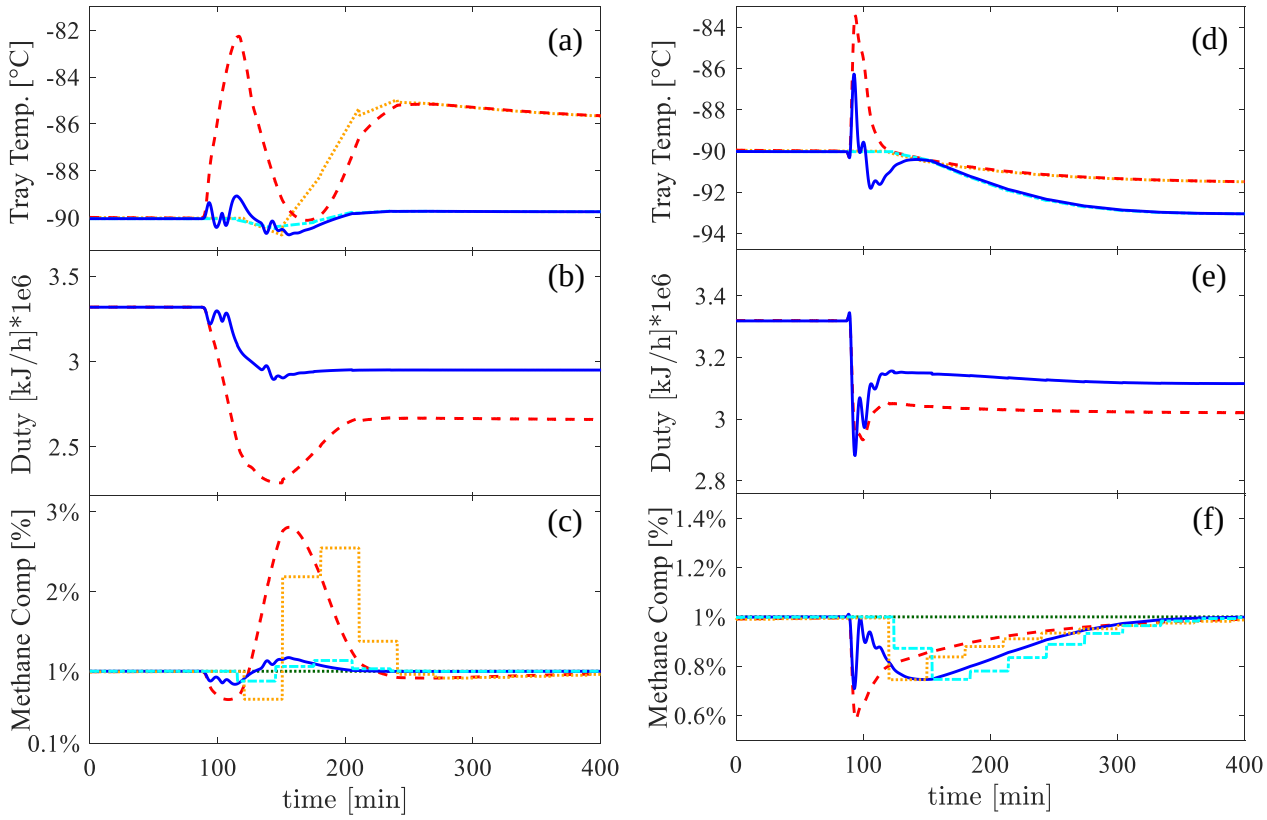

Figure 5.22: Responses obtained for the demethanizer column of the GSP unit by the CS5 scheme (dashed red lines) and the CS4 scheme (continuous blue lines) for a 10% decrease in the plant feed flowrate (left panel graphs) and for a 40% decrease in the ethane inlet composition to the plant (right panel graphs). The green dotted lines depict the control targets. The dash-dotted cyan and the dotted orange lines depict the tray temperature setpoint and the methane composition measurements respectively for the CS4 and CS5 control schemes.

Similar results are also obtained with the GSP and CRR recovery units under the decreasing disturbance of the ethane inlet composition which respectively depicted in the right panels of Figure 5.22 and Figure 5.23. In the tray temperature profile the results, shown in Figure 5.22d and Figure 5.23d, it is possible to observe that also in case of composition disturbances, the initial variation from the setpoint variable is reduced with the CS4 control scheme, although with CS5 the temperature can trace the setpoint earlier in time. Also, with CS4 it is possible to obtain less variability in the action of the manipulated variables (Figure 5.22e and Figure 5.23e). By considering the methane impurity profiles reported in Figure 5.22f and Figure 5.23f, it is possible to observe that the CS5 control depicts a higher initial variation. Regarding the speed of response, the two control schemes are overall comparable, but the one obtained with CS4 appears to be faster, despite what was found in the work of Mandis et al. (2021), where the CS5 control showed a higher speed of convergence. However, the results shown further corroborate the results obtained in the cited work, as the higher response speed obtained with the C5 control was due to the initial error of the composition controller in the CS5

configuration, which led to a more aggressive initial control action. Again, the initial error of the CS5 composition controller is higher, but due to the different sampling position, it is lower than the error reported from Mandis et al., this time allowing observation that CS4 correlates with a higher response speed.

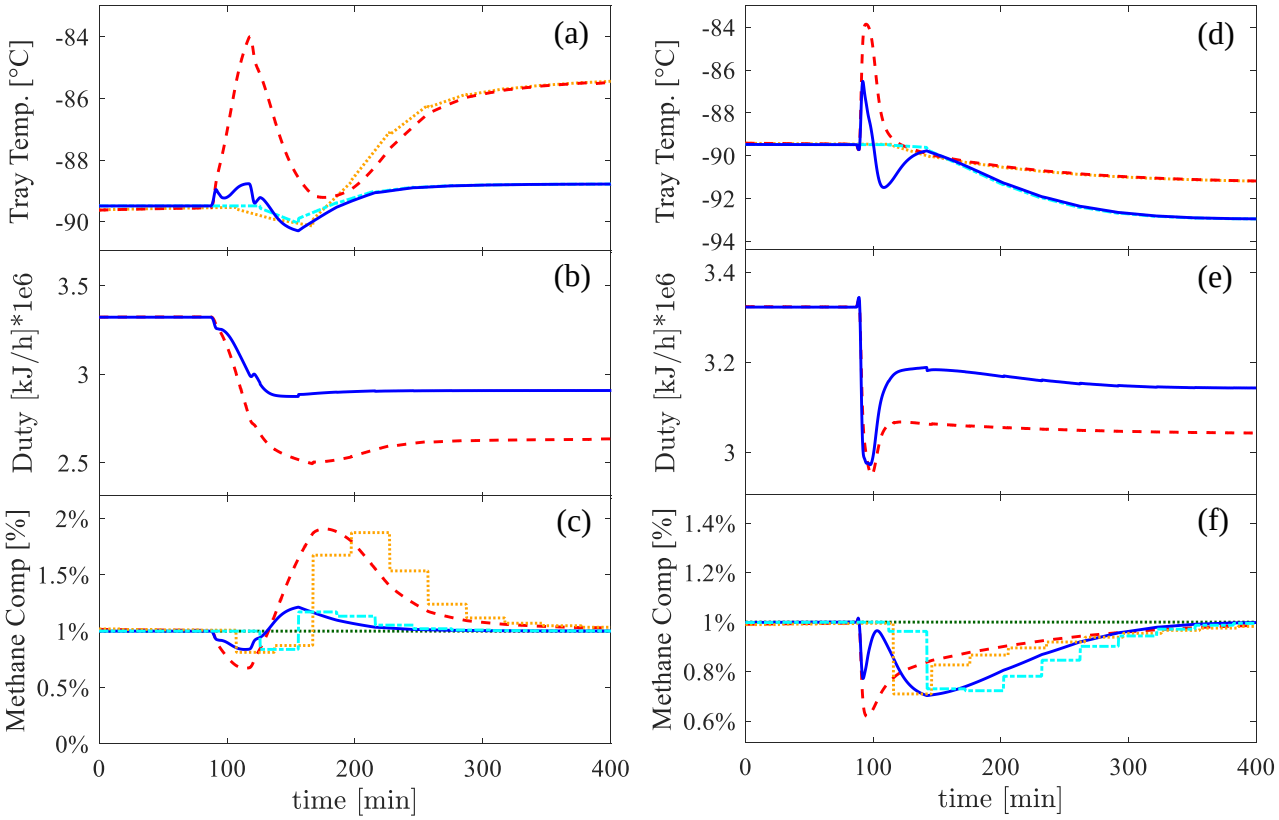

Figure 5.23: Responses obtained for the demethanizer column of the CRR unit by the CS5 scheme (dashed red lines) and the CS4 scheme (continuous blue lines) for a 10% decrease in the plant feed flowrate (left panel graphs) and for a 40% decrease in the ethane inlet composition to the plant (right panel graphs). The green dotted lines depict the control targets. The dash-dotted cyan and the dotted orange lines depict the tray temperature setpoint and the methane composition measurements respectively for the CS4 and CS5 control schemes.

As observed in this section the use of an offline methane concentration controller as a setpoint controller in the cascade temperature controller allows for the elimination of the steady state offsets for all applied disturbances. Additionally, the proposed control scheme demonstrated that CS4 not only provides the best control performance for the composition of interest but also enhances overall column operation in the CRR and GSP separation units, leading to more exergy-efficient disturbance rejection along the column. The superiority of CS4 over CS5 further demonstrates the benefits of introducing enhancements such as control of PCT and the cascade control where the approximated ratio flow controller acted as the slave of the tray temperature controller necessary to assure the required bottom methane composition in case of changes in feed composition.

Also in this case, to have a quantitative measure of the control performances comparison of CS4 and CS5 for conventional, GSP and CRR process schemes the IAE associated with controlled and target variables has been calculated and reported in Table 5.10 and Table 5.11.

Table 5.10: Integral Absolute Error (IAE) obtained for CS4 and CS5 under the considered decreasing variation in the plant inlet flowrate

		Conventional	**GSP**	**CRR**
Controlled outputs				
Tray Temperature	CS5	31.38	373.94	274.96
	CS4	2.43	33.71	33.57
Methane Concentration	CS5	0.20	1.12	0.90
	CS4	0.06	0.11	0.16

Table 5.11: Integral Absolute Error (IAE) obtained for CS4 and CS5 under the considered decreasing variation in the plant inlet ethane composition

		Conventional	**GSP**	**CRR**
Controlled outputs				
Tray Temperature	CS5	50.29	86.84	84.54
	CS4	29.65	58.25	69.08
Methane Concentration	CS5	0.72	0.28	0.30
	CS4	0.49	0.32	0.36

The IAE values reported in Table 5.10 are inherent to the CS4 and CS5 control schemes under the decreasing inlet feed disturbance inlet to the plant for the three considered separation units. As it is possible to observe the use of the CS4 scheme allows for better control performances in the column tray temperature control, and it also improves the methane impurity level indirect control in the three units. Methane composition IAE reduction of 70.0%, 90.2% and 82.2% are obtained with this control structure respectively for the conventional, the GSP and the CRR units. Table 5.11 shows the IAE values obtained under the decreasing variation of the inlet ethane composition for CS4 and CS5. Also, in this case, the implementation of the CS4 control strategy allows better control performances in the controlled variables for all the separation units. For the conventional separation scheme also the methane composition shows better control performances, with a reduction of 31,9%. While higher IAE values are found for this target variable for the GSP and CRR units. Nevertheless, the increase registered is not

excessively large and could be still due to the higher initial error of the methane composition controller registered for the CS5.

5.2.2. Effects of the controlled structures on the separation train

This section is intended to verify the influence of the control strategies developed to optimize the achievement of the demethanizer column production targets on the other distillation column of the train. Considering the results obtained for the quality control of the demethanizer column bottom product, it was chosen to compare the effects of the CS1 and the CS3 control structures in presence of feed flowrate disturbances. With this purpose, the dynamics profiles obtained for impurity composition levels and reboiler duty of the deethanizer, depropanizer and debutanizer columns are evaluated under the presence of the inlet feed disturbances in the NGL recovery plant incorporating a CRR unit.

Deethanizer column results

The composition and the reboiler duty dynamic profiles obtained for the deethanizer column with the conventional and the proposed control structure, in presence of the considered decreasing and increasing variation in the plant feed, are depicted in Figure 5.24.

Here, it is possible to assert that, by increasing and decreasing the plant inlet flowrate with an amplitude of 10%, with the proposed configuration, the propane composition profiles (Figure 5.24a) show a lower initial variation and a higher speed of response. Additionally, for decreasing variation in the feed flowrate, the propane concentration profile exhibits, with the CS1 control, a much higher offset in the new steady state conditions when compared with the CS3. Nevertheless, under the considered increase of the feed flowrate, the propane composition profile obtained with the CS1 depicts a slightly lower offset that can be negligible considering the small entities of the variations. In presence of both the considered plant feed variations, the ethane composition profiles (Figure 5.24b) obtained with the CS3 depicted an improvement in the control performance. Indeed, lower initial variations, higher speed of response and a lower offset at the new steady states are registered with this control structure. Under opposite variations of the same amplitude in the feed flowrate, propane and ethane concentration profiles achieved with CS3 show symmetric behaviors. Thus, with the use of the cascade structure with PCT control, it is possible to obtain more linear behaviors for the deethanizer product targets. Moreover, by considering the action of the reboiler duty (Figure 5.24c) with the CS3 control, it shows a lower variability, with registered reductions of 22% and 28%, respectively under the

decreasing and increasing variation in the inlet feed to the plant. This allows for reaching the product target with lower power consumption.

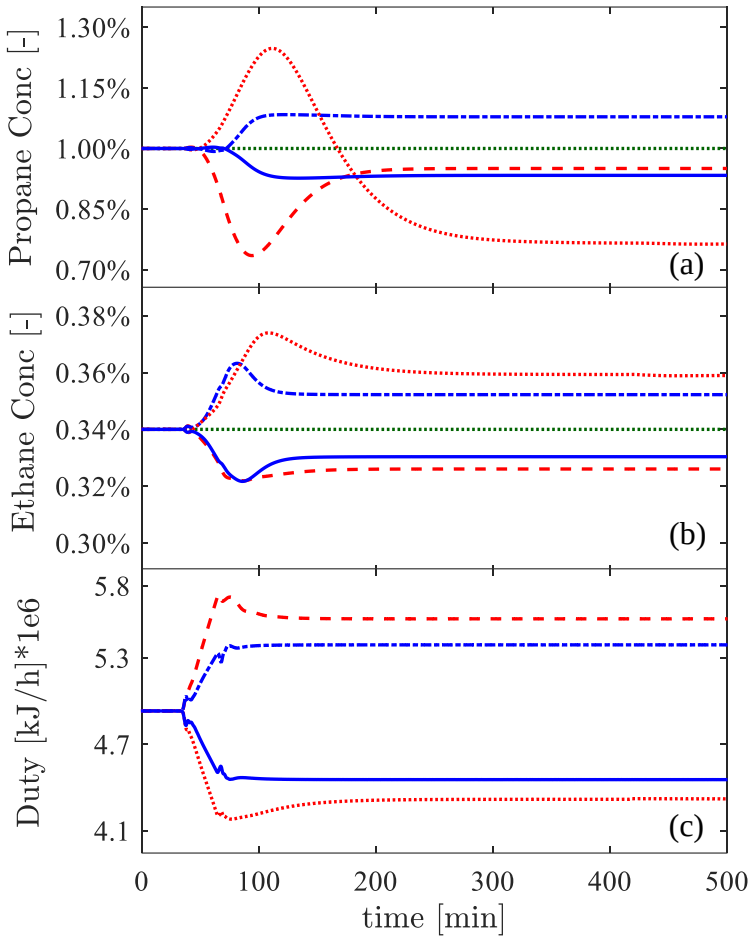

Figure 5.24: Responses obtained with the deethanizer column by the CS1 scheme (red lines) and the CS3 scheme (blue lines) for a 10% increase (dash and dash-dotted lines) and a 10% decrease (continuous lines and dotted) in the plant feed flowrate. The green dotted lines depict the control targets.

Depropanizer column results

The depropanizer dynamic profiles obtained for impurity concentration and reboiler duty with the CS1 and the CS3 control structures under the increasing and decreasing variation of 10% in the inlet feed flowrate to the plant are depicted in Figure 5.25. By looking at the graphs obtained it is possible to assert that the impurity in the top product of the depropanizer (sum of the concentrations of isobutane and n-butane depicted in Figure 5.25a) exhibits different behaviors. The impurity concentration profile shows, with the CS1, a slightly higher initial variation, and a lower offset under the effect of an increase in the feed flowrate to the plant. In contrast, under the worst-case variation, represented by a decrease in the feed flowrate, the top product impurity shows a lower initial variation and a lower offset with the CS3.

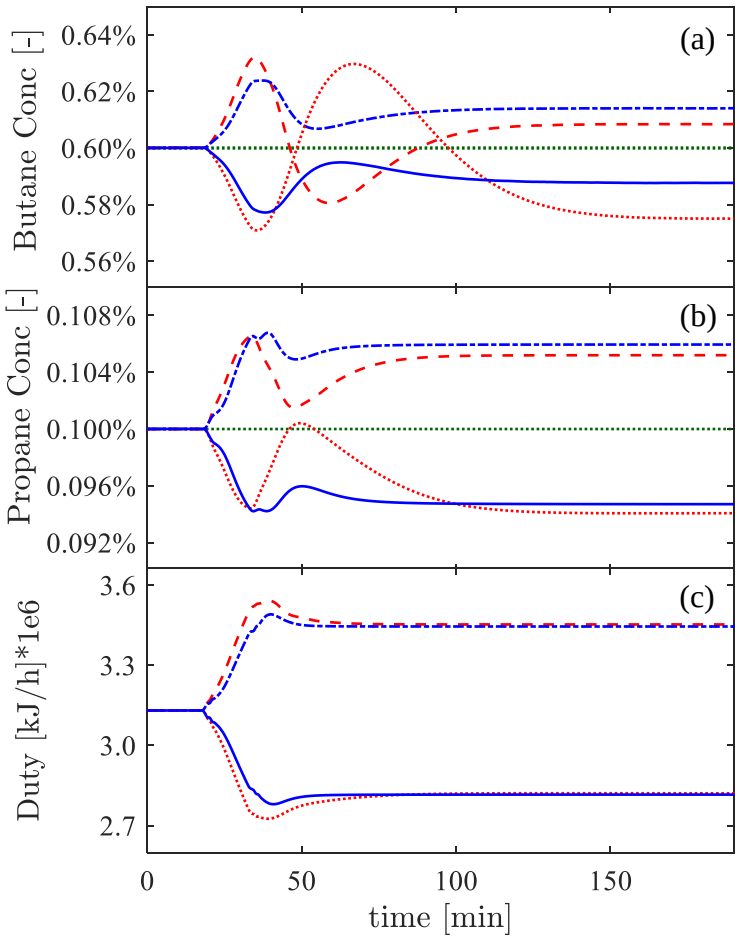

Figure 5.25: Responses obtained with the depropanizer column by the CS1 scheme (red lines) and the CS3 scheme (blue lines) for a 10% increase (dash and dash-dotted lines) and a 10% decrease (continuous lines and dotted) in the plant feed flowrate . The green dotted lines depict the control targets.

Under the effect of both the applied disturbances, the same behaviors are observed for the propane concentration profiles (Figure 5.25c). Nevertheless, for meeting the control objective in the depropanizer outflows top and bottom impurities levels, with the CS3, it is possible to mitigate the effects of the worst variation, the decreasing of the feed flowrate to the plant. Additionally, with the CS3, the impurity concentration profiles in the top and bottom products depict more linear behaviors, in response to opposite variations of the same aptitude in the disturbance applied. Also, with this configuration, the actions of the reboiler duty (Figure 5.25c) show a lower initial variation but in general, the actions obtained with the conventional and proposed control structure are comparable for both the variations applied.

Debutanizer column results

The results of the comparison between the transient profiles, achieved with the CS1 and CS3 control strategies, of bottom and top product quality targets and the action of the reboiler duty,

obtained for the debutanizer column under a 10% increase and decrease in the plant feed flowrate, are depicted in Figure 5.26.

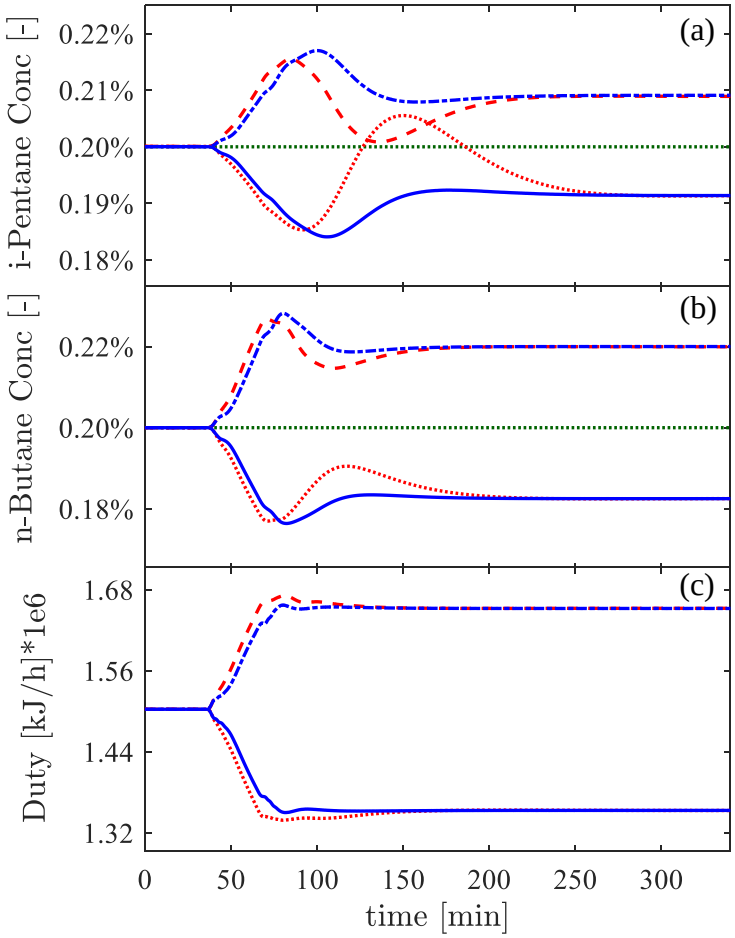

Figure 5.26: Responses obtained with the debutanizer column by the CS1 scheme (red lines) and the CS3 scheme (blue lines) for a 10% increase (dash and dash-dotted lines) and a 10% decrease (continuous lines and dotted) in the plant feed flowrate. The green dotted lines depict the control targets.

By looking at the profiles depicted in Figure 5.26, it is possible to assert that, considering the little composition variations, the iso-pentane impurity level profiles in the top product of the debutanizer (Figure 5.26a) show similar behavior with both control configurations. Nevertheless, with the CS1 the deviation from the target value appears to be lower during the transient. Under the effect of the two disturbances applied, by considering the n-butane profiles (Figure 5.26b) obtained with the CS3, it is possible to observe a lower initial variation and a higher speed of response. By considering the actions of the reboiler duty (Figure 5.26c), using the CS3, depicts a lower initial variation, but also in this case, generally the profiles obtained with the two control structures are comparable under both the considered disturbances.

A qualitative comparison of the influence in the indirect product quality control performances for deethanizer, depropanizer and debutanizer due to the implementation of CS1 and CS3

control for demethanizer column product quality control is given in Table 5.12. Here are reported the IAE values for top and bottom impurity levels of the three columns under the presence of the considered ramp variations in the plant inlet flowrate.

Table 5.12: Integral Absolute Error (IAE) obtained for the deethanizer, depropanizer and debutanizer product quality control with CS1 and CS3 under the considered decreasing and increasing variation in the plant inlet flowrate

			Deethanizer	**Depropanizer**	**Debutanizer**
Controlled outputs					
Top product impurity	Increasing variation	CS1	0.55	0.08	0.07
		CS3	0.64	0.12	0.08
	Decreasing variation	CS1	1.78	0.20	0.07
		CS3	0.54	0.10	0.08
Bottom product impurity	Increasing variation	CS1	0.12	0.04	0.17
		CS3	0.11	0.05	0.17
	Decreasing variation	CS1	0.17	0.05	0.15
		CS3	0.08	0.04	0.15

The IAE results reported in Table 5.12 agree with the qualitative analysis reported in this section. It is possible to observe that the effect of using the CS2 instead of the CS1, for demethanizer quality control, mostly affects the product quality control performances of the deethanizer column. Considering the use of the CS3, in presence of the decreasing variation in the plant feed flow rate, the IAE value related to the top product impurity indirect control (propane concentration in the distillate) is reduced by 69.7%. In the same situation, the IAE value associated with the bottom product impurity indirect control (ethane concentration in the residue) shows a reduction of 52,9%. The improvement was not registered under the increasing variation in the plant feed flow rate: the top product impurity is associated with a minor increase of about 16.4%, while in the bottom product impurity, only a reduction of 8.3% was obtained.

5.3. Conclusion of the Chapter

The control of methane composition and ethane recovery is a critical aspect of the whole NGL recovery process operation, as it impacts the overall efficiency and the performances of the whole separation process since the bottom product of the demethanizer column represents the feed stream to the downstream separation train. For this reason, in this chapter initially, several control strategies were compared with the main objective of achieving the methane composition of 1 mol% while maintaining ethane recovery at 84% in the demethanizer column bottom product. The results obtained showed that indirect composition controllers through temperature controllers were not effective in rejecting the flow and composition disturbances considered as input to the plant. This highlighted the need to design alternative control strategies.

The indirect control of ethane recovery was improved by compensating for pressure variations in the flash tank (TK-100) by controlling the PCT in this unit. This allowed the reduction of ethane recovery offset registered in presence of flow disturbances. The PCT control demonstrated under the same disturbance to have a positive effect also in the indirect control of the methane composition. However, those improvements were not observed under inlet composition disturbances, as the realization of pressure compensation did not consider the plant inlet change in composition, and its influence slows down the action of the direct tray temperature controller. To speed up the action of the column tray temperature controller a cascade control configuration (CS3) was realized. For this purpose, a ratio flow controller was implemented to maintain a constant ratio between a boilup approximation and the column bottom product. The ratio flow controller, manipulating the reboiler duty, acted as a slave for the column tray temperature controller, which was necessary to assure the required bottom methane composition in case of changes in feed composition. The CS3 configuration shows the fastest response and maximum speed of convergence for controlling the tray temperature and methane composition in the demethanizer bottom product. It was shown that this control scheme also improves the overall operation of the column, allowing for better disturbance rejection along the column, and lower power consumption in the CRR and GSP units.

Due to changes in the column inlet composition, the implementation of the ratio controller as a cascaded secondary loop was not able to maintain the methane composition at the target value of 1 mol%. To eliminate the methane composition offset, the use of a methane concentration controller, using offline and delayed composition measurements, as a third control loop in the

cascade control strategy (CS4 control structure) was considered. This allowed for the elimination of methane composition steady state offset for all applied disturbances. The obtained control strategy was effective in controlling the methane composition in the column, while also improving the overall operation of the column in the CRR and GSP units and achieving a faster response and maximum convergence speed.

To examine the impact on the production targets of the deethanizer, depropanizer, and debutanizer columns of the optimized control structure developed for the control of the demethanizer column, the whole NGL separation process, including a CRR unit, was simulated under the effect of plant inlet flow disturbances. With this aim, the effects of the CS1 and CS3 control structures on the separation train have been compared. It was demonstrated that the use of the CS3 control, given by the cascade and PCT control, not only can improve the control performance achieved on the demethanizer column and the corresponding energy consumption but has also positive effects on the rest of the plant. Furthermore, this control strategy proves to be able to guarantee a more linear dynamic behavior of the impurity concentrations, allowing for a more efficient and stable operation of the whole NGL recovery process.

Chapter 6

State estimation

With the perspective of improving the control strategy developed for the achievement of the desired product quality in the demethanizer column of the NGL separation process without the use of online analyzers, artificial neural networks (ANNs) with a data-driven approach have been employed for real-time estimation of critical variables. Due to their simple structure and fast learning rate, feed forward neural networks (FNNs) have been used for the realization of soft sensors for methane concentration, ethane recovery and column boilup flowrate. The performances of the soft sensors developed were evaluated offline and after their implementation in the control strategy.

6.1. Feedforward neural networks

Feedforward neural networks are a type of artificial neural network in which data flows through the network in only one direction. The input is passed through multiple layers of nodes (neurons). Each neuron receives input from the previous layer, performs a computation on it, and then passes the result to the next layer. The computation performed by each neuron is typically a linear combination of its input, followed by a nonlinear activation function. In this way, the network can learn complex relationships between the input and output data. The number of layers and the number of neurons in each layer determine the capacity of the network. The more layers and neurons, the more complex relationships the network can learn. The selection of a proper number of layers and neurons is necessary to avoid overfitting problems. A general scheme of a Feedforward neural network is reported in Figure 6.1.

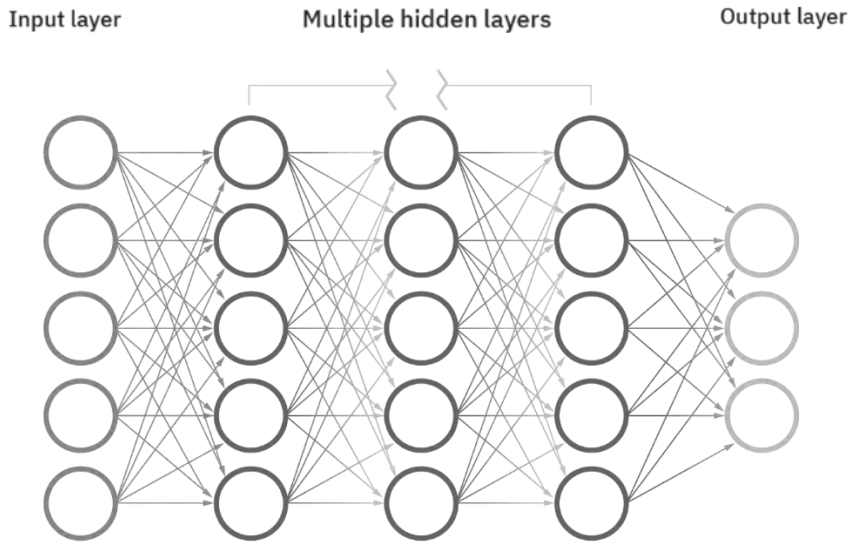

Figure 6.1: Feedforward neural structure. The image is taken from (*What are Neural Networks? - United Kingdom | IBM*, s.d.).

6.2. Development of the FNNs based soft sensor

FNNs have been utilized to develop three different models to infer in real-time boilup, methane concentration and ethane recovery in the demethanizer column. With this purpose the input data for each network was chosen with a knowledge-based approach supported by statistical tools, considering easily measurable variables in real plants that were the most informative and most affecting the target outputs. Table 6.1 shows the input variables selected for the three developed neural models.

The network architecture consisted of only one hidden layer with hyperbolic tangent activation function and a number of hidden neurons selected by considering firstly a model with only one hidden unit and adding one more neuron until a significant change in the model performance had been observed (Spigno & Tronci, 2015; Tronci et al., 2019). An extra neuron was introduced to the input and hidden layers, the bias, which provides a constant output signal equal to one. The selection of the best neural network model has been carried out by utilizing the determination coefficient (R^2) and mean squared error (MSE) as performance indexes. The training script was implemented in the MATLAB® computing environment and updates the weight and bias values according to the Levenberg-Marquardt optimisation available in the Neural Network Toolbox.

Table 6.1: Selected input variables for boilup methane composition and ethane recovery soft sensors

Outputs	Inputs
Boilup	Column (T-100) temperature difference between tray 28 and bottom; column (T-100) bottom temperature; column (T-100) bottom product flowrate and temperature.
Methane composition	Column (T-100) temperature difference between tray 28 and bottom; column (T-100) bottom product flowrate; flash tank (TK-100) temperature and pressure.
Ethane recovery	Column (T-100) temperature difference between tray 28 and bottom; column (T-100) bottom product flowrate; flash tank (TK-100) temperature; flash tank (TK-100) pressure; flash tank (TK-100) liquid product flow and level.

Data collected for training and testing the neural networks have been obtained by varying the feed flowrate and inlet composition in the CRR unit simulated in the process simulator Aspen HYSYS®. To simulate the actual variability of natural gas processed daily, which is due to the variation in the corresponding daily demand, sinusoidal variations of the raw gas inlet to the plant have been considered, with a range of variation between 4500 and 5500 kmol/h. The changes in extraction basin characteristics were mimicked by considering step variations of ethane inlet composition and changing accordingly the inlet methane composition (range of variation for methane: 0.92-0.94; range of variation for ethane: 0.02-0.04%). To obtain a more realistic representation of real plant data, the measured data collected include noise normally

distributed with zero-mean. Standard deviation equal to 20kPA and 0.04 °C has been used for pressure and temperature measurements, respectively. Since dealing with a cryogenic process the standard deviation considered for temperature measurement is chosen considering the use of a high accuracy temperature sensor. Variations of ±1% have been considered for flowrate measurements, ±0.2% for level measurements and ±2% for composition measurements.

6.3. Soft sensors estimation and control performances

The estimation performances of the software sensors realised using FNN are reported and analysed in this section. The developed soft sensors have been implemented in the control structures replacing the actual measurement of column boilup and methane concentration used as process variables. Since the soft sensors developed are implemented in the methane impurity level control structure, and the ethane soft sensor is employed only for monitoring purposes, the results are obtained considering the implementation of the direct control of temperature in the flash tank (TK-100).

Table 6.2: Control structure and data-driven control structure developed for demethanizer bottom product methane impurity level control

		CS1		**CS6**		**CS7**		**CS8**	
Manipulated variables	Chiller heat loss	✓		✓		✓		✓	
	Column reboiler duty		✓		✓		✓		✓
Controlled variables	Flash tank temperature	✓		✓		✓		✓	
	Column tray temperature		✓		✓		✓		✓
	Approximated ratio flow						✓		
	Methane composition						✓		
	Methane soft sensor								✓
	Boilup soft sensor				✓				✓

The control structure considered, which are summarized in Table 6.2, comprehend: (i) the CS1 scheme (direct temperature control in the flash tank (TK-100) and demethanizer column), (ii) two loops cascade with boil-up estimated with the neural network (referred to as CS6), (iii) three loops cascade with delayed methane measurements (referred to as CS7) and (iv) three loops cascade with methane estimated with the neural network (referred to as CS8).

6.3.1. Soft sensors validation

The results obtained in the training and structure optimization of the feedforward neural models for the estimation of boilup, methane and ethane optimization are reported in Table 6.3 along with the statistical performance indexes.

Table 6.3: Soft sensors training and test results

Outputs	Hidden neurons	R2 Train	MSE Train	R2 TEST	MSE TEST
Boilup	6	0.997	3.88E-02	0.990	3.59E-02
Methane conc.	3	0.985	2.55E-07	0.953	1.59E-07
Ethane rec.	3	0.941	1.34E-04	0.807	1.37E-04

To validate the estimation capabilities of the developed soft sensors, they were implemented in the Aspen HYSYS® simulation and compared with the actual values of the target variables by varying the input flowrate with ramp changes of different amplitudes and duration. The results of this comparison are reported in Figure 6.2.

The transient profiles obtained in the validation campaign, reported in Figure 6.2, shows that the software sensors for boilup (Figure 6.2a) and methane composition (Figure 6.2b) can reproduce the trend of the actual variables quite accurately. The two models developed can predict not only the general trend of the profiles over time but also the peaks of variation following the applied inlet flowrate changes. Some inaccuracies still occur, but overall, the models prove to be suitable to be used as boilup and methane soft sensors. Figure 6.2c depict the comparison obtained with the ethane recovery neural model and the actual measurement. Here the soft sensor for ethane recovery shows poorer performance compared to the others, indeed as it is possible to visualize it is not able to detect the peaks but only the average trend.

It is nevertheless useful for monitoring this production index if no other information is available in the plant.

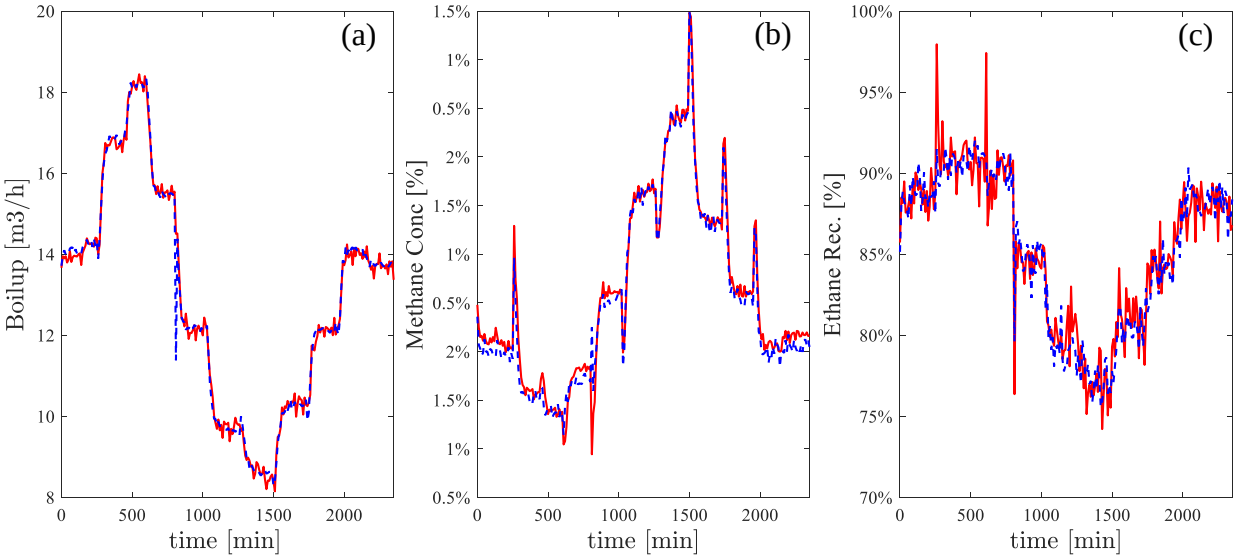

Figure 6.2: Validation campaign results: comparison of actual boilup and boilup soft-sensor measurements (a); comparison of actual methane concentration and methane soft-sensor measurements (b); comparison of actual ethane recovery end ethane recovery soft-sensor measurements (c). The actual profiles are indicated by the continuous red lines, while the estimations are depicted by the dashed blue lines.

6.3.2. Soft sensors control performances

The process conducted in the CRR unit was simulated under feed disturbances considering ramp variations in the inlet flowrate of ±10%. The performances of the data-driven control structures have been evaluated in their ability to keep a methane composition of 1 mol% in the bottom product of the demethanizer column and an ethane recovery of 84% under inlet feed disturbances. The results obtained with the CS6 are compared to the profiles obtained with the CS1 control structure, given by the direct temperature control in the flash tank (TK-100) and the demethanizer column. While the profiles obtained with the CS8 were compared with the ones obtained with the CS7, the three loops cascade with delayed methane measurements. The software sensor developed for the estimation of ethane recovery was implemented in the plant, to further test its performance and as a tool for monitoring production targets. For sake of brevity, only the results obtained in presence of an increase in the plant inlet flowrate are reported and shown in Figure 6.3 and Figure 6.4.

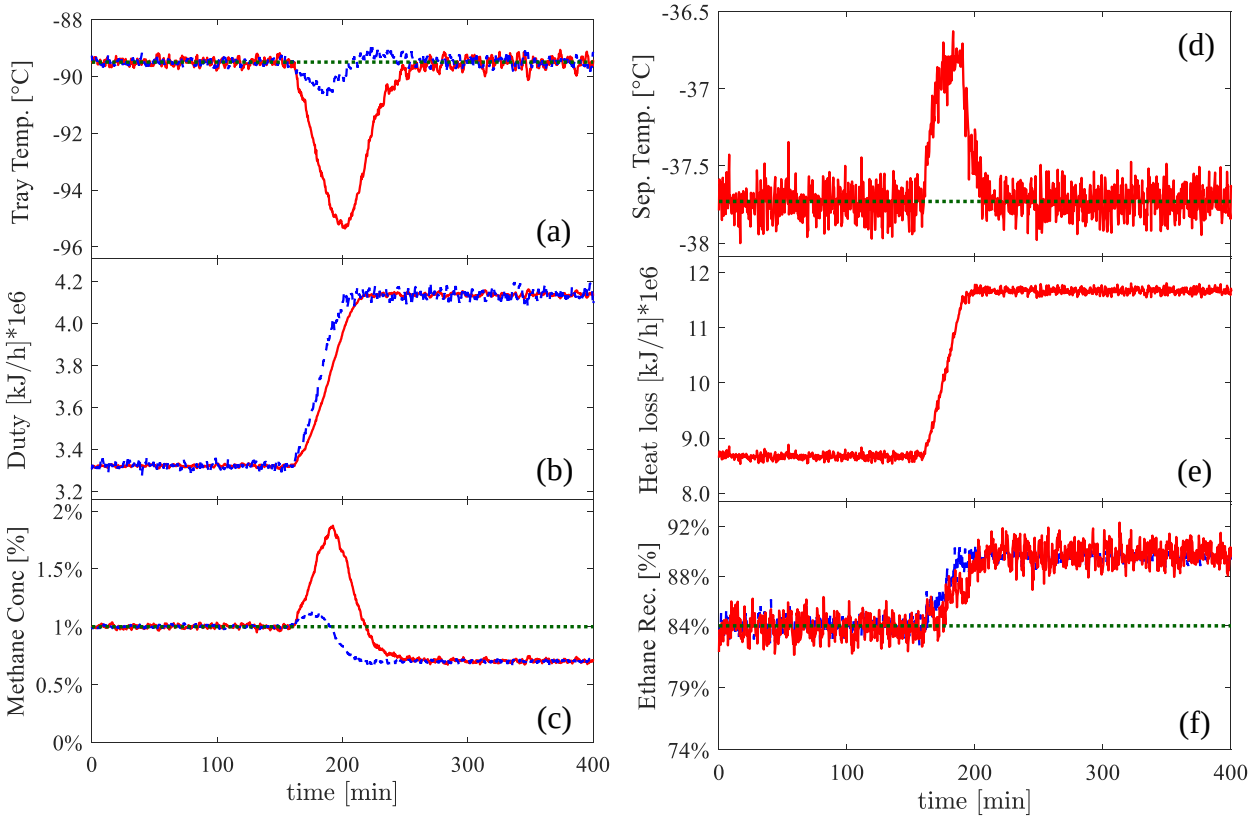

Figure 6.3: Profiles obtained with CS1 (continuous red lines) and CS6 (dashed blue lines) for methane impurity level (on the left panel) and for ethane recovery (right panel) for a 10% increase on the inlet flowrate.

The comparison of the profiles obtained with the CS1 and CS6 control schemes is depicted in Figure 6.3 for a 10% increase in the inlet flowrate to the plant. None of the configurations under consideration involve the use of a composition controller. In this case, only the estimation performance of the soft sensor for the boilup flowrate is analyzed. The left panel depicts the results obtained for the indirect control of the methane impurity while the right panel depicts the profiles obtained in the indirect control of ethane recovery. Considering the temperature profile of the column tray (Figure 6.3a), it is possible to observe that the CS6 control drastically reduces the initial variation compared to the CS1 control. Consequently, the initial deviation of the methane impurity (Figure 6.3c) is considerably reduced. Furthermore, this control strategy allows the achievement of a faster response of the control system arriving at the steady state with the same offset value of 0.3% much earlier than with CS1. The implementation of the soft sensor for ethane recovery (Figure 6.3f), can reduce the impact of noise in the measurement and provide a proper reconstruction of ethane recovery behavior.

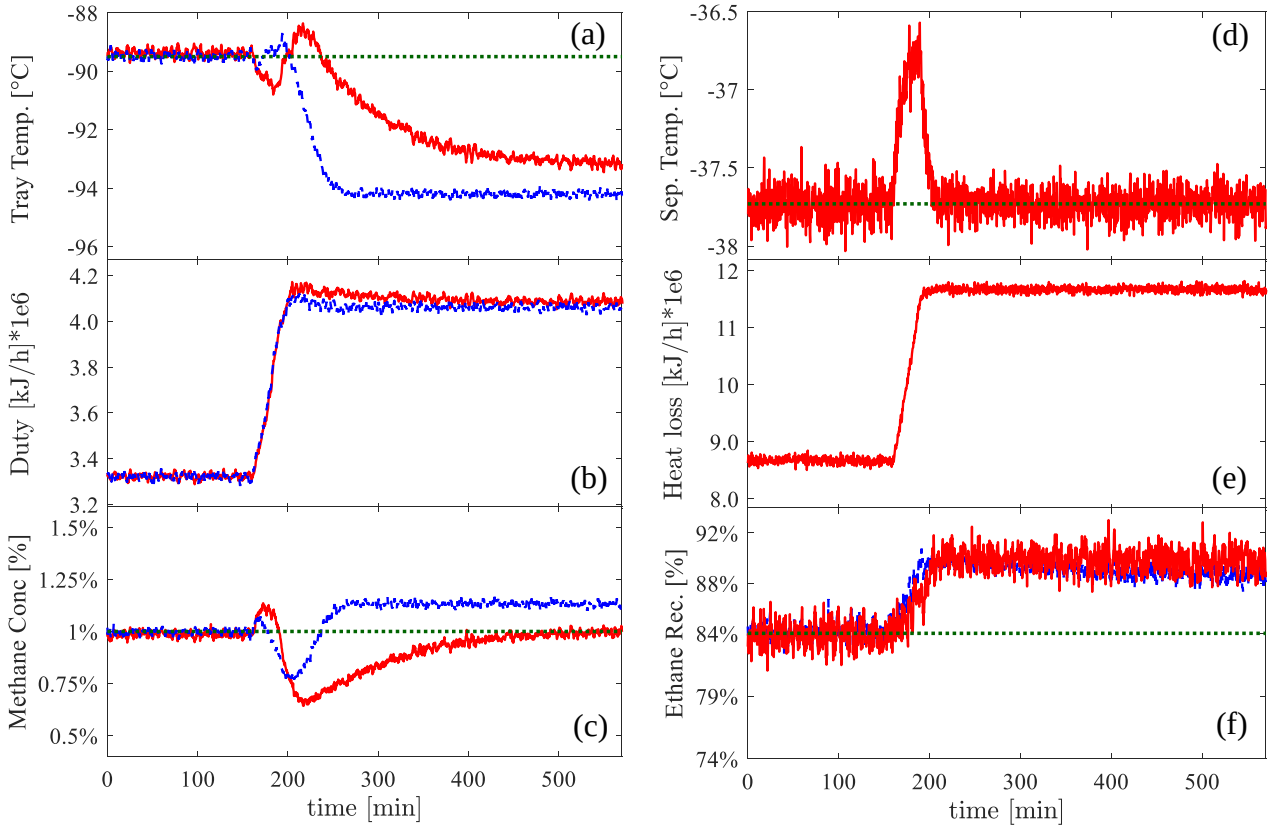

Figure 6.4: Profiles obtained with CS7 (continuous red lines) and CS8 (dashed blue lines) for methane impurity level (on the left panel) and for ethane recovery (right panel) for a 10% increase on the inlet flowrate.

Figure 6.4 depicts the comparison of the profiles obtained with the CS7 and CS8 control schemes in response to a 10% increase in the inlet flowrate. As mentioned in the previous chapter, using the composition analyzer makes only discrete and delayed measurements available. The methane soft sensor is instead used as an online analyzer with the availability therefore of a continuous estimation of the methane concentration to be used as a controlled variable in the composition controller. As a result, the methane composition profiles (Figure 6.4c) with the CS7 control show a higher initial deviation and slower response. With the CS8, thus with estimation available in real-time, the performance of the controlled system shows a smaller initial deviation and a faster response. Nevertheless, due to the estimation error of the soft sensor, the use of the methane soft sensors was not able to eliminate the registered offset at the new steady state conditions. A small offset is indeed still present when using the inferential control. For what concerns the implementation of the soft sensor for ethane recovery (Figure 6.4f) it shows good abilities in filtering the measurement noise and gives an adequate reconstruction of the ethane response.

6.4. Conclusion of the Chapter

In the chapter, the obtained results showed that the developed feedforward soft sensors of the boilup and the methane concentration in the bottom product of the demethanizer column were able to effectively reconstruct the dynamic behavior of the actual variables. The obtained neural models were successfully used as controlled variables in two different control configurations to guarantee the required target for feed flowrate inlet variations. It was shown that as a composition analyzer takes time to perform the analysis, an accurate real-time estimation of such variables can indeed improve control performances by speeding up the action of the controller. The same data-driven approach was also applied to estimate the recovery of ethane recovery obtaining a valuable tool for monitoring the process in real-time when the analyzer has a long delay or is not present. However, the use of these software sensors in the control structure was not able to eliminate the offset obtained under the new steady state conditions. Since estimation errors are bound to exist between the actual value and the soft sensor estimated values, one way to apply a correction is to use both the estimate and the composition measurements, when available, employing filters. For instance, in the study conducted by Randek & Mandenius (2018) various types of Kalman filters were utilized to correct soft sensor errors.

Chapter 7

Digital twin

This section focuses on the formulation and development of a digital twin for a demethanizer column, providing a useful tool for optimization, monitoring and quality control of the NGL recovery process. Deep learning methods for the development of Recurrent neural networks (RNNs) were used to build the demethanizer data-driven model. The choice of working with RNNs is based on the necessity of obtaining an adaptive neural model capable of detecting the temporal dependencies between data.

7.1. Long Short-Term Memory neural networks

Thanks to their ability to detect the time dependencies between input and output data, as well as the fact that they were developed to overcome the vanishing gradient problem, LSTM neural networks were used to obtain real-time estimations more accurately than what is achievable with FNNs. The recurrent structure of an LSTM neural network and the single unit, the LSTMcell, are shown in Figure 7.1.

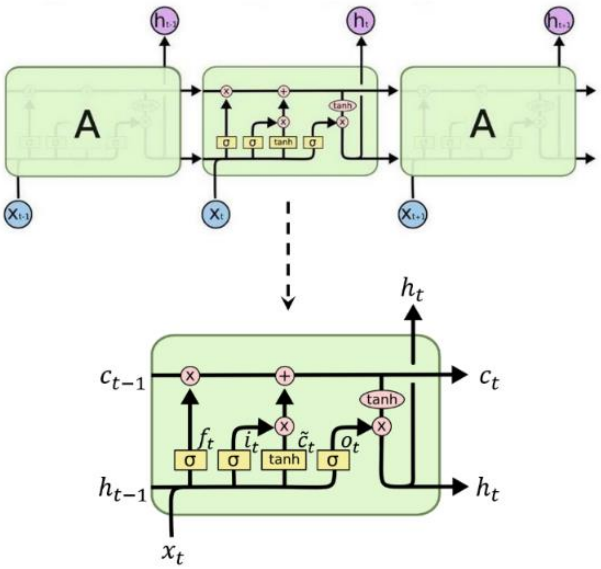

Figure 7.1. Recurrent LSTM network and LSTMcell structure. Image readapted from (*Understanding LSTM Networks -- colah's blog*, s.d.).

The calculation of the outputs, referred to as hidden states, is performed in the single LSTM cell by three gates: the forget gate, the input gate, and the output gate. Those gates determine what information should be remembered by the network and used for hidden state calculation by considering the input information stored in the current internal cell state, which represents the long-term memory of the network, in the hidden state at the previous time and in the input data at the current time. The operation applied by those gates is defined by the relationships reported in Equations 7.1-7.4.

$$f_t = \sigma(W_{if}x_t + b_{if} + W_{hf}h_{t-1} + b_{hf}) \quad 7.1)$$

$$i_t = \sigma(W_{ii}x_t + b_{ii} + W_{hi}h_{t-1} + b_{hi}) \quad 7.2)$$

$$o_t = \sigma(W_{io}x_t + b_{io} + W_{ho}h_{t-1} + b_{ho}) \quad 7.3)$$

$$\tilde{c}_t = tanh(W_{ig}x_t + b_{ig} + W_{hg}h_{t-1} + b_{hg}) \quad 7.4)$$

Where σ and $tanh$ are respectively the sigmoid and hyperbolic tangent activation functions; f_t indicates the forget gate that defines what information in the internal cell state should be forgotten; i_t indicates the input gate that determines what information stored in $\tilde{c}_t$, the new candidate vector for the internal cell states, are worthily memorized; o_t denotes the output gate that determines what information stored in the actual internal cell state should be considered in the currently hidden state calculation; W_{ij} and b_{ij} are the weights and biases related to the current inputs x_t, with j identifying the considered gate, while W_{oj} and b_{oj} are the weights and biases related to the previous hidden states h_{t-1}. The calculations performed by the presented gates to obtain the internal cell state and hidden state in each time instant are expressed by the relations reported in Equations 7.5 and 7.6.

$$c_t = f_t \cdot c_{t-1} + i_t \cdot \tilde{c}_t \qquad 7.5)$$

$$h_t = o_t \cdot tanh\,(c_t) \qquad 7.6)$$

Where c_{t-1} is the internal cell state calculated at the previous time while c_t and h_t are the calculated internal cell states and hidden states at the current time.

7.2. Digital twin structure

To obtain a digital surrogate of the column with shorter calculation times than the simulator, which can be used for both control and optimization of the process, the demethanizer column was modelled by decomposing the problem into three main tasks. The first tasks concern the estimation of the column's top and bottom compositions and the column's internal and external flows. Two different LSTM neural models were designed and developed for this purpose. Subsequently to estimate the internal separation operations in column three different neural model architectures were developed and compared to establish the best structure in terms of estimation performances. These two models were then integrated with the best architecture for the development of the digital column model for the demethanizer column employs only easily and economically available variable measurements as input data, the demethanizer digital twin will be referred to as demethanizer digital twin (DDT). The architectures of the neural models employed for the digital twin realization are described in the following subsections.

7.2.1. Product composition estimation LSTM neural networks

To estimate the demethanizer top and bottom product compositions, LSTM neural networks were employed for the realization of a neural model that will be referred to as NMPC (Neural Model for product composition estimation). The NMPC architecture, which is schematized in Figure 7.2, involves the use of two LSTM cells, each of which is responsible for calculating the compositions in one of the two product streams. The cells used are independent of each other and have as common input data the pressure and temperature of all column feed streams and top and bottom product streams, reboiler duty, power of the cryogenic compressor and flash tank (TK-100) pressure and temperature. The input data selected for each network was chosen with a knowledge-based approach, thus considering the variables mostly correlated with the desired outputs and by considering easily measurable variables in real plants.

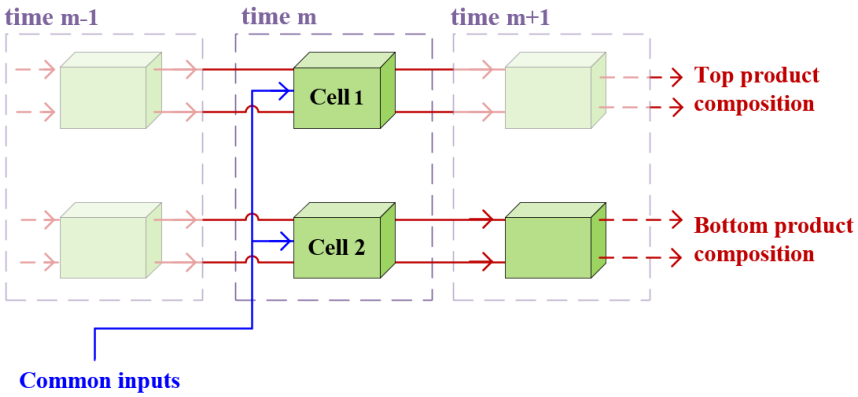

Figure 7.2: Schematic representation of the NMPC recurrent structure.

7.2.2. Column flows LSTM neural networks

To estimate the top and bottom product streams as well as the reflux and the boilup streams, a neural model, referred to as NMCF (Neural Model for Column Flow estimation), was developed. The architecture of the NMCF, schematized in Figure 7.3, involves the use of three interacting LSTM cells. The first cell is responsible for calculating the material balance around the cryogenic compressor, and, as shown in Figure 7.3, has the goal of estimating the reflux stream. The second cell is responsible for calculating the total column material balance and gives as outputs the flows of the top and bottom column products. The third cell is responsible for estimating the material balance around the reboiler and is responsible for the estimation of boilup flow. The input data considered in the model was chosen with a knowledge-based approach and differed from cell to cell. The cells' outputs are also provided as input in the other

cells to simulate the behavior of flows in the column. The first cell receives as input the reflux ratio in addition to the estimation of boilup and distillate. The second cell receives as input the measurement of the input flowrates and reflux and boilup streams estimations. The third cell receives as input column bottom temperature and bottom product temperature and bottom product and reflux streams estimations.

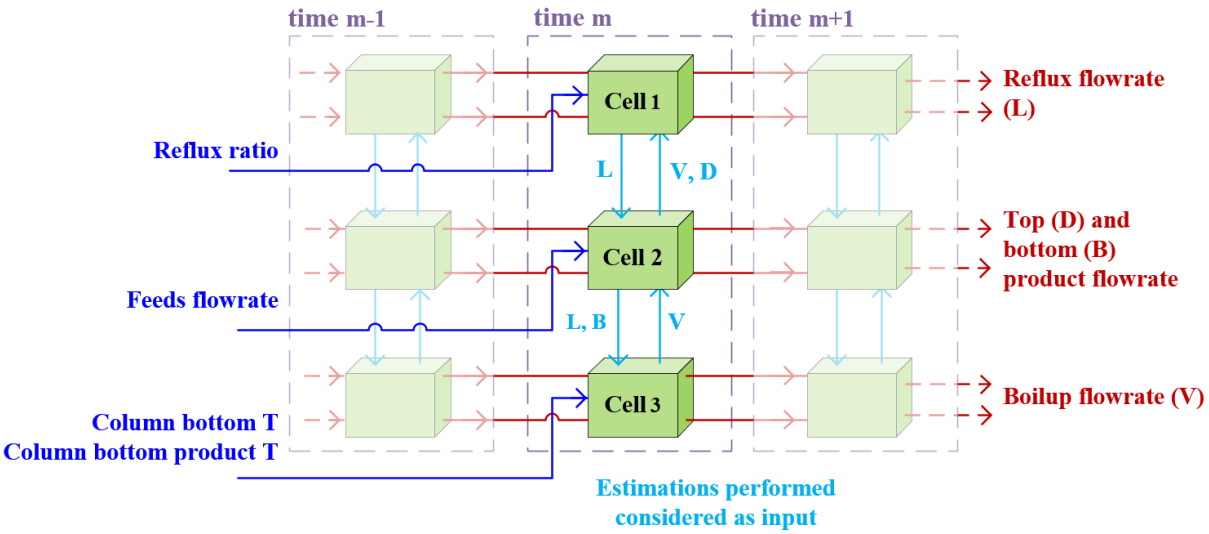

Figure 7.3: Schematic representation of the NMCF recurrent structure.

7.2.3. Column Neural model proposed architectures

Different neural model architectures were developed and compared to achieve accurate estimations for the temperature, pressure and compositions of all column trays and reboiler of the demethanizer column. Those models differ in the way the information is exchanged between the single LSTM units and had the purpose to estimate the separation operation occurring in all trays of the column. Thus, the hidden states calculated by every cell of the networks were the temperature, pressure, and compositions of the corresponding demethanizer tray. These models share a common base layout that involves the utilization of a dedicated LSTM cell to mimic the operations of each stage of the distillation column and the reboiler, allowing the dynamics inherent in the separation process occurring in each column stage to be captured in the model. Also, bidirectional connections have been considered to account for the interactions between adjacent stages, mimicking the action of internal flows within the distillation column. The described layout is the core body of the models, estimating the

demethanizer operation at a certain instant of time and representing the recursive part of the model. As common inputs to every cell of the networks, the following variables were considered: pressure and temperature of all column feed streams, reboiler duty, power of the cryogenic compressor and flash tank (TK-100) pressure and temperature. In the following, the characteristics of the different architectures are presented.

Neural Model 1

The first developed model referred to as neural model 1 (NM1), is designed to obtain a single model capable of detecting and simulating the separation operations occurring in the distillation column. Developing individual neural models for each column stage using a dedicated LSTM network, and from these creating a single model representing the operations of the entire column, the interconnections between the utilized LSTM networks have been modified at the expense of the temporal connection between cells. To better visualize the structure of the resulting model, a schematic representation of the NM1 layout is reported in Figure 7.4 while a schematic of the corresponding inner LSTM cell is depicted in Figure 7.5.

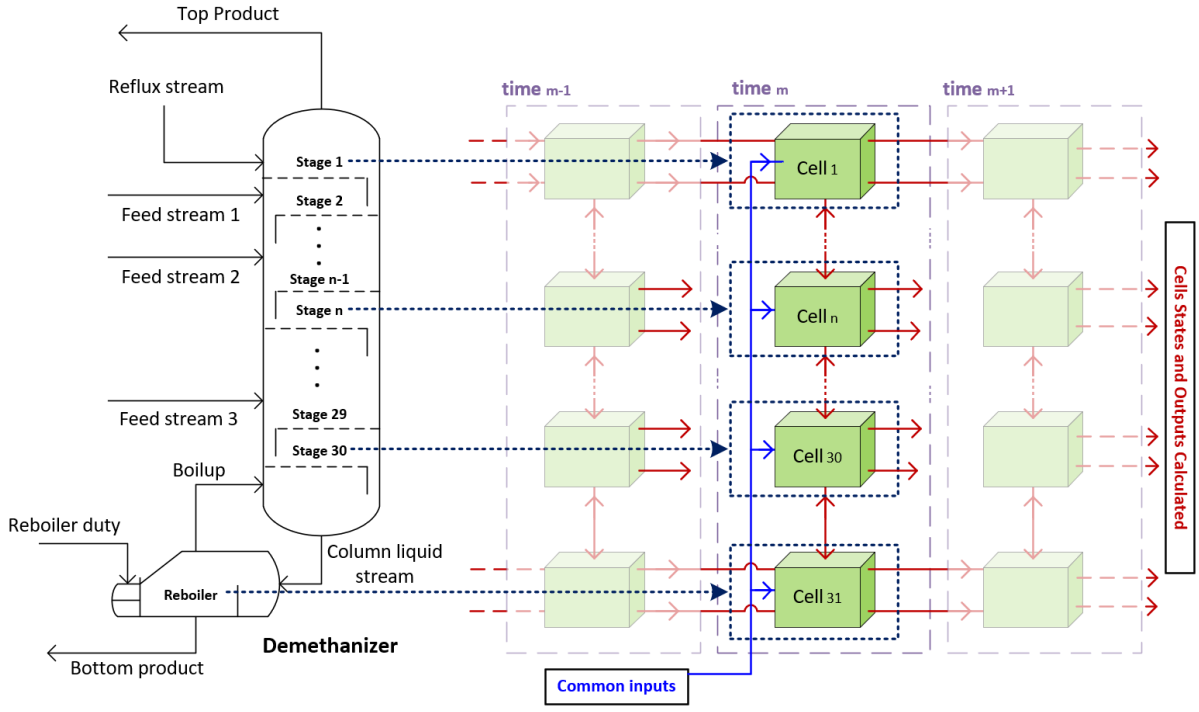

Figure 7.4: Schematic representation of the NM1 recurrent structure.

As can be seen in Figure 7.5, where the considered cell is referred to by the subscript s, the previous states for the cell are given by the hidden states and internal cell states calculated by the adjacent LSTM cells (indicated with subscripts $s-1$ and $s+1$) at the current time. As can

be seen from the layout in Figure 7.4, the usual LSTM time connection is only considered in the terminal LSTM cells of the network. For inner cells, the dependence on the states calculated by the same cell in previous instants is dropped and the only temporal dependencies are given by the information stored in the hidden cell state. Regarding the time-dependent input tensor, this retains the same information for each cell of the network.

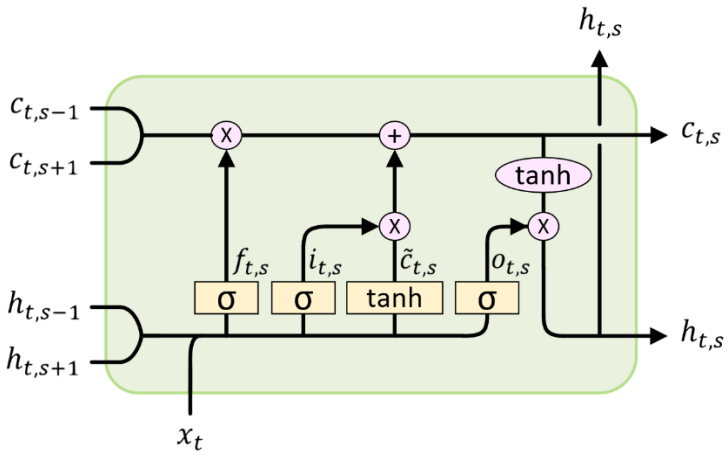

Figure 7.5: Schematic representation of an inner LSTM cell for NM1.

Neural Model 2

The second neural model, referred to as neural model 2 (NM2), has been developed to account for the neglected time dependence in the inner cells of NM1. With this purpose the previous model layout has been modified while maintaining the preexisting connection that mimics the progression of the internal flows in the column. The modification applied are observable in Figure 7.6 and Figure 7.7 where respectively, a schematic representation of the NM2 layout and a specific inner LSTM cell are depicted.

As can be seen in Figure 7.7, in the considered cell (also in this case referred to by the subscript s), the previous states for the cell are provided by combining the actual previous hidden states and internal cell states ($h_{t-1,s}$ and $c_{t-1,s}$) with the hidden states and internal cell states calculated by the adjacent LSTM cells (indicated with subscripts $s-1$ and $s+1$) in the current time. In addition, for the connections of the network terminal cells mimicking the column top tray and the reboiler, the calculated hidden states from the missing adjacent cell ($h_{t,0}$ and $h_{t,32}$) are replaced by the actual measurement of the corresponding variables of the reflux and the liquid stream entering the reboiler respectively for the first and the last cell of the network.

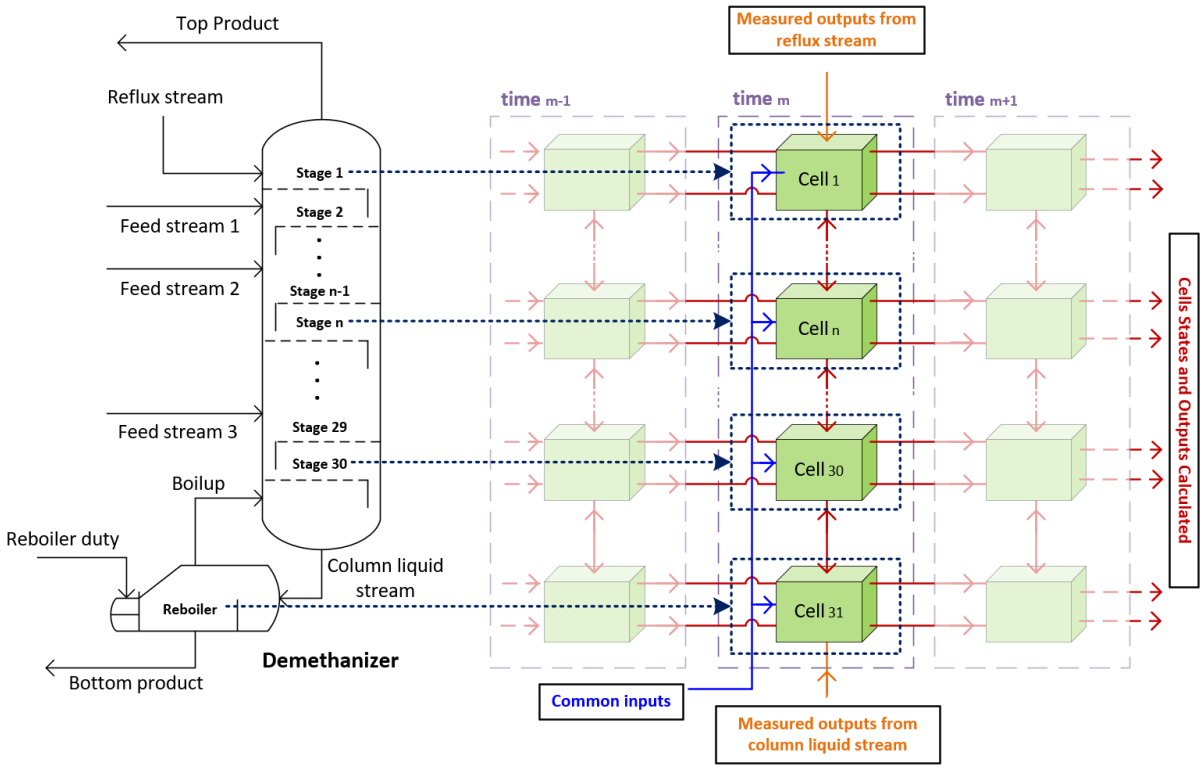

Figure 7.6: Schematic representation of the NM2 recurrent structure.

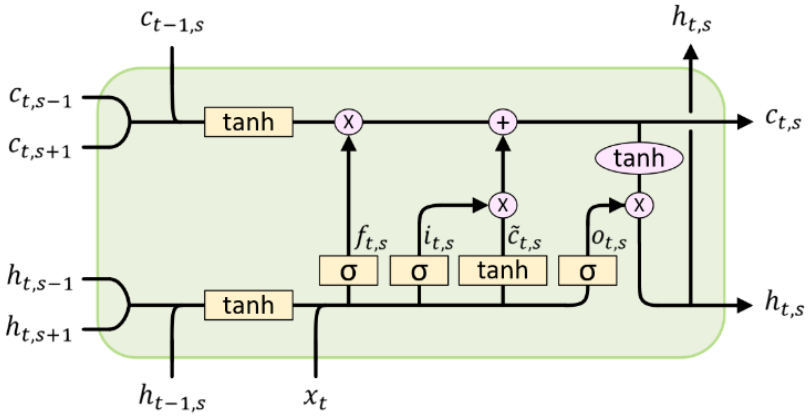

Figure 7.7: Schematic representation of an inner LSTM cell for NM2.

Neural Model 3

The third presented model for the demethanizer column, referred to as neural model 3 (NM3), is a modification of the NM2. In this case, the connection between a cell and the corresponding adjacent cells is realized by providing the calculated hidden states of $cell_{s-1}$ and $cell_{s+1}$ as inputs for the $cell_s$ in addition to the time dependent common input vector. The temporal connection between the cells corresponds to the conventional LSTM cell connection, considering as previous outputs the hidden and internal cell states calculated in the previous instant of time by the same cell. The described cell structure is schematically represented in Figure 7.9, while the

described model layout, responsible to approximate the demethanizer operation at a certain instant of time is depicted in Figure 7.8. In this model, the actual measurement of the corresponding variables of the reflux and the liquid stream entering the reboiler are provided in inputs respectively for the first and the last cell of the network instead of the calculated hidden states from the missing adjacent cell.

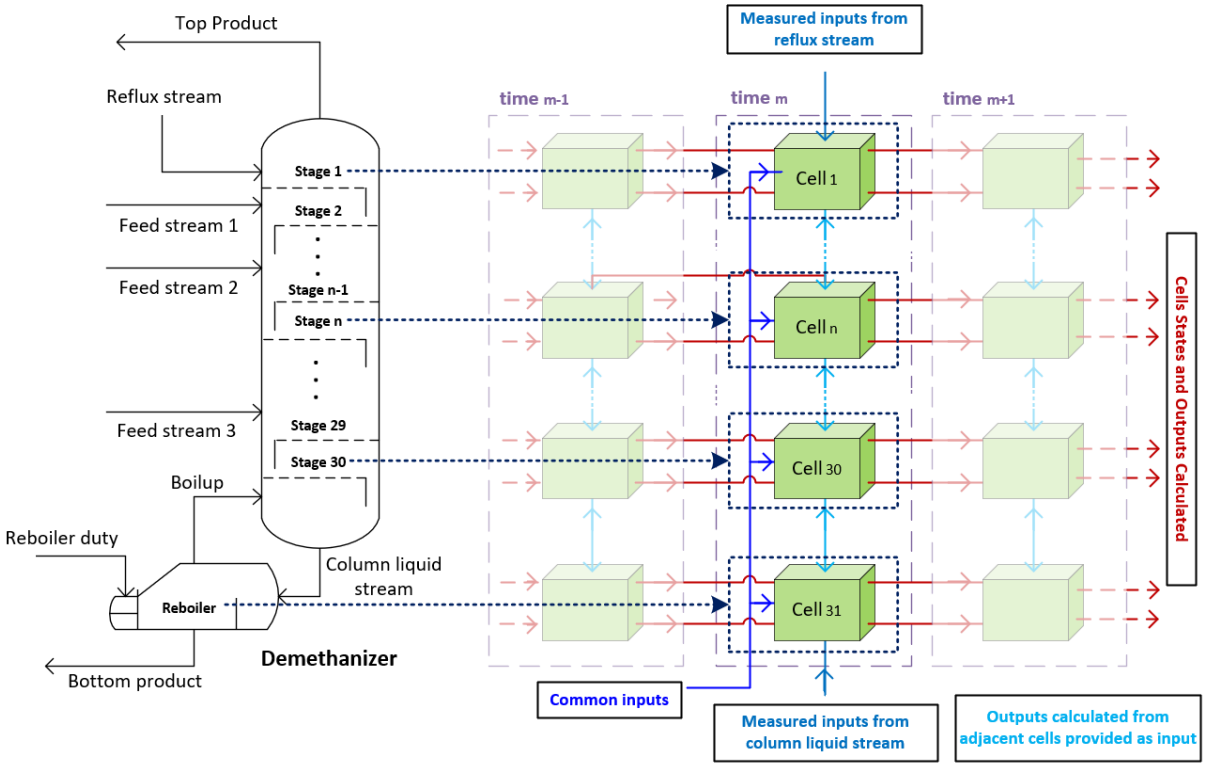

Figure 7.8: Schematic representation of the NM3 recurrent structure.

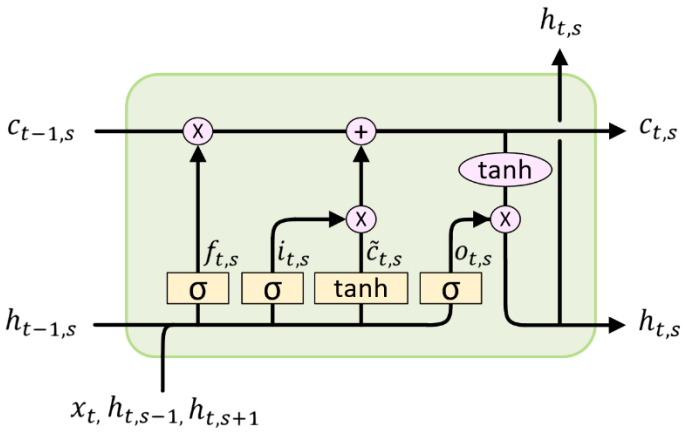

Figure 7.9: Schematic representation of an inner LSTMcell for NM3.

7.3. Neural models development

All the presented neural models have been implemented and trained in the Python programming environment by using the functions available in the open-source library PyTorch (Paszke et al., 2019). The data used for training, testing, and validating the models are described in the following, along with the functions used for training the different models.

7.3.1. Datasets

The datasets employed for training and testing of the developed neural models were simulated by considering two months of plant operation of the CRR separation unit simulated in the process simulator Aspen HYSYS®. To generate these sets of data, ramp changes of varying amplitude and duration in the plant feed flowrate were applied in the process simulator. Those variations were used to emulate the daily demand for natural gas, which exhibits an increasing trend during daylight hours and a decreasing trend during night hours (with variation peaks of 10% of the plant feed nominal value). Of all recorded datasets, 80% were used for network training, while the remaining 20% were used for the testing campaign. To validate the performance of presented neural models, 2 days of plant operation were simulated by applying ramp variations of 5% in the plant feed flowrate nominal value. All the datasets used were registered by considering a sampling time of 20 seconds and without measurement delays, as the data were treated as historical plant data. To provide a more realistic situation measurement noise was applied, using the standard deviations reported in Table 7.1.

Table 7.1: Values of maximum measurement noise considered for input and output data in train, test, and validation datasets

	Duty	**Temperatures**	**Pressures**	**Flows**	**Concentrations**
maximum measurement noise	1.3%*	0.1 [◦C]	1%*	1%*	2%*

** Referred to the maximum value of the considered variable for the given column stage.*

7.3.2. Model Training

The loss function considered in the training optimization problem is given by the Mean Square Error (MSE) defined as reported in Equation 7.7.

$$MSE = \frac{1}{N_b}\sum_{j=1}^{O}\sum_{n=1}^{N}\sum_{m=1}^{M}(\hat{y}_{j,n,m} - y_{j,n,m})^2 \qquad 7.7)$$

where: $N_b$corresponds to the number of observations in the current iteration; O is the number of considered outputs in a given cell, while the general output is denoted by j; N represent the length of the selected time sequence; M is the number of cells employed by the different models;and $\hat{y}$ and y denote a general hidden state calculated by the considered model and the corresponding actual value, respectively.

The loss function is calculated at each iteration in which the Backpropagation through time algorithm is used to calculate the associated gradient with respect to weights and biases. The obtained gradient is then used for the parameter updating performed by the Adaptive Moment Estimation optimizer (ADAM) (Kingma & Ba, 2017). The network hyperparameters were obtained by multiobjective optimization using the NSGA-II algorithm available in the pymoo package (Blank & Deb, 2020). The hyperparameters that were optimized include batch size, which determines the number of time-sequential data series processed by the network in each iteration; sequence length, which corresponds to the length of the time sequence considered and determines the number of cells performing calculations in each iteration; hidden size, which determines the number of cell states considered by the network cells; and learning rate, which determines the step size used by the optimization algorithm in the learning process. The resulting hyperparameters used are shown in Table 7.2.

Table 7.2: Neural Models' optimized hyperparameters

	NMPC	**NMCF**	**NM1**	**NM2**	**NM3**
Batch size	16	5	11	26	17
Sequence length	11	10	12	7	29
Hidden size	18	6	14	15	16
Learning rate	10^{-2}	10^{-2}	$10^{-1,51}$	$10^{-1,54}$	$10^{-1,53}$

7.4. Demethanizer digital twin estimation performances

This section first reports the results obtained in the validation campaign for the NMPC and NMCF models, together with a comparison of the estimation performance of the NM1, NM2 and NM3 models. After that, the results obtained for DDT are compared with those obtained using only the model for estimating the separation operations in the column plates that showed the best performance.

7.4.1. NMPC estimation performances

The results of the control performance achieved in the validation campaign from the NMPC neural model are depicted in Figure 7.10 and Figure 7.11, respectively for the estimation of the distillate composition and bottom product compositions. The results are obtained considering the imposition of inlet feed flowrate variations realized with increasing and decreasing ramp variation with an amplitude of 5% in the CRR process unit.

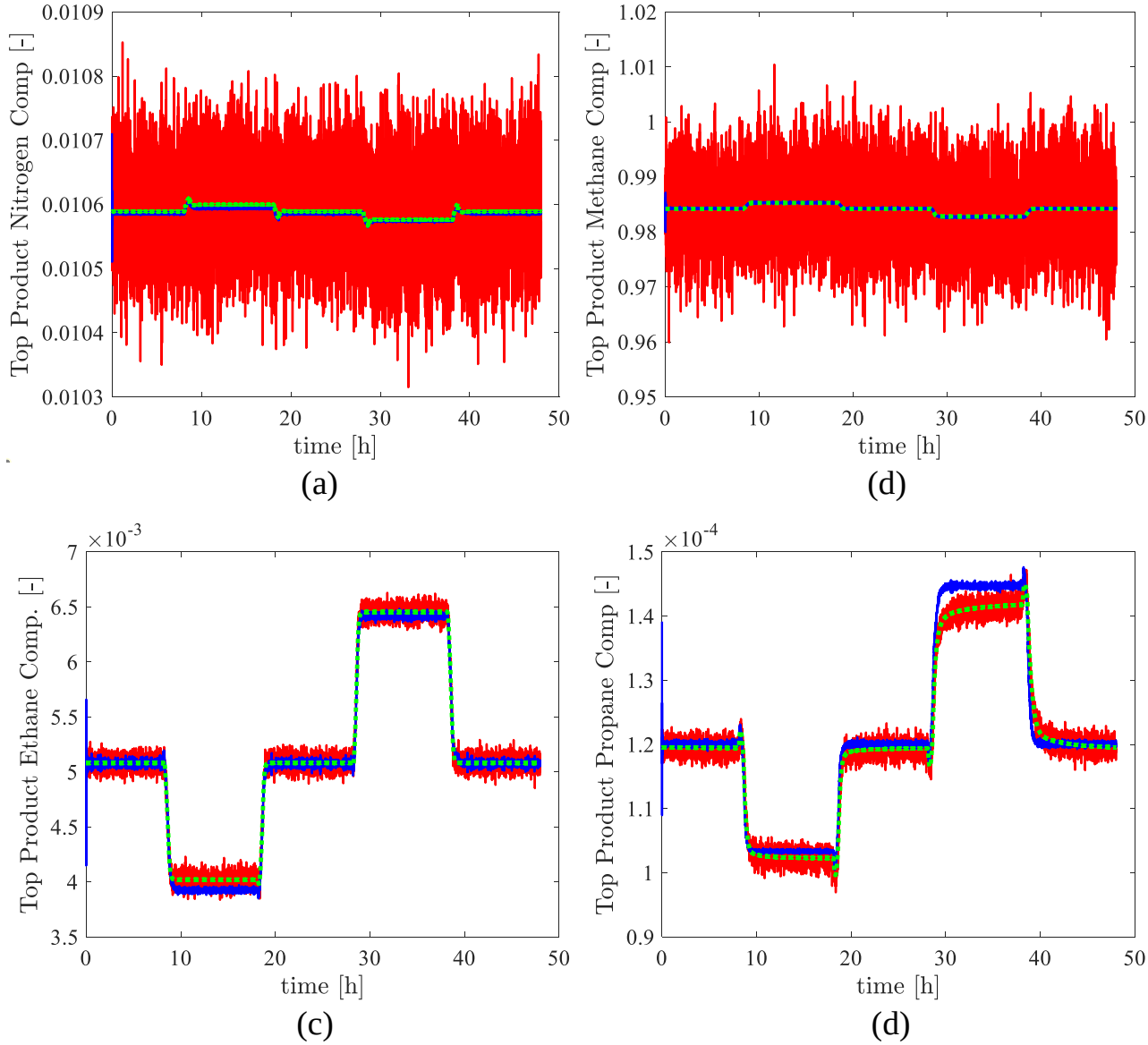

Figure 7.10: Comparison of the estimated transient profiles (blue lines) obtained by for top product compositions with the actual (green lines) and measure profiles (red lines) during the validation campaign.

Figure 7.10a and Figure 7.10b depict the comparison of the measured and the actual profiles respectively of nitrogen and methane composition, with the estimated profiles obtained with

the NMPC. Here it is possible to observe that even though the measurement noise considered is so large, compared to the actual concentration changes, such that the two measured composition profiles appear to be constant, the model can perfectly filter out the considered measurement noise. The obtained estimations accurately approximate the actual transient trend in nitrogen and methane concentrations, as well as the new steady state conditions reached in the column top product. The comparison of the measured, actual and estimated profiles of ethane concentration is depicted in Figure 7.10c. Again, the estimation obtained by the developed model shows good capabilities in filtering the considered measurement noise and the ethane estimate is perfectly capable of reconstructing the transient evolution of ethane in the top product of the demethanizer. Figure 7.10d depicts the validation campaign results obtained for the propane composition in the demethanizer distillate.

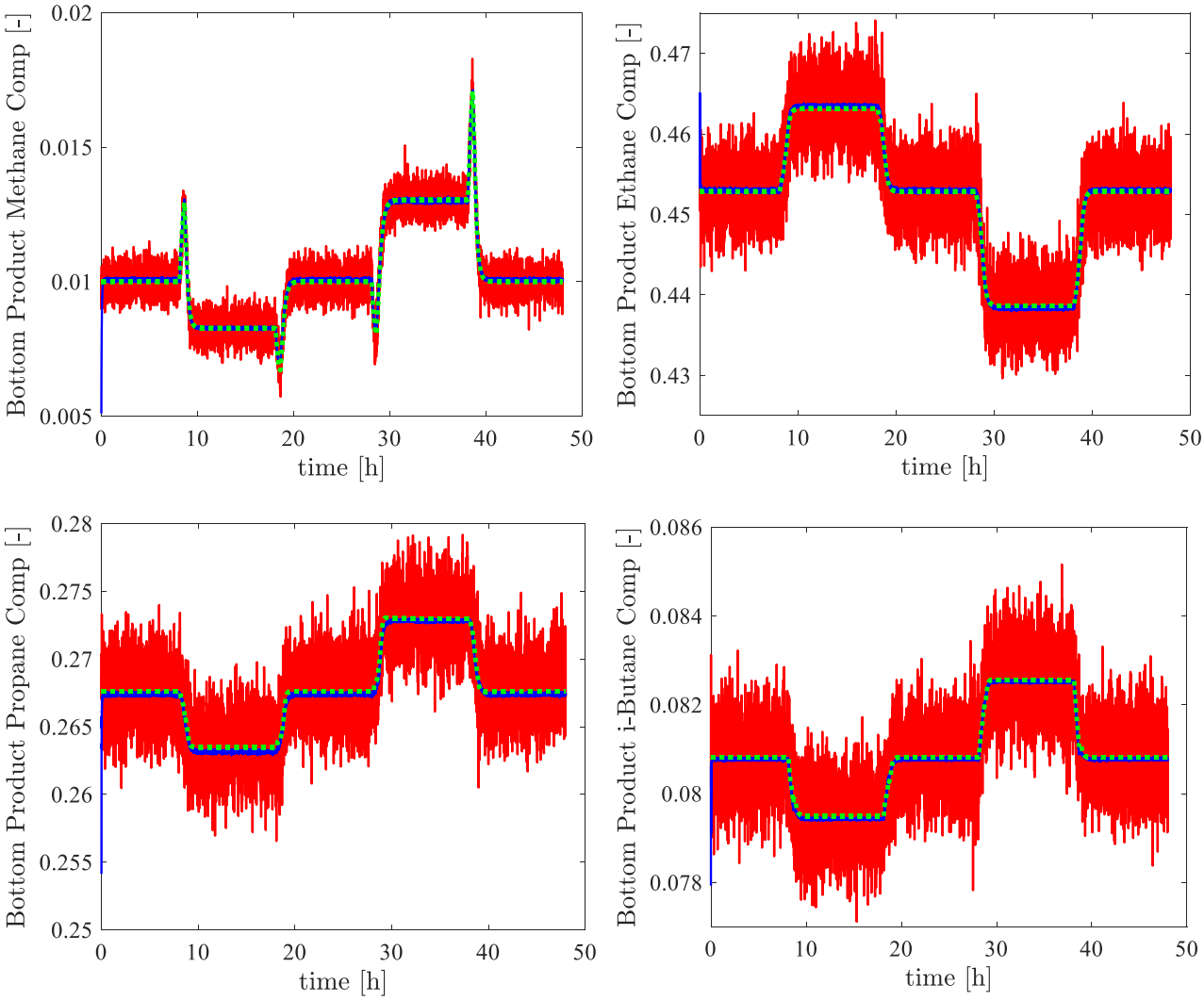

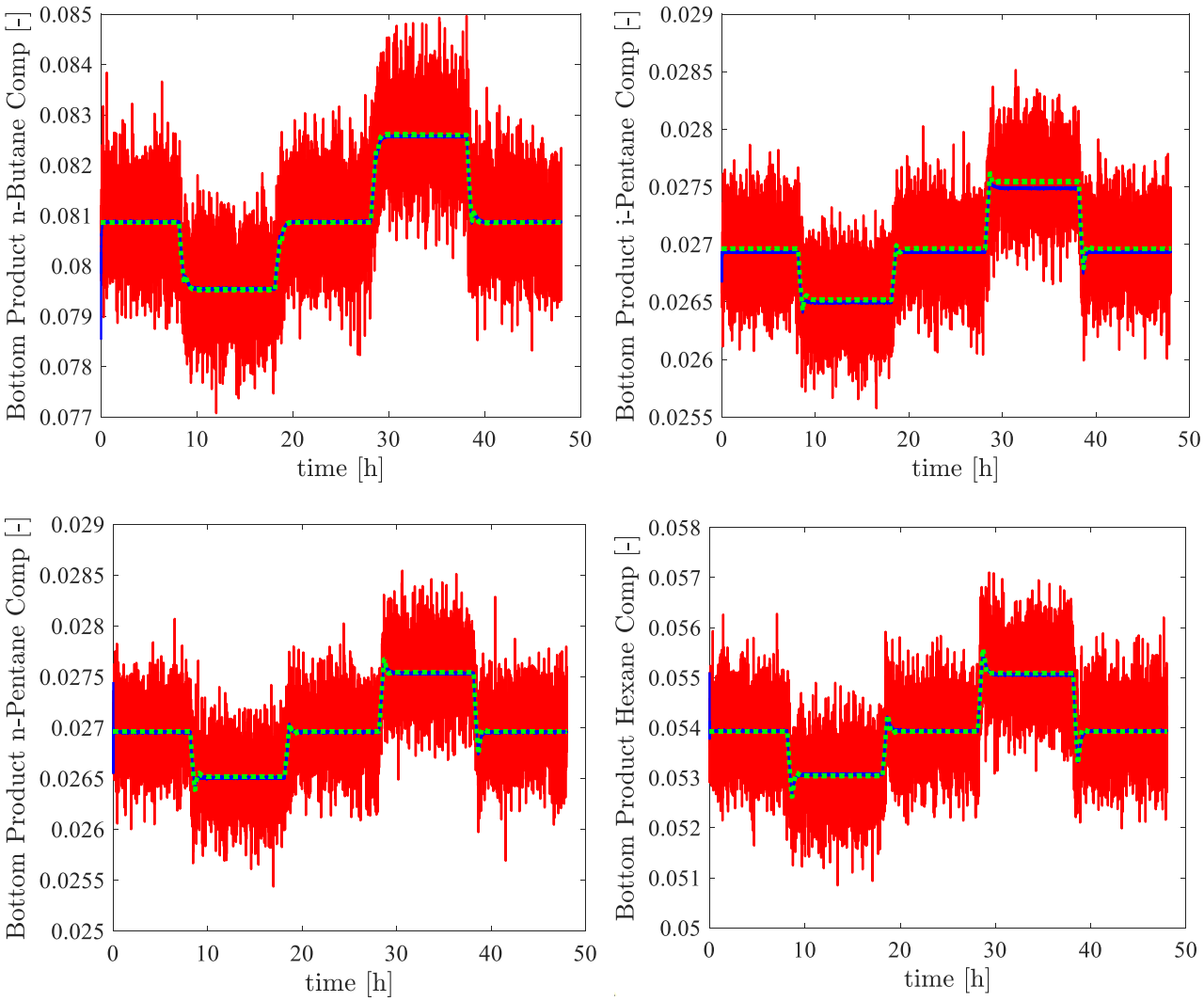

Figure 7.11: Comparison of the estimated transient profiles (blue lines) obtained by for bottom product compositions with the actual (green lines) and measure profiles (red lines) during the validation campaign.

Also in this case, the model manages to filter out the measurement noise, providing a more accurate estimate of the actual profile both in the steady state and in the transient time following the application of the increasing flowrate disturbance to the plant. Nevertheless, we can observe that in the presence of the decreasing flow disturbance, the model failed to properly estimate the composition of the propane with an error higher than the considered measurement noise. The performance of the model in estimating the concentrations in the top product deteriorates as heavier components are considered and thus as the concentrations of the compounds considered in the estimation approach zero.Regarding the estimation results obtained by the model during the validation campaign for the composition estimations in the bottom product of the demethanizer column depicted in Figure 7.11, similar results were obtained. The NMPC model was able to successfully and accurately reconstruct the transient profiles obtained for all

the compositions in the bottom product of the demethanizer column except nitrogen whose presence is, however, negligible.

7.4.2. NMCF estimation performances

The validation campaign results obtained with the NMCF model for the reconstruction of the dynamic profiles of the top and bottom product flowrates as well as the reflux and boilup flowrates are depicted in Figure 7.12.

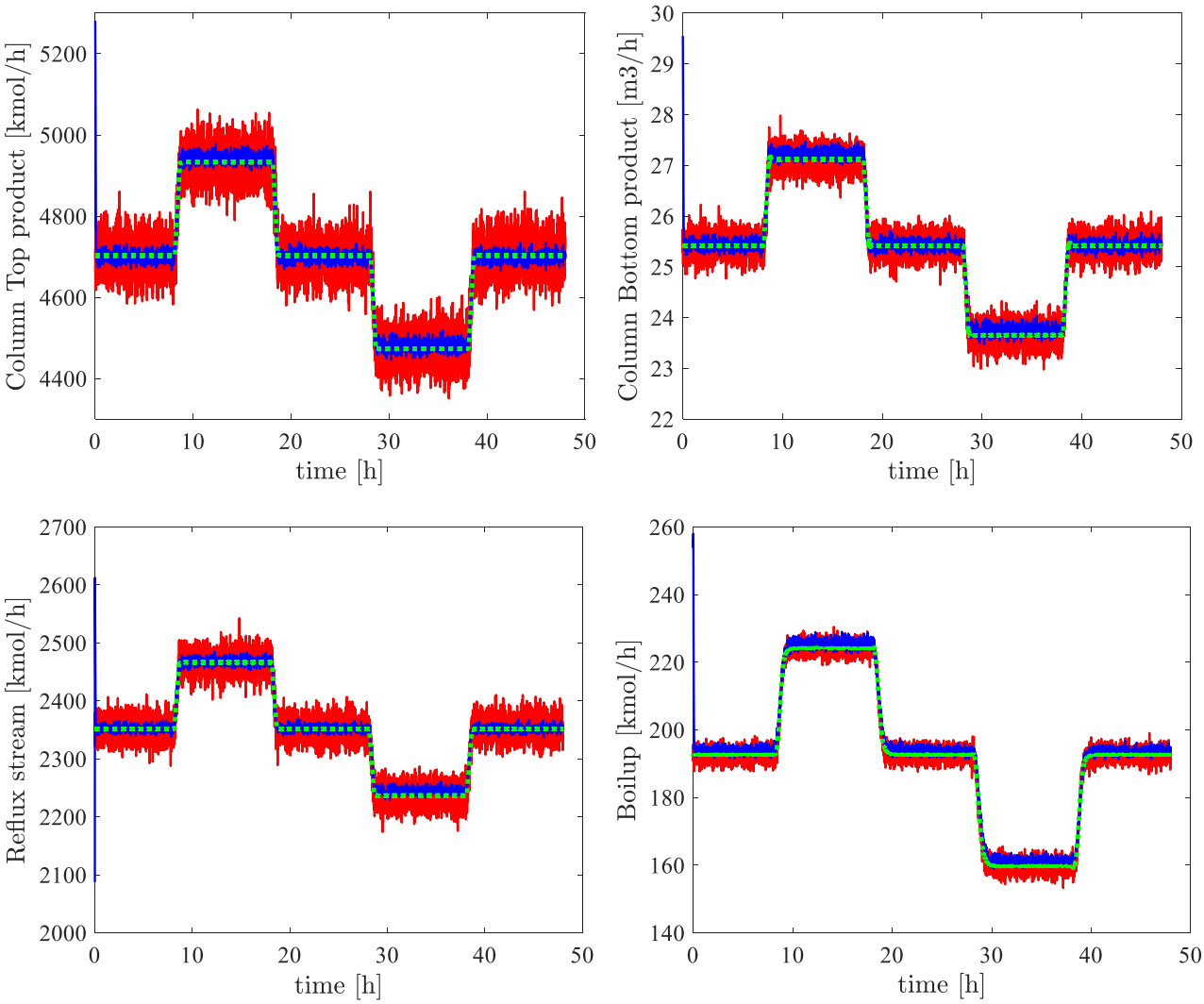

Figure 7.12: Comparison of the estimated transient profiles (blue lines) obtained by for distilate, bottom product, reflux and boilup streams with the actual (green lines) and measure profiles (red lines) during the validation campaign.

The results obtained with this neural model depict similar results to those obtained for the model for the estimation of product compositions. Again, it can be observed that, for all the considered estimation outputs, the model demonstrates good filtering capabilities with

estimated profiles with estimated errors lower than the measurement noise considered. The obtained estimates prove to be very accurate and able to follow the actual output profiles.

7.4.3. Selection of column neural model architecture

The performances of the three models developed to select the best architectures to estimate the column's internal behaviour are evaluated considering the Loss function as well as comparing the temperature and concentration profiles obtained in steady state and during transients for the validation campaign. For the sake of brevity, only the results obtained in the presence of the decreasing flow disturbances are shown.

The values obtained for the Loss functions during training, test, and validation campaign for the considered models, are reported and confronted in Table 7.4.

Table 7.3: Loss function evaluated for the three neural models test and validation campaign

	NM1	**NM2**	**NM3**
Training loss	1.518E-03	1.324E-03	1.368E-03
Test loss	1.636E-03	1.324E-03	1.366E-03
Validation loss	2.273E-03	2.125E-03	2.133E-03

As it is possible to visualize considering the loss function values obtained at the end of the training campaign the NM2 model registers a smaller error, followed by the NM3 model, while the highest value is obtained for NM1. The same results are obtained with the loss function values obtained during the test and validation campaign. This suggests that the changes applied to the NM1 model for maintaining the temporal connection between cells led to an improvement in the column model. Considering that the NM2 show the lowest loss function values in all the campaigns this may be the best model among those proposed to approximate the operations of the demethanizer column.

Model comparison

The ability of NM1, NM2 and NM3 in the reconstruction of temperature and key-component profiles are evaluated under the worst-case variation represented by a decrease in the feed plant nominal value.

The results achieved during the validation campaign are depicted in Figure 7.13-Figure 7.15.

Figure 7.13 illustrates the predicted temperature steady state column profiles, along with the related predicted transient profiles in the trays where the deviation from the true steady state value is maximum.

Considering the column temperature steady state profiles depicted in Figure 7.13a, it is possible to visualize that all three models are generally able to reconstruct the actual column temperature profile. However, in the last two stages of the column, the estimation performed deviates from the trend, with a major deviation registered for NM1.

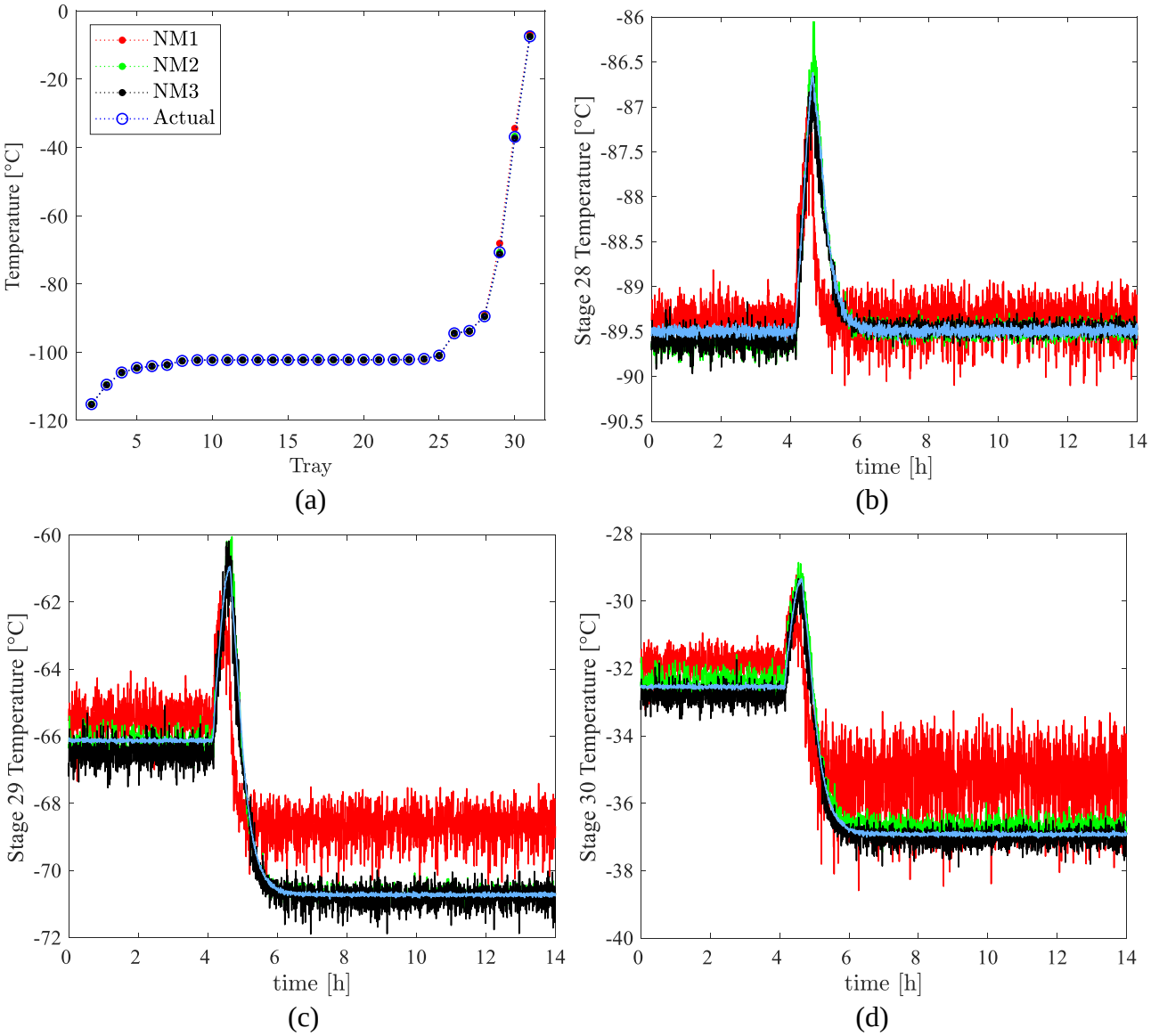

Figure 7.13: Column temperature profiles at the new steady state (a). Transient profiles of 28th stage temperature (b), 29th stage temperature (c), 30th stage temperature (d) obtained in the validation campaign for NM1 (red lines), NM2 (green lines) and NM3 (black lines) under decreasing variation of 5% in the plant feed nominal value.

It is worth noting that most of the column temperature variation is concentrated in the latter three stages of the column, with about 80°C of variation due to the presence of methane in the

gas phase. Furthermore, the temperature in the 28th stage has been controlled, and as a result of these, temperature data are not enough informative to obtain an accurate estimation.

To analyze further the temperature estimation obtained in this column region the time evolution of the temperature in the 28th, 29th and 30th column trays are reported in Figure 7.13b, Figure 7.13c and Figure 7.13d respectively. As it is observed in those Figures none of the presented models can reconstruct the temperature profile in the tray with an error lower than the measurement noise. In particular, the NM1 estimation not only presents a noisier estimation but also deviates from the actual profile with a maximum deviation of around 2 °C in the 28th tray, 5.5°C in the 29th tray and 4 °C in the 30th tray. The deviations registered for NM2 are generally lower than NM3 estimations, except in the 28th tray where the maximum deviation obtained with NM3 is around 0.7 °C while the one obtained with NM2 is around 0.8 °C. Furthermore, the prediction obtained in this region with NM2 always has an error lower than 1°C except in the 29th tray where the maximum error reaches the value of 1.8°C. The prediction error obtained with NM3 exceeds the value of 1°C in the 29th tray with a maximum deviation of 2 °C and in the 30th tray with a maximum deviation of 1.5 °C.

Figure 7.14 illustrates the predicted methane composition steady state column profiles, along with the predicted transient profiles obtained in the trays where the deviation from the true steady state value is maximum. In these trays, the methane fraction is over its critical temperature, thus in the gas phase and due to this fact, the methane gradient in this column region is the highest.

Figure 7.14a depicts the steady state methane composition column profile reached after the imposed disturbance in the plant feed. Here the NM2 and NM3 can reconstruct the profile for all the column trays. Although NM1 succeeds in correctly approximating the measurement of most of the stages, it fails to approximate the methane concentration in the 29th and 30th trays. Indeed, by considering the transient profiles in the 28th tray depicted in Figure 7.14b it is possible to visualize that here all the models well approximate the new steady state values with an error lower than the assumed measurement error, with a resulting estimation noise that is higher for NM1 while it is comparable for the estimations performed by NM2 and NM3. It is also shown that the NM1 estimation deviates from the measured profiles during the transient with a maximum deviation of 0.022. Figure 7.14c and Figure 7.14b depict the methane composition transient profiles respectively in the 29th and 30th trays. Here the predictions obtained with NM2 and NM3 show to be able to predict not only the general trend but also the

transient peaks with comparable estimation noise in the 29th tray and a less noisy estimation with NM2 in the 30th tray. For what concerns the prediction obtained with NM1 it is confirmed that in both the 29th and 30th tray the model fails to reconstruct the time evolution of methane concentration profiles and results in noisier responses compared with the other two models.

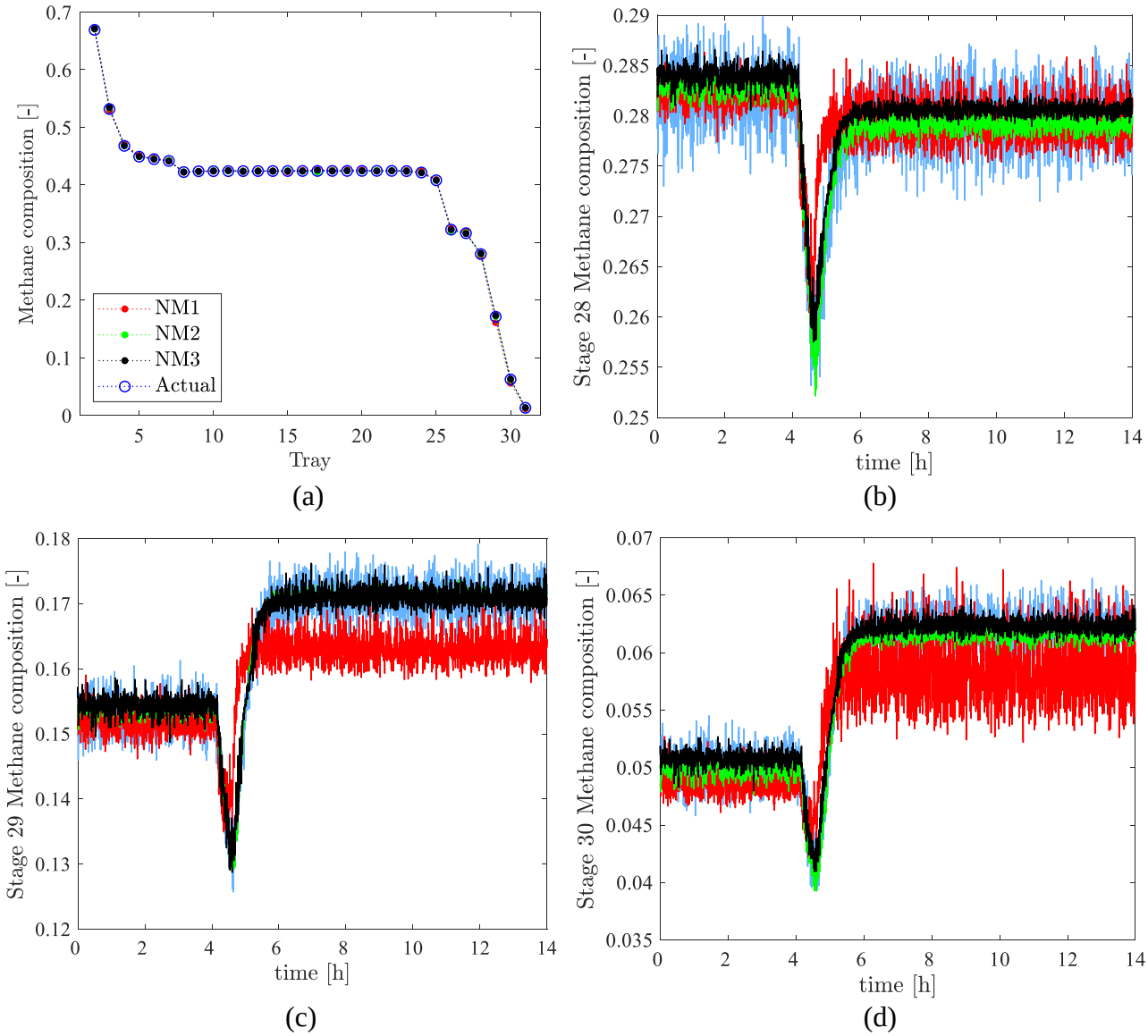

Figure 7.14: Column methane composition profiles at the new steady state (a). Transient methane composition profiles of 28th stage (b), 29th stage (c), 30th stage (d) obtained in the validation campaign for NM1 (red lines), NM2 (green lines) and NM3 (black lines) under decreasing variation of 5% in the plant feed nominal value.

Figure 7.15 shows the results of the estimation performed by the three presented models on ethane composition steady state column profiles, and transient profiles obtained in the trays where the registered deviations from the actual profiles are maximum. As it is possible to visualize in Figure 7.15a, again, models NM2 and NM3 are perfectly able to accurately

reconstruct the column concentration steady state profiles, however, model NM1 shows to provide a poorer prediction in the 29th and 30th trays.

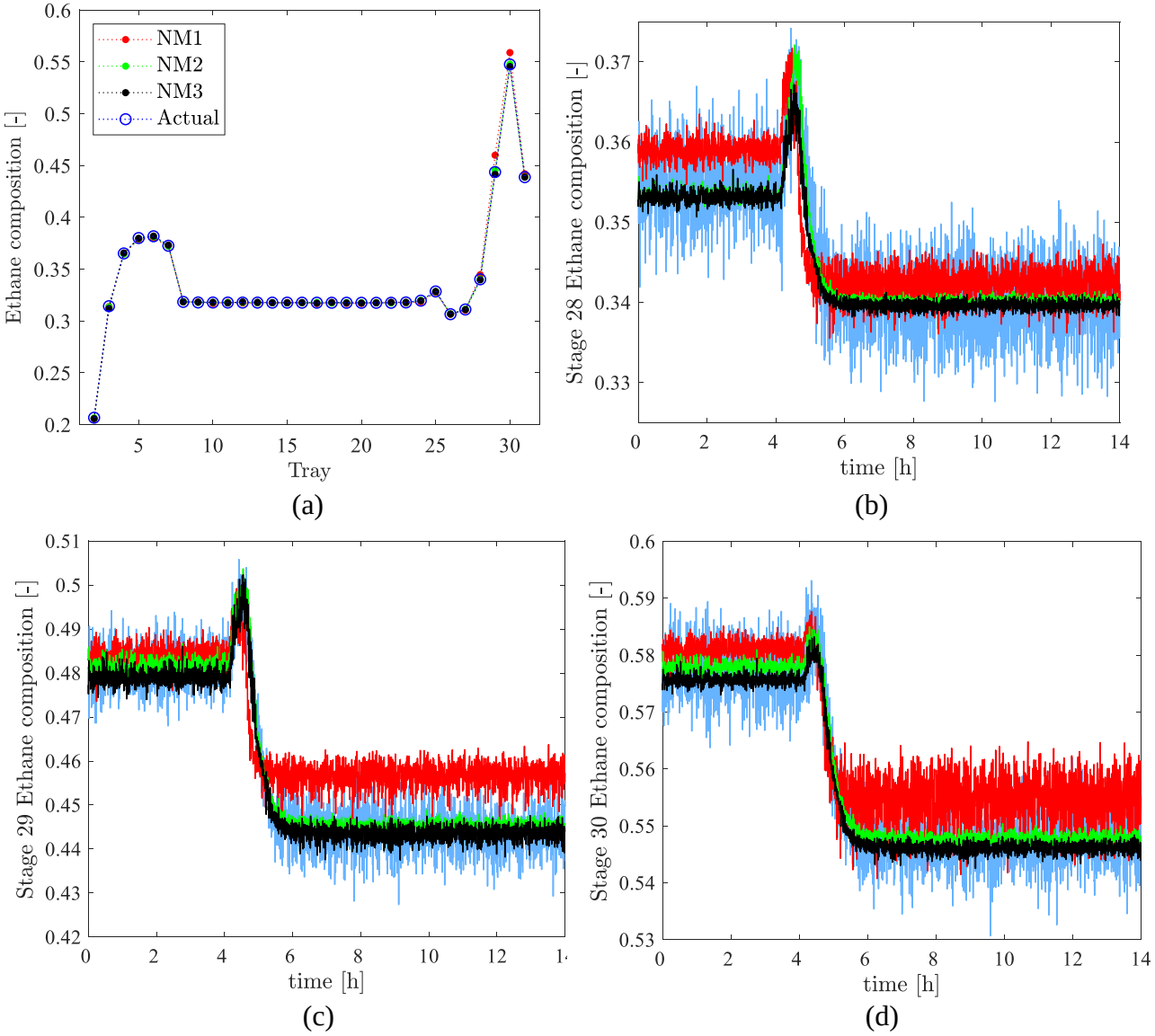

Figure 7.15: Column ethane composition profiles at the new steady state (a). Transient ethane composition profiles of 28th stage (b), 29th stage (c), 30th stage (d) obtained in the validation campaign for NM1 (red lines), NM2 (green lines) and NM3 (black lines) under decreasing variation of 5% in the plant feed nominal value.

Observing the transient profiles obtained for the 28th tray (Figure 7.15b), it appears that all the models can predict the trend of the ethane concentration. Nevertheless, NM1 shows poorer estimation performances when compared with the other models that can more accurately predict and filter the concentration profiles. Indeed, the prediction obtained with NM2 and NM3 has lower noisy profiles compared with NM1. It is also possible to observe that NM3 cannot well approximate the transient peaks of the measured profile and NM1 has a slightly offset in the nominal conditions, even if, thanks to the model's ability to reduce the

measurement noise, the prediction lies under the measurement profiles. Analyzing the transient profiles correspondent to the ethane concentration profiles in the 29th and 30th tray of the column (Figure 7.15c and Figure 7.15d respectively), model NM1 prediction shows an error greater than the considered measurement error, while the other two models can obtain an estimation that remains within the measurement range with a less noisy response compared to NM1.

In the present results, the NM1 turns out to have the worst prediction performance when considering most of the estimation target variables. This is probably due to the reduced temporal dependency in the structure of this model, as well as the impossibility of benefiting from the presence of the actual measures of the output variables used by the end cells of NM2 and NM3. On the other hand, the NM2 seems to be a more suitable neural model since it can adequately represent and predict the dynamic behavior of the whole column, except for the temperature profile in the 29th tray. Therefore, this model architecture may represent a viable candidate for the demethanizer column digital twin development.

Validation transient profiles

The results reported in the above section identify the NM2 as the model with the best architecture for the prediction of the demethanizer separation operations. To examinate the prediction obtained in the validation campaign by this model, the estimated transient profiles and the actual column pressure, temperature and concentration profiles are depicted in Figure 7.16. For the sake of brevity, only the transient composition profiles of column key components are included in the discussion.

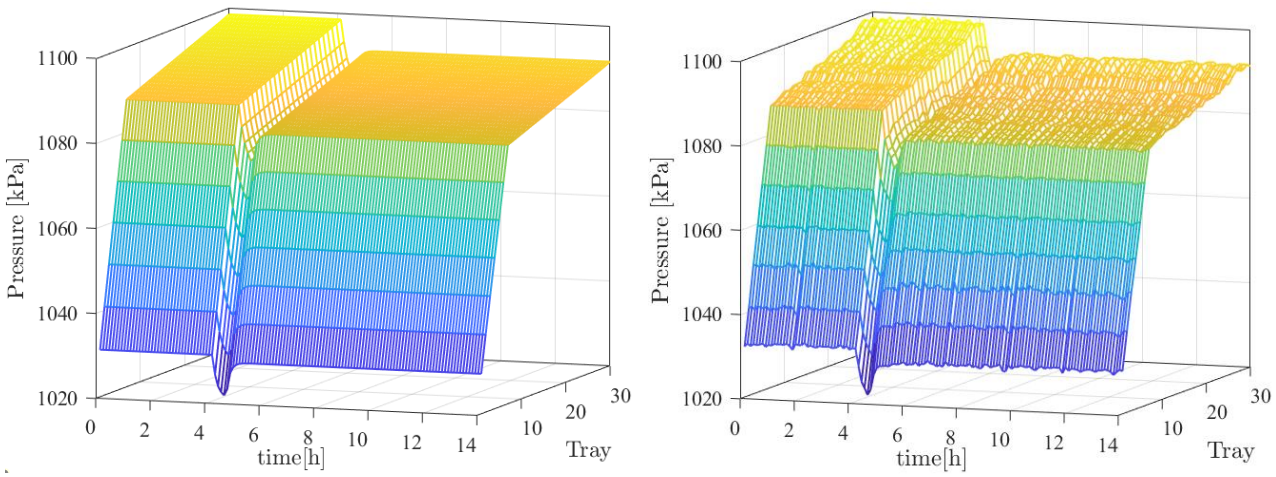

(a) (b)

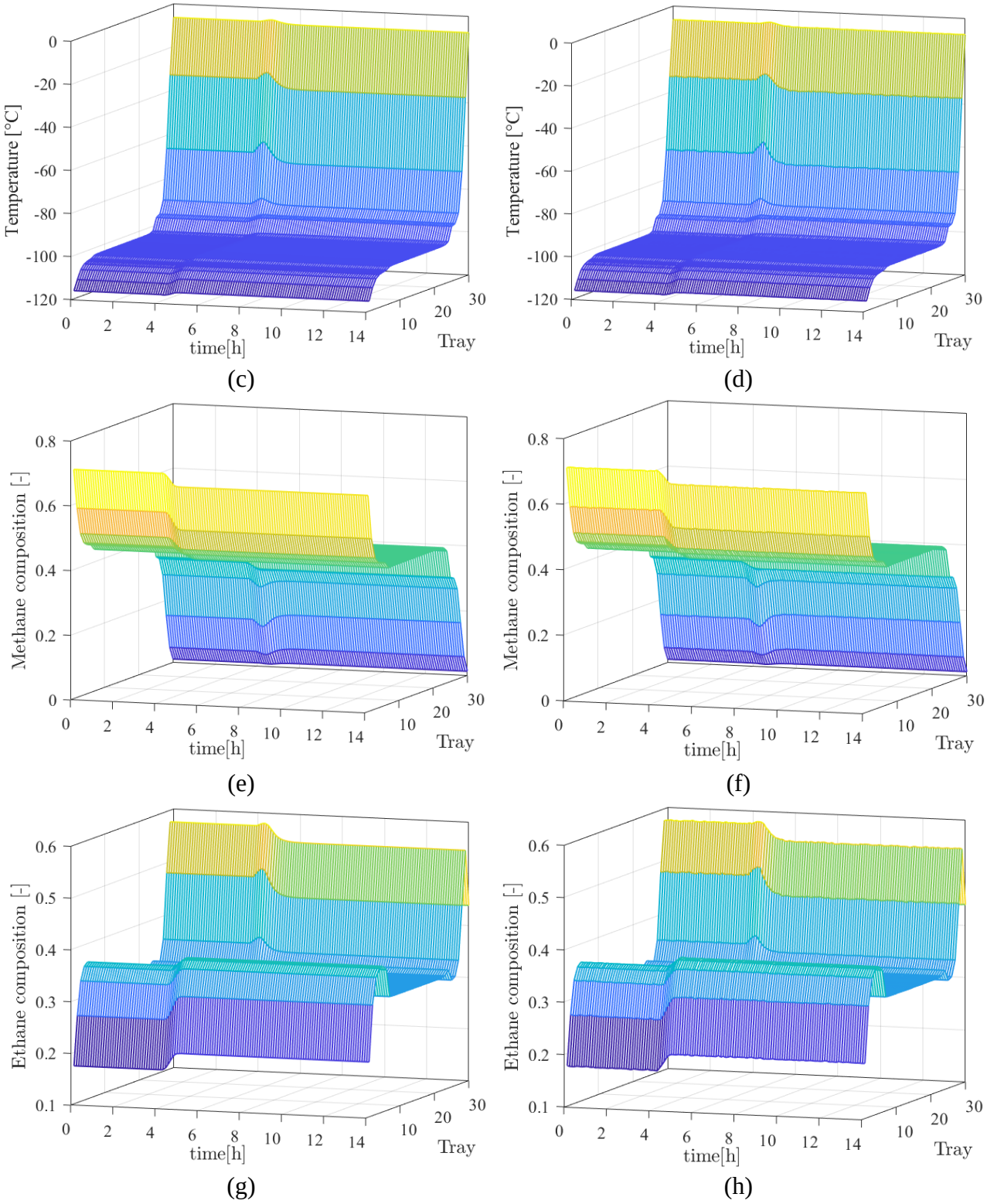

Figure 7.16: Transient column profiles obtained with the NM2 under a decreasing variation of 5% in the plant feed nominal value for: actual pressure (a) and estimated pressure (b); actual temperature (c) and estimated temperature (d); actual methane composition (e) and estimated methane composition (f); actual ethane composition (g) and estimated ethane composition (h).

As shown in Figure 7.16, the profile obtained by the NM2 model, for the estimation of the actual column pressure transient profile (Figure 7.16a), which is depicted in Figure 7.16b

shows that the model is perfectly able to accurately reconstruct the actual profiles with a profile whose noise is lower than the considered measured error. The real-time predictions obtained with the NM2 for the column temperature profile (Figure 7.16d) provide accurate estimation with no detectable deviations from the actual column temperature profiles (Figure 7.16b). As it is possible to visualize, the neural model proves to be able to predict not only the steady state condition but also reconstruct the time evolution of the profiles. The same results are obtained for the estimated methane concentration (Figure 7.16f) and ethane concentration (Figure 7.16h) profiles in the column estimation. In both cases, the model can accurately reconstruct the trend of the actual profiles (Figure 7.16e and Figure 7.16g) of key components, also related to the quality indexes of the column. Analogue results are obtained for the non-key component prediction. Table 7.4 shows the MSE and the maximum deviation, obtained by considering the predictions for non-key components of the transient composition profiles and the actual profiles in all column trays. The NM2 model can accurately reconstruct all the composition transient column profiles, with extremely low values obtained for MSE and maximum estimation error. The latter always results under the assumed measurement error, confirming the model's ability to filter the measurement noise.

Table 7.4: Mean square error and max error obtained for the non-key components in the validation campaign of NM2 under a decreasing variation of 5% in the plant feed nominal value

	Propane	**Butanes**	**Pentanes**	**Hexane**
MSE	3.17e-07	1.89e-07	2.53e-07	6.27e-06
Max Error	3.31e-05	1.96e-05	3.30e-05	5.69e-04

Remarks on neural model comparison

The results of the comparison showed that the NM2 model has the best estimation performance. This model had an enhanced ability to approximate the trends of the actual target variable profiles and to filter out measurement noise. Furthermore, NM2 was able to predict the actual trend of temperature transient profiles quite accurately for most of the column trays, while it allows the monitoring of the temperature in the final stages of the column and the reboiler. The predictions obtained for column temperatures may be improved by using datasets involving the use of different control strategies to increase data insights in the later stages of the column.

7.4.4. DDT estimation performances

As NM2 showed the best estimation performances of the target variables, this model architecture was thus selected for the development of the demethanizer digital twin (DDT). The DDT integrates the structure of the NM2 model with NMPC and NMCF models. In particular, the estimation of reflux and boilup flows obtained with the NMCF were given as model inputs and the composition estimations obtained by the NMPC model were employed instead of the composition measurements required in the NM2 architecture, eliminating the dependence of the NM2 architecture on the presence of composition analyzers. In this way, it was possible to obtain a complete model of the column, whereby it was possible to estimate the demethanizer column operations employing only readily available measurements. In this section, to evaluate the performance of the DTT and to show how information about the terminal compositions of the column is necessary to obtain adequate target estimations, the results obtained by comparing the estimation performances of the DDT with the NM2 and with a modified version of the NM2 model not depending on concentration measurements, referred to as NM2mod, are reported in Figure 7.17. Subsequently, the column transient profiles of pressure, temperature, and composition of the key components in the column estimated with the DDT are compared with the actual profiles in Figure 7.18. To quantify the magnitude of the prediction errors, the transient error profiles are shown in Figure 7.19.

Model comparison

For comparing the results obtained by the DDT, NM2 and NM2mod, the profiles obtained in the column's most critical area, i.e. the end of the column and the reboiler, were analyzed. In Figure 7.17 the measured methane and temperature profiles are compared with the profiles estimated from the 27^{th} and 29^{th} trays of the column and in the reboiler. For the sake of brevity, only the profiles obtained in the validation campaign in response to the 5% decrease in the plant inlet flowrate are reported.

The graphs shown in Figure 7.17 are intended to show the trend in the estimates obtained for methane and temperature as moving towards the bottom of the column. The graphs on the left show the results obtained for the methane composition in the liquid phase of the considered tray, while the graphs on the right show the results obtained in estimating the temperature in the same trays. In the profiles estimated in the 27^{th} plate, it is observable that all three models considered can estimate the methane concentration (Figure 7.17a) with good accuracy.

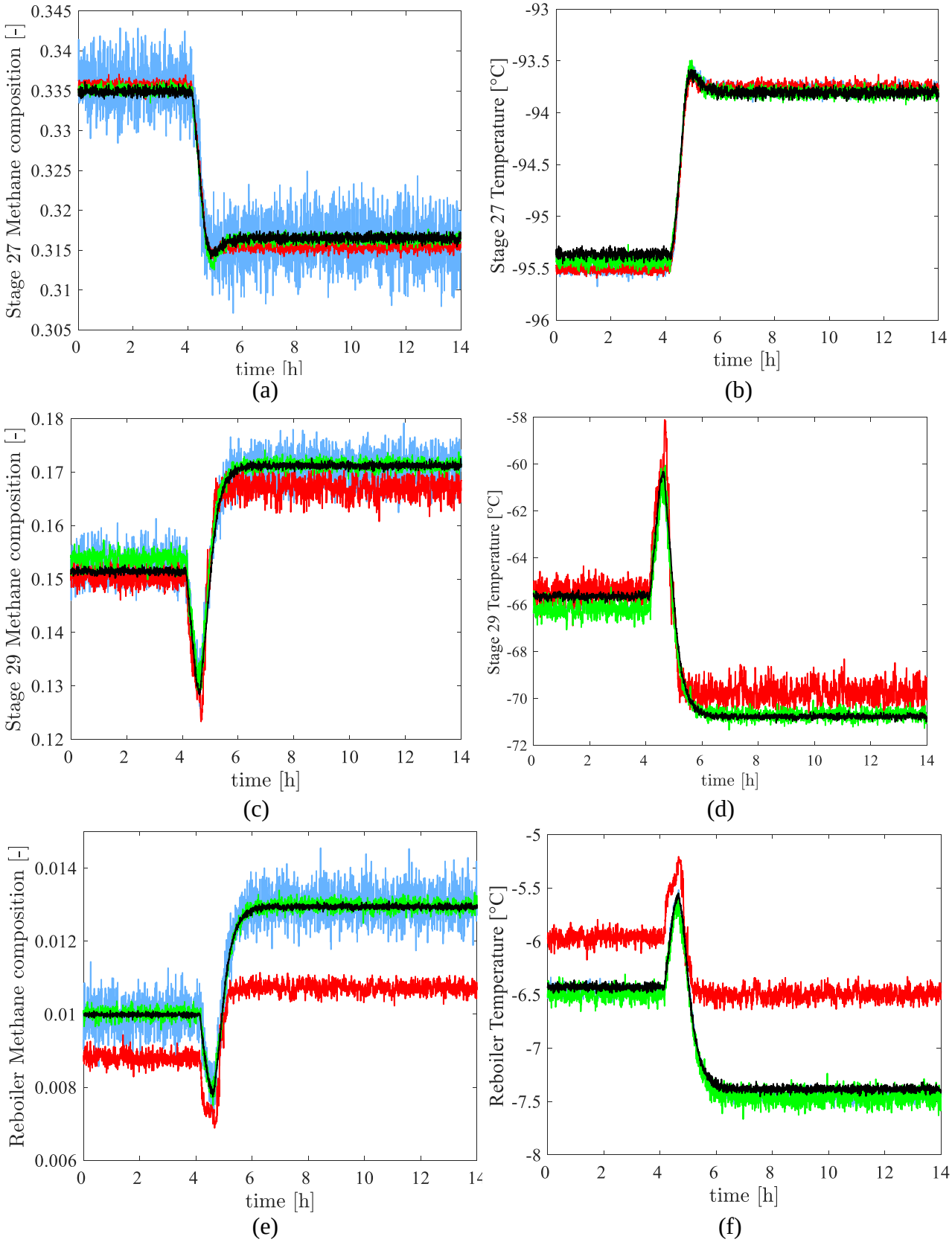

Figure 7.17: Comparison of transient profiles of methane composition and tray temperature of 27th stage (a and b respectively), 29th stage (c and d respectively), reboiler (e and f respectively) obtained in the validation campaign for NM2 (green line), NM2mod (red line), and DDT (black line) under a decreasing variation of 5% in the plant feed nominal value. The light blue line depicts the measured profiles.

The same results are obtained for the temperature profiles (Figure 7.17b) where the maximum estimation error obtained with the models is about 0.15°C. Methane composition and temperature profiles, in the 29th tray, are depicted in Figure 7.17c and Figure 7.17d respectively. Here it is possible to observe a deterioration in the estimation performance obtained by NM2mod. Although the methane composition profiles estimated by this model managed to remain within the measurement error considered, the average estimated profile starts to deviate from the actual profile at the new steady state conditions. For what concerns the NM2mod temperature profile a maximum deviation of about 2.8°C from the mean value of the measured temperature profile is registered. Also, it is possible to observe a deviation from the mean value of the measured profiles in the new steady state conditions. The estimation obtained with the other models can well approximate the methane and temperature profiles with an estimation error of less than 0.5°C.

From the comparison of the profiles obtained for the column reboiler the lack of information in the NM2mod model, it is evident from the fact that it cannot estimate either methane composition (Figure 7.17e) or temperature profiles (Figure 7.17f). The estimated methane composition profile obtained by this model shows an estimation error greater than the considered measurement error during the transient and the new steady state conditions. For what concerns the estimated profiles obtained for the reboiler temperature, here the MN2mod model does not follow the trend of the actual measurement, with a maximum estimation error of around 1°C. By comparing the performances of the other models, the NM2 shows to provide more noisy estimations for both methane and temperature profiles compared to the estimated profiles obtained with the DDT. This is due to the use of the NMPC concentration estimations, which, as stated previously, demonstrated excellent measurement noise reduction abilities.

Validation transient profiles

To have a complete overview of the results obtained by the DDT model, developed for the prediction of demethanizer column operations, the comparison of the transient profiles obtained for column pressure, temperature and key components composition and the actual transient profiles is depicted in Figure 7.18.

As shown in Figure 7.18, the estimated transient profiles obtained by the DDT show similar results to the ones obtained with the NM2 model (Figure 7.16). As it is possible to visualize, the model can predict not only the steady state condition but also accurately reconstruct the time evolution of the profiles with no detectable deviations from the actual column profiles.

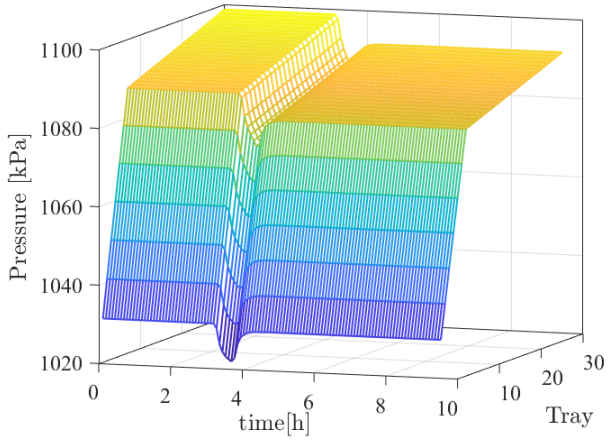
Pressure [kPa]
1100
1080
1060
1040
1020
0 2 4 6 8 10
time[h]
10 20 30
Tray

(a)

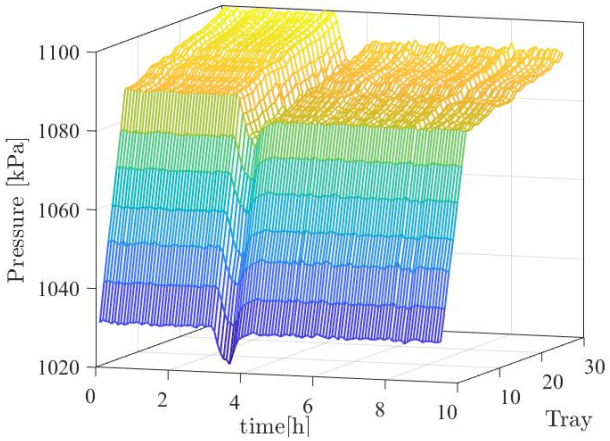
Pressure [kPa]
1100
1080
1060
1040
1020
0 2 4 6 8 10
time[h]
10 20 30
Tray

(b)

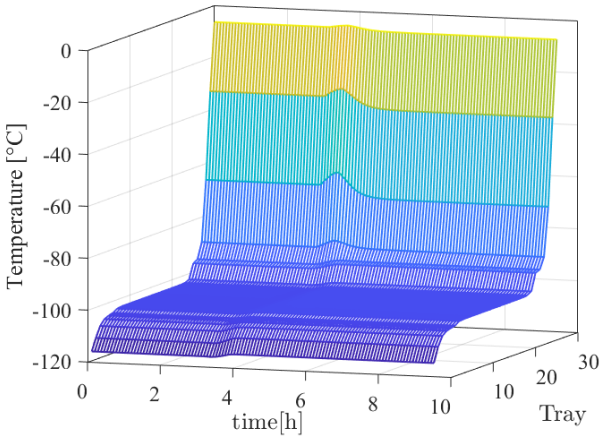
Temperature [°C]
0
-20
-40
-60
-80
-100
-120
0 2 4 6 8 10
time[h]
10 20 30
Tray

(c)

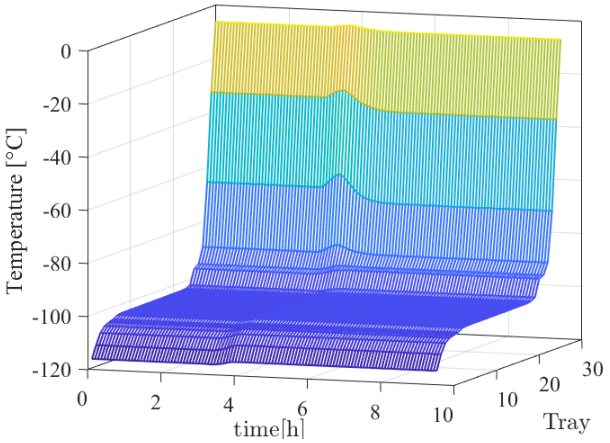
Temperature [°C]
0
-20
-40
-60
-80
-100
-120
0 2 4 6 8 10
time[h]
10 20 30
Tray

(d)

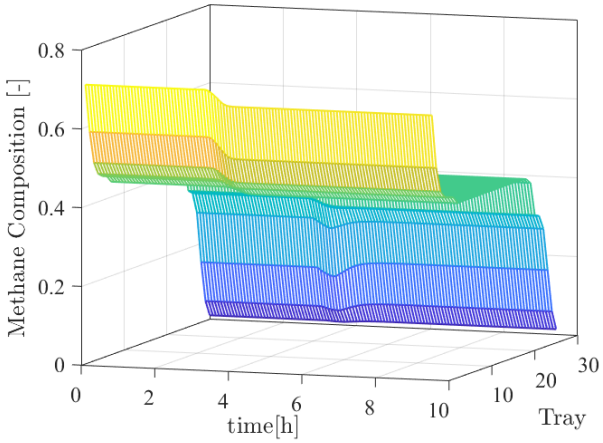
Methane Composition [-]
0.8
0.6
0.4
0.2
0
0 2 4 6 8 10
time[h]
10 20 30
Tray

(e)

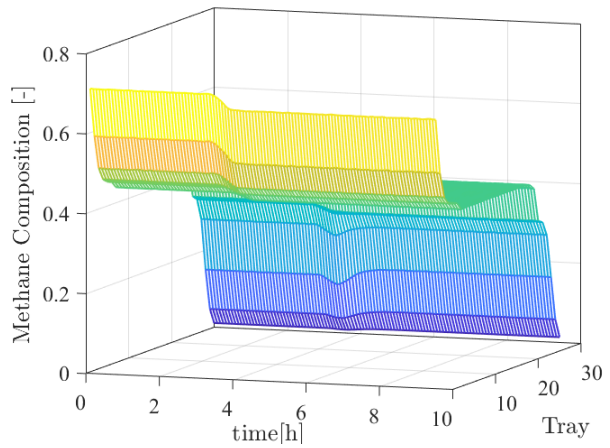
Methane Composition [-]
0.8
0.6
0.4
0.2
0
0 2 4 6 8 10
time[h]
10 20 30
Tray

(f)

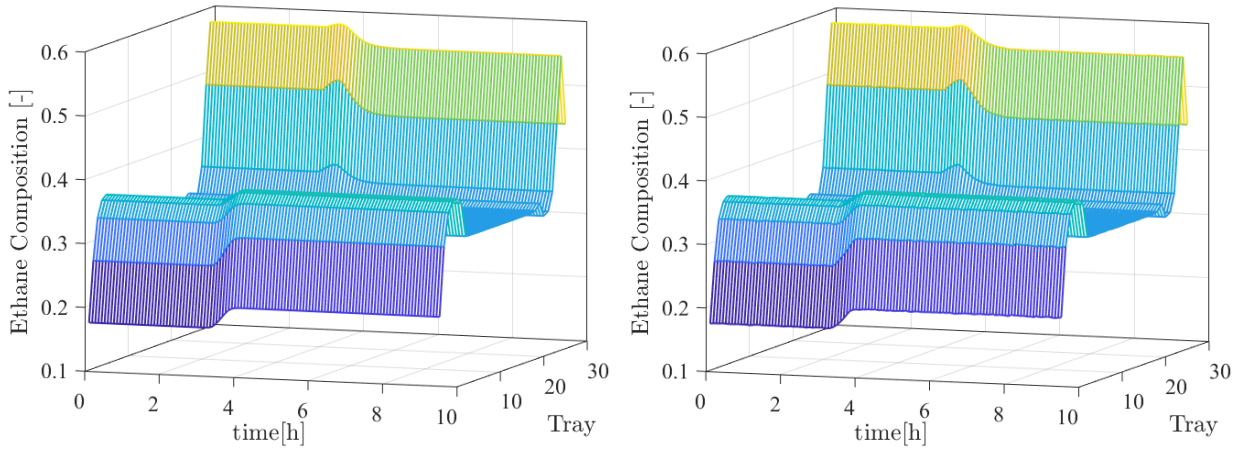

Figure 7.18: Transient column profiles obtained under a decreasing variation of 5% in the plant feed nominal value for: actual pressure (a) and estimated pressure (b); actual temperature (c) and estimated temperature (d); actual methane composition (e) and estimated methane composition (f); actual ethane composition (g) and estimated ethane composition (h).

The model is also able to predict the time evolution of the other components in the column. Thus, from a qualitative point of view, the model developed correctly approximates the target variables. It succeeds in extrapolating the information contained in the inputs provided, and those provided by the outputs of the adjacent cells of the model, to produce a mathematical model that succeeds in estimating the separation that occurs in each column tray.

By considering the estimation error of the transient profiles obtained by the DDT in the validation campaign for pressure, temperature, and key components composition, the goodness of the derived model was analyzed quantitatively in Figure 7.19. The performances obtained in the estimation of the transient profiles of non-key components are analysed in terms of Mean square error (MSE). Also, in this case for the sake of brevity, only the results obtained under the worst-case variation represented by the application of a 5% decrease in the feed plant nominal value.

As it is possible to visualize from the estimation error of the column pressure profile, which is depicted in Figure 7.19a, the DDT is perfectly able to predict the pressure time evolution in all column trays, with a maximum error below 3kPa, way below the maximum assumed measurement deviation of 16kPa. The model is thus not only able to accurately predict the column pressure profiles, but it also can filter the measurement error.

Figure 7.19b illustrates the estimation error obtained for the column temperature profile during the considered transient time. Here, it is possible to observe that the temperature profile obtained with the DDT always predicts the actual general trend of the transient column temperature profile. The model can perform an accurate transient prediction for the trays

between the 2nd to 23rd with an estimation error below 0.1 °C. While a higher error but still lower than 0.2°C is registered in the first tray. As moving to the ends of the column, starting from the 28th tray the estimation error increases remaining below 1°C. Most of the column temperature variation is concentrated in the latter three stages, with about 80°C of variation due to the presence of methane in the gas phase. Furthermore, since the temperature in the 28th stage has been controlled, the resulting temperature data are not enough informative to obtain an accurate estimation.

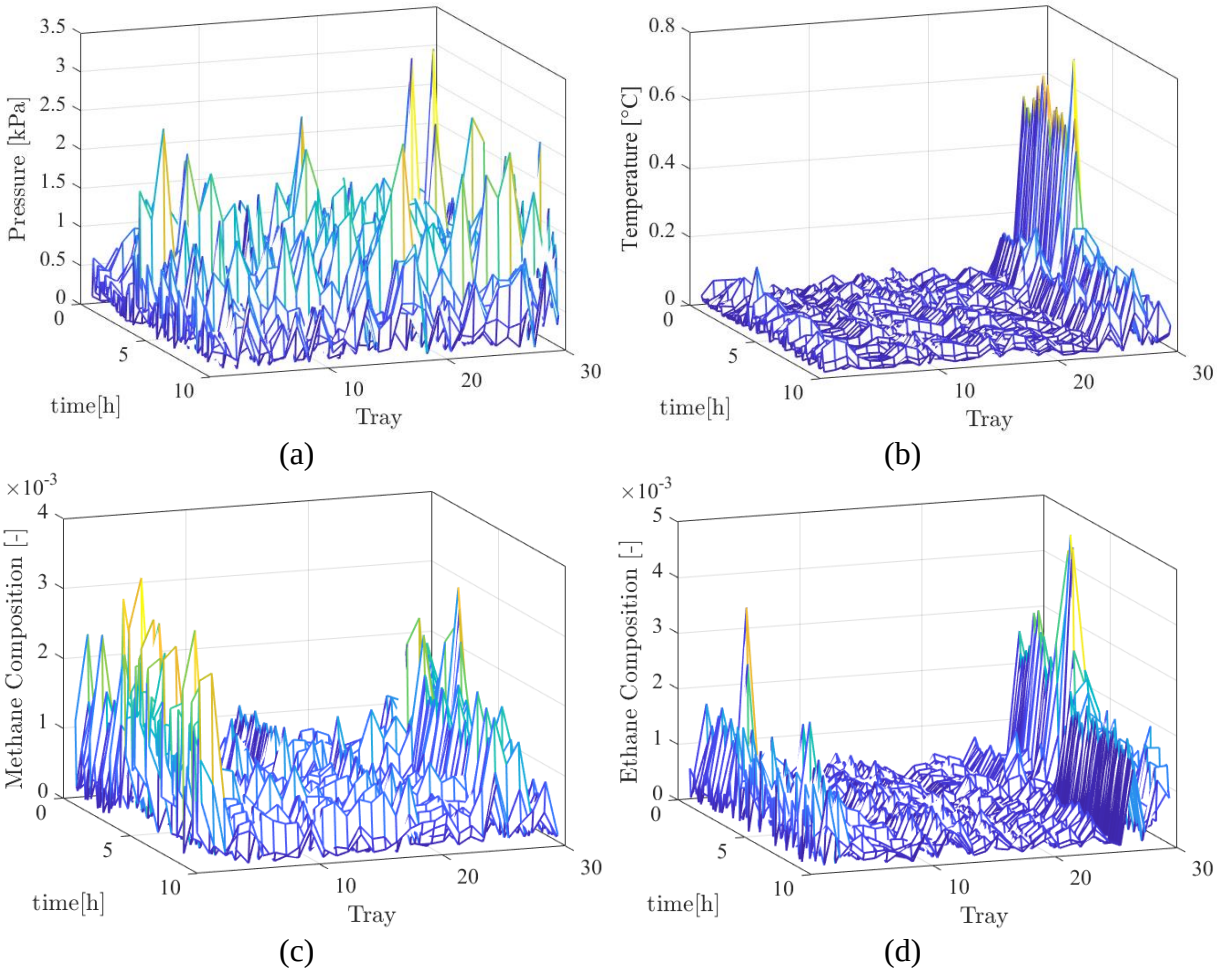

Figure 7.19: Error transient profiles obtained in the validation campaign under the decreasing variation of plant feed nominal value for pressure (a), temperature (b), methane (c) and ethane (d) composition.

For what concerns the key components, the estimation error of the column transient profiles of methane and ethane composition are shown in Figure 7.19a and Figure 7.19b respectively.

Here, is it shown that for both components, the DDT can accurately predict the actual composition transient profiles for all the column trays. The estimation errors increase in correspondence to the column region where most of the variations for the considered component occur. Indeed, the estimation error for methane increases around the column feed

trays, and for both the components it is higher in the column terminal regions, where most of the separation takes place. For both the key components the deviations of the predicted transient column profiles from the actual profiles are always lower than the maximum assumed measurement error, leading to the achievement of estimates more accurate than the measures achievable with measurement sensors considering the standard deviations reported in Table 7.1. Analogue results are obtained for the non-key components prediction. Table 7.5 shows the MSE and the maximum deviation, obtained by considering the predictions of the transient composition profiles in all column trays and the actual profiles, for non-key components in the validation campaign. The proposed neural model was able to accurately reconstruct the all the composition transient column profiles, with extremely low values of MSE and maximum estimation error. The latter always results under the assumed measurement error, confirming the model's ability to filter the measurement noise.

Table 7.5: Mean square error and max error obtained for the non-key components in the validation campaign of the DTT under a decreasing variation of 5% in the plant feed nominal value

	Propane	**Butanes**	**Pentanes**	**Hexane**
MSE	7.24E-8	1.22E-8	1.49E-9	2.57E-9
Max Error	0.0011	7.62E-4	2.60E-4	2.64E-4

Calculation time comparison

As stated in the motivation of this work, the development of the Demethanizer column digital twin is linked to the necessity to obtain a tool suitable for controlling and monitoring the process in real time. To assess the fulfilment of this goal, a calculation times comparison between the Aspen HYSYS® simulation and the DDT was performed. To meet a more realistic situation, the use of the interactive platform SimWiz (PSE research group, LSU, s.d.) is also considered in this analysis. The use of this platform gives us a measure of how much computation time is required in Aspen HYSYS® for simulated data to be exchanged in real-time by other software avoiding loss of data. Indeed, SimWiz is a powerful tool developed by the PSE research group of Louisiana State University (LSU) that emulates a DCS environment. The use of this platform allows the simulated data generated by the Aspen HYSYS® simulation to be shared in a Python environment and allows the easy collection and analysis of simulated data. The presented analysis has been performed by simulating two datasets, one with Aspen HYSYS® and the other with SimWiz, under the presence of the inlet disturbances considered

in the registration of the dataset used in the neural networks' validation reported in section 7.3.1. The DDT calculation time has been recorded in the Python environment during the validation campaign. Thus, the calculation times obtained by the three considered tools are associated with the same plant operations, the result of this comparison is depicted in Figure 7.20.

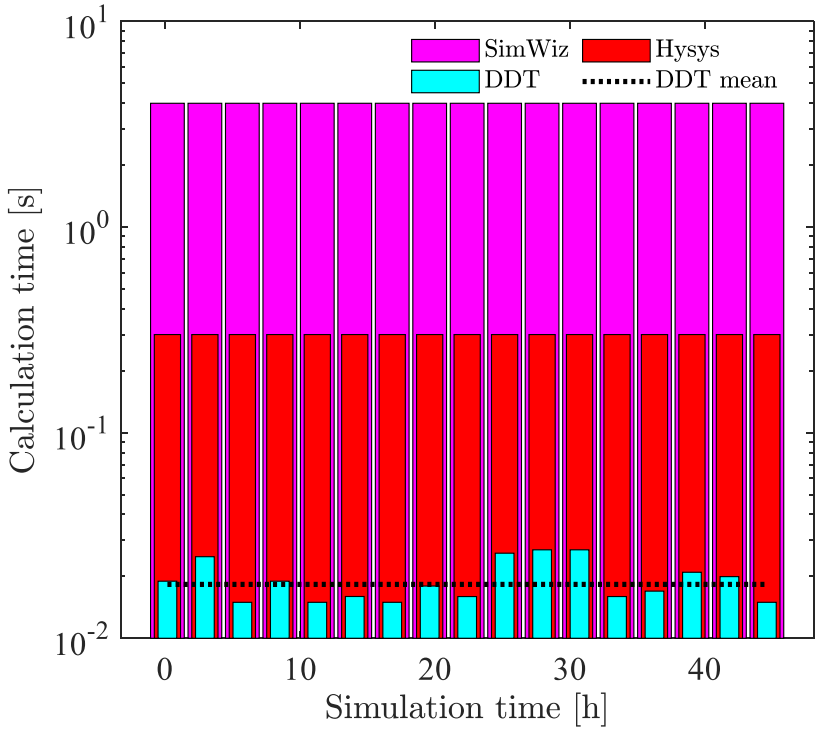

Figure 7.20: Calculation times comparison between the Aspen HYSYS® simulation, the DDT and SimWiz.

In Figure 7.20 it is possible to observe the comparison computational time of the DDT SimWiz and Aspen HYSYS®. The results reported for SimWiz and Aspen HYSYS® are referred to as average calculation times, since in the Aspen HYSYS® environment the actual timing recording is not possible, and therefore the registration of the actual computation times was not practicable. In the case of the Aspen HYSYS® simulation, the average computation time was calculated by dividing the actual timing accounted for performing the simulation by the number of samplings considered for each variable. As showed in Figure 7.20 the average computation time obtained for the Aspen HYSYS® simulation was found to be equal to 0.3 s. In the case of SimWiz, on the other hand, a fixed calculation time of 4 s was used, as found to be the lowest calculation time allowing for no data loss in the connection between Python and Aspen HYSYS® determined based on trial-and-error tests. For the DDT both the computation time and the average computation time (black dotted line) are depicted in Figure 7.20, in particular

the latter was found to be equal to 0.0183 s. To the DDT is thus associated a reduction in the calculation time of 99.54% compared to SimWiz and of 93.9% compared to Aspen HYSYS®. The DDT was able to perform around 48 hours of plant operation estimation in about 2.7 minutes, while the Aspen HYSYS® simulation required about 43 minutes and SimWiz required 9.62 hours.

7.5. Conclusion of the Chapter

This chapter has exploited the possibility of using a data-driven approach and neural networks to model a demethanizer column of a simulated CRR unit, intending to use the developed model as a demethanizer digital twin (DDT), allowing for more efficient and accurate monitoring and control of the column's performance. The DDT was realized by integrating three different neural models: one for column material balance approximation (NMCF), another for column product composition estimation (NMPC), and a model that estimates the demethanizer separation occurring in all the trays and the reboiler. To select the most suitable network architecture capable of estimating separation operations in all column trays, several neural network models, differing in the interconnections between the network cells, were compared. The NM2 model has proved to have the best estimation performance and its architecture was employed for the DDT realization. The estimation of reflux and boilup flows obtained with the NMCF were given as model inputs to the DDT, while the NMPC estimations were used in the DDT replacing the NM2 required the compositions at column ends. As a result, the developed digital twin employs only easy and economical to-measure variables, making it more feasible to use in real plants. Furthermore, the need for composition data as input to the surrogate model was confirmed by the comparison of it with an NM2mod model realized by modifying the structure of the NM2 model to remove the dependency of composition data. The developed demethanizer digital twin was able to predict the actual trend of the considered output quite accurately with also a great ability to filter the measurement noise. Thus, it was found to be a possibly useful tool for estimating the dynamic behavior of the demethanizer column and for optimizing, monitoring, and controlling the NGL recovery process.

Chapter 8

Conclusions

In this Thesis, the research work concerning the control and estimation problems of an NGL recovery process was presented. With this purpose, three plant schemes largely used in the industry, using cryogenic distillation for methane separation, were considered in the work. The conventional, GSP, and CRR separation units were, in turn, simulated in the Aspen HYSYS® process simulator, each representing the first part of the plant for NGL separation. The remaining columns required for NGL recovery were designed and dynamically simulated in the same simulation environment. The full plant obtained, thus, consists in a train of distillation columns where the demethanizer column for methane separation is followed by the deethanizer, depropanizer, and debutanizer column for the heavier hydrocarbon separation. This is an energy-intensive process subject to typical input disturbances, such as changes in the inlet flowrate and composition which have a large influence on the product quality attained in the distillate and residue of the multicomponent distillation columns considered in the plant. The main equipment of the plant is the demethanizer column, which provides the NGL liquid stream supplied to the subsequent distillation train for further separation. In this separation unit, the cryogenic operations and the presence of methane in supercritical conditions solved in the liquid mixtures in the last stages of the column require attention over the power consumption used for the separation. Due to the unconventional separation operations performed by this unit, the low performances of temperature control for the indirect control of product quality would require the use of expensive composition analyzers to attain the product specification targets, mitigate the effects of disturbances in the other column of the plant as well as reducing the power consumption of the plant. However, the use of direct control of composition is less attractive due to the high cost of purchasing and maintenance of composition analyzers. Furthermore, also the associated long measurement delays contribute to making them less reliable for estimation and control purposes. To find a control strategy that combined the cost-effectiveness of temperature controllers with the achievement of optimum control performances, several indirect composition control strategies were developed in this research

work to mitigate the effects of disturbances while retaining the desired product specifications and enhancing the plant's energy efficiency.

To select and design the indirect composition controllers for the considered column, firstly an analysis of temperature gradients, with a per-component contribution diagram, was carried out to determine the most suitable location for temperature sensors. The results indicated that the temperature variation in the demethanizer columns was mostly dependent on the methane composition changes. The influence of the variations of this component increases significantly at the bottom of the column due to its solubility in the mixture. The variations in light key components had a significant impact on the temperature gradient in the stripping section of the other columns leading to the selection of the temperature sensor location where this was the maximum. The analysis also recommended implementing a reflux ratio controller to mitigate the effect of feed disturbances on the heavy-key components in the top product, as the variation of this component has a negligible impact on the temperature gradient in this column section. Based on these considerations, control strategies for indirect purity control of the products of the various columns were developed.

Different control schemes were proposed to keep a methane composition of 1 mol% and an ethane recovery of 84% in the bottom product of the demethanizer column under the presence of feed and composition disturbances. The initial control strategy (CS1) using only indirect composition controllers was found to be insufficient in managing flow and composition disturbances. Alternative control strategies were developed, including CS2, where the control of the pressure-compensated flash tank (TK-100) temperature was introduced, and CS3 which utilized a cascade control configuration to speed the controller of the column tray temperature, introducing as slave loop a ratio flow controller between a boilup approximation and the demethanizer bottom product. From the analysis of the control structures presented, the CS3 gave the best control performances also improving the overall operation of the column and reducing the plant power consumption, although this was unable to meet the methane composition target. The offset was eliminated only with the introduction of a methane composition controller as a third control loop in the cascade (CS4).

To overcome the need for concentration measures, and thus composition analyzers, to achieve the required production targets, deep learning techniques were applied, for the development of composition soft sensors for methane composition, ethane recovery and demethanizer boilup. The results demonstrated that methane composition and boilup feedforward soft sensors were

capable of accurately reproducing the dynamic behavior of the actual variables and were successful in enhancing the performances of the control strategy in terms of response speed, although offset elimination under new steady state conditions was not achieved. In addition, the realized ethane recovery soft sensor proved to be a useful tool for real-time process monitoring.

The final part of the presented research work was focused on the development of a data-driven digital twin for a simulated demethanizer column of a CRR unit. The goal was the achievement of an efficient tool for monitoring, controlling, and optimizing the plant that would benefit from a reduced estimation time compared to the commercial simulator. To achieve this goal, LSTM recurrent neural networks were employed with a data-driven approach for surrogate model development. Different neural network architectures were designed to approximate, as far as possible, the separation operation performed in the column. The developed architecture differs in the organization of the modified LSTM cells, in particular, the interconnections between the cells of the networks and the information flow attempted to recreate the internal behaviour of a distillation column. Three architectures were compared in their capability to estimate the thermodynamic equilibrium established in the column trays, as temperature pressure and composition of all column trays were the desired output of the network. The result of the comparison shows that the NM2 architecture proved to be the best approximation for the internal behavior of the column. This structure combines the presence of a temporal link between cells with the possibility of determining which information calculated from the adjacent cells and received by a given NM2 cell is useful for calculating the desired output. The NM2 architecture was then employed in the column digital twin development, by integrating it with the LSTM models for column material balance and column product composition estimation. The introduction of those models made possible the use of only easily accessible and inexpensive measure variables, leading to the realization of a surrogate model attractive for use in real plants. The resulting demethanizer digital twin could predict the actual output trend with accuracy and filtering measurement noise, making it a valuable tool for monitoring and controlling the NGL recovery process and estimating the dynamic behavior of the demethanizer column.

Index of acronyms

ANN	Artificial neural network
ANNs	Artificial neural networks
ADAM	Adaptive Moment Estimation optimizer
CRR	Cold residue reflux separation scheme
CNG	Compressed natural gas
CS1	Control structure with Flash tank (TK-101) temperature control and direct control of column (T-101) tray temperature
CS2	Control structure with Flash tank (TK-101) PCT control and direct control of column (T-101) tray temperature
CS3	Control structure with the two loops cascade with column tray temperature controller and ratio controller and Flash tank (TK-101) PCT control
CS4	Control structure with the three loops cascade and Flash tank (TK-101) PCT control
CS5	Control structure with the two loops cascade with composition controller and column tray temperature controller and direct control of column (T-101) tray temperature
CS6	Control structure with the two loops cascade with column tray temperature controller and ratio controller with boil-up soft sensor estimation and Flash tank (TK-101) temperature control
CS7	Control structure with the three loops cascade with delayed methane measurements and Flash tank (TK-101) temperature control
CS8	Control structure with the three loops cascade with methane soft sensor estimation and Flash tank (TK-101) temperature control
DDT	Demethanizer column digital twin
EKF	Extended Kalman Filter
EOS	Equations of state
FNN	Feedforward neural network
FNNs	Feedforward neural networks
GE	Geometric Estimator
GSP	Gas Subcooled Process separation scheme

IAE	Integral Absolute Error
MSE	Mean squared error
NGL, NGLs	Natural gas liquids
NMPC	Neural Model for product composition estimation
NMCF	Neural Model for Column Flow estimation
NM1	Neural model 1
NM2	Neural model 2
NM3	Neural model 3
PCR	Partial component regression
PLS	Partial least square
PCT	Pressure compensated temperature
RNN	Recurrent neural network
RNNs	Recurrent neural networks
SVD	Singular value decomposition

Bibliography

Al Kalbani, F., & Zhang, J. (2023). Inferential Composition Control of a Distillation Column Using Active Disturbance Rejection Control with Soft Sensors. *Sensors*, *23*(2), Articolo 2. https://doi.org/10.3390/s23021019

Alvarez, J., & López, T. (1999). Robust dynamic state estimation of nonlinear plants. *AIChE Journal*, *45*(1), 107–123. https://doi.org/10.1002/aic.690450110

Bassani, A., Previtali, D., Pirola, C., Bozzano, G., Colombo, S., & Manenti, F. (2020). Mitigating Carbon Dioxide Impact of Industrial Steam Methane Reformers by Acid Gas to Syngas Technology: Technical and Environmental Feasibility. *Journal of Sustainable Development of Energy, Water and Environment Systems*, *8*, 71–87. https://doi.org/10.13044/j.sdewes.d7.0258

Blank, J., & Deb, K. (2020). pymoo: Multi-objective Optimization in Python. *IEEE Access*, *8*, 89497–89509. https://doi.org/10.1109/ACCESS.2020.2990567

Brambilla, A. (2014). *Distillation Control and Optimization*. McGraw-Hill Education.

Brigida, M. (2014). The switching relationship between natural gas and crude oil prices. *Energy Economics*, *43*(C), 48–55.

Campbell, R. E., & Wilkinson, J. D. (1981). *Hydrocarbon gas processing*.

Caporin, M., & Fontini, F. (2017). The long-run oil–natural gas price relationship and the shale gas revolution. *Energy Economics*, *64*(C), 511–519.

Chebbi, R., Al-Amoodi, N. S., Abdel Jabbar, N. M., Husseini, G. A., & Al Mazroui, K. A. (2010). Optimum ethane recovery in conventional turboexpander process. *Chemical Engineering Research and Design*, *88*(5–6), 779–787. https://doi.org/10.1016/j.cherd.2009.11.003

Chebeir, J., Salas, S. D., & Romagnoli, J. A. (2019). Operability assessment on alternative natural gas liquids recovery schemes. *Journal of Natural Gas Science and Engineering*, *71*, 102974. https://doi.org/10.1016/j.jngse.2019.102974

Chetouani, Y. (2007). *Using Artificial Neural networks for the modelling Of a distillation column*. *Vol 4*(Issue 3), 119–133.

Elman, J. L. (1990). Finding structure in time. *Cognitive Science*, *14*(2), 179–211. https://doi.org/10.1016/0364-0213(90)90002-E

Feng, G.-F., Wang, Q.-J., Chu, Y., Wen, J., & Chang, C.-P. (2021). Does the shale gas boom change the natural gas price-production relationship? Evidence from the U.S. market. *Energy Economics*, *93*(C). https://ideas.repec.org//a/eee/eneeco/v93y2021ics0140988319300799.html

Ferreira, J., Pedemonte, M., & Torres, A. I. (2022). Development of a machine learning-based soft sensor for an oil refinery's distillation column. *Computers & Chemical Engineering*, *161*, 107756. https://doi.org/10.1016/j.compchemeng.2022.107756

Frau, A. (2011). *Composition control and estimation with temperature measurements for multicomponent distillation columns*.

Ge, Z. (2017). Review on data-driven modeling and monitoring for plant-wide industrial processes. *Chemometrics and Intelligent Laboratory Systems*, *171*, 16–25. https://doi.org/10.1016/j.chemolab.2017.09.021

Getu, M., Mahadzir, S., Long, N. V. D., & Lee, M. (2013). Techno-economic analysis of potential natural gas liquid (NGL) recovery processes under variations of feed compositions. *Chemical Engineering Research and Design*, *91*(7), 1272–1283. https://doi.org/10.1016/j.cherd.2013.01.015

Grieves, M. (2015). *Digital Twin: Manufacturing Excellence through Virtual Factory Replication*.

Hochreiter, S., & Schmidhuber, J. (1997). Long Short-Term Memory. *Neural Computation*, *9*(8), 1735–1780. https://doi.org/10.1162/neco.1997.9.8.1735

Hori, E. S., & Skogestad, S. (2007). Selection of control structure and temperature location for two-product distillation columns. *Chemical Engineering Research and Design*, *85*(3 A), 293–306. https://doi.org/10.1205/cherd06115

Hudson, H. M., Wilkinson, J. D., Cuella, K., & Pierce, M. C. (2003). Integrated liquids recovery technology improves LNG production efficiency. In *82nd Gas Processors Association (GPA) Annual Convention* (p. 36).

Joseph, B., & Brosilow, C. B. (1978). Inferential control of processes: Part I. Steady state analysis and design. *AIChE Journal*, *24*(3), 485–492. https://doi.org/10.1002/aic.690240313

Kalman, R. E. (1960). A New Approach to Linear Filtering and Prediction Problems. *Journal of Basic Engineering*, *82*(1), 35–45. https://doi.org/10.1115/1.3662552

Ke, W., Huang, D., Yang, F., & Jiang, Y. (2017). *Soft sensor development and applications based on LSTM in deep neural networks* (p. 6). https://doi.org/10.1109/SSCI.2017.8280954

Kherbeck, L., & Chebbi, R. (2015). Optimizing ethane recovery in turboexpander processes. *Journal of Industrial and Engineering Chemistry*, *21*, 292–297. https://doi.org/10.1016/j.jiec.2014.02.035

Kidnay, A. J., Parrish, W. R., & McCartney, D. G. (2011). Fundamentals of Natural Gas Processing. In *Fundamentals of Natural Gas Processing*. CRC Press.

Kingma, D. P., & Ba, J. (2017). *Adam: A Method for Stochastic Optimization* (arXiv:1412.6980). arXiv. https://doi.org/10.48550/arXiv.1412.6980

Lu, L., Jin, P., & Karniadakis, G. E. (2021). DeepONet: Learning nonlinear operators for identifying differential equations based on the universal approximation theorem of operators. *Nature Machine Intelligence*, *3*(3), 218–229. https://doi.org/10.1038/s42256-021-00302-5

Luyben, W. L. (2005). Evaluation of criteria for selecting temperature control trays in distillation columns. *AIChE Annual Meeting Conference Proceedings, 2005*.

Luyben, W. L. (2013a). Control of a train of distillation columns for the separation of natural gas liquid. *Industrial and Engineering Chemistry Research*, *52*(31), 10741–10753. https://doi.org/10.1021/ie400869v

Luyben, W. L. (2013b). *Distillation Design and Control Using AspenTM Simulation*. https://www.academia.edu/34975308/DISTILLATION_DESIGN_AND_CONTROL_USING_ASPEN_TM_SIMULATION

Luyben, W. L. (2013c). NGL demethanizer control. *Industrial and Engineering Chemistry Research*, *52*(33), 11626–11638. https://doi.org/10.1021/ie400454y

Mandis, M., Chebeir, J. A., Tronci, S., Baratti, R., & Romagnoli, J. A. (2021). Control of a natural gas liquid recovery plant in a GSP unit under feed and composition disturbances. *IFAC-PapersOnLine*, *54*(3), 182–187. https://doi.org/10.1016/j.ifacol.2021.08.239

Manning, F., & Thompson, R. (1991). *Oilfield Processing: Natural Gas*.

McCulloch, W. S., & Pitts, W. (1943). A logical calculus of the ideas immanent in nervous activity. *The Bulletin of Mathematical Biophysics*, *5*(4), 115–133. https://doi.org/10.1007/BF02478259

Mehrpooya, M., Vatani, A., & Ali Mousavian, S. M. (2010). Introducing a novel integrated NGL recovery process configuration (with a self-refrigeration system (open-closed cycle)) with minimum energy requirement. *Chemical Engineering and Processing: Process Intensification*, *49*(4), 376–388. https://doi.org/10.1016/j.cep.2010.03.004

Mejdell, T., & Skogestad, S. (1991). Estimation of distillation compositions from multiple temperature measurements using partial-least-squares regression. *Industrial & Engineering Chemistry Research*, *30*(12), 2543–2555. https://doi.org/10.1021/ie00060a007

Mokhatab, S., Poe, W. A., & Mak, J. Y. (2015). Handbook of Natural Gas Transmission and Processing. In *Handbook of Natural Gas Transmission and Processing: Principles and Practices*. Gulf Professional Publishing.

Nakhjiri, A. T., Heydarinasab, A., Bakhtiari, O., & Mohammadi, T. (2020). Numerical simulation of CO2 / H2S simultaneous removal from natural gas using potassium carbonate aqueous solution in hollow fiber membrane contactor. *Journal of Environmental Chemical Engineering*, *8*, 104130. https://doi.org/10.1016/j.jece.2020.104130

Natural gas—Composition and properties of natural gas | Britannica. (s.d.). https://www.britannica.com/science/natural-gas/Composition-and-properties-of-natural-gas

Oisiovici, R. M., & Cruz, S. L. (2000). State estimation of batch distillation columns using an extended Kalman filter. *Chemical Engineering Science*, *55*, 4667–4680. https://doi.org/10.1016/S0009-2509(00)00088-9

Olsen, C., Kozman, T. A., Lee, J., & Yuvamitra, K. (2012). A Comparative Study of Natural Gas Liquids Recovery Methods. *Distributed Generation & Alternative Energy Journal*, *27*(2), 42–55. https://doi.org/10.1080/21563306.2012.10505411

Pang, C., Duan, D., Zhou, Z., Han, S., Yao, L., Zheng, C., Yang, J., & Gao, X. (2022). An integrated LSTM-AM and SPRT method for fault early detection of forced-oxidation system in wet flue gas desulfurization. *Process Safety and Environmental Protection*, *160*, 242–254. https://doi.org/10.1016/j.psep.2022.01.062

Park, J. H., Khan, M. S., Andika, R., Getu, M., Bahadori, A., & Lee, M. (2015). Techno-economic evaluation of a novel NGL recovery scheme with nine patented schemes for offshore applications. *Journal of Natural Gas Science and Engineering*, *27*, 2–17. https://doi.org/10.1016/j.jngse.2014.12.023

Paszke, A., Gross, S., Massa, F., Lerer, A., Bradbury, J., Chanan, G., Killeen, T., Lin, Z., Gimelshein, N., Antiga, L., Desmaison, A., Köpf, A., Yang, E., DeVito, Z., Raison, M., Tejani, A., Chilamkurthy, S., Steiner, B., Fang, L., … Chintala, S. (2019). *PyTorch: An Imperative Style, High-Performance Deep Learning Library* (arXiv:1912.01703). arXiv. https://doi.org/10.48550/arXiv.1912.01703

Pitman, R., Hudson, H., Wilkinson, J., & Cuellar, K. T. (1998). Next generation processes for NGL/LPG recovery. United States: N. p., 1998. Web.

Porru, M., Alvarez, J., & Baratti, R. (2013). Composition estimator design for industrial multicomponent distillation column. *Chemical Engineering Transactions*, *32*, 1975–1980. https://doi.org/10.3303/CET1332330

PSE research group, LSU. (s.d.). *SimWiz*. Louisiana State University. https://pse.che.lsu.edu/sw.php

Qu, X., Song, Y., Liu, D., Cui, X., & Peng, Y. (2020). Lithium-ion battery performance degradation evaluation in dynamic operating conditions based on a digital twin model. *Microelectronics Reliability*, *114*, 113857. https://doi.org/10.1016/j.microrel.2020.113857

Rademaker, O., Rijnsdorp, J., & Maarleveld, A. (1975). *Dynamics and control of continuous distillation units*.

Randek, J., & Mandenius, C.-F. (2018). On-line soft sensing in upstream bioprocessing. *Critical Reviews in Biotechnology*, *38*(1), 106–121. https://doi.org/10.1080/07388551.2017.1312271

Ratner, M. (2018). Natural Gas Liquids: The Unknown Hydrocarbons. *EveryCRSReport.com*. https://www.everycrsreport.com/reports/R45398.html#_Ref518912625

Rivera, D. E., Morari, M., & Skogestad, S. (1986). Internal model control: PID controller design. *Industrial & Engineering Chemistry Process Design and Development*, *25*(1), 252–265. https://doi.org/10.1021/i200032a041

Rosyadi, I., Wardhana, A. W., Aliim, M. S., Ediati, R., & Ristiawan, D. (2023). Multivariate soft sensor for product monitoring in the debutanizer column with deep learning. *Proceeding ICMA-SURE*, *2*(1), Articolo 1. https://doi.org/10.20884/procicma.v2i1.7762

Shinskey, F. G. (1996). *Process Control Systems: Application, Design, and Tuning*. McGraw-Hill.

Singh, V., Gupta, I., & Gupta, H. (2005). ANN based estimator for distillation—Inferential control. *Chemical Engineering and Processing - CHEM ENG PROCESS*, *44*, 785–795. https://doi.org/10.1016/j.cep.2004.08.010

Spigno, G., & Tronci, S. (2015). Development of Hybrid Models for a Vapor-Phase Fungi Bioreactor. *Mathematical Problems in Engineering*, *2015*, 11. https://doi.org/10.1155/2015/801213

Tao, F., Zhang, L., Nee, A. Y. C., & Pickl, S. W. (2016). Editorial for the special issue on big data and cloud technology for manufacturing. *The International Journal of Advanced Manufacturing Technology*, *84*(1), 1–3. https://doi.org/10.1007/s00170-016-8495-6

The MathWorks Inc. (2019). *System identification Toolbox™* (Versione R2019b) [MATLAB]. The MathWorks Inc. https://www.mathworks.com

The world's biggest natural gas reserves. (s.d.). https://www.hydrocarbons-technology.com/features/feature-the-worlds-biggest-natural-gas-reserves/

Tronci, S., Bezzo, F., Barolo, M., & Baratti, R. (2005). Geometric Observer for a Distillation Column: Development and Experimental Testing. *Industrial & Engineering Chemistry Research*, *44*(26), 9884–9893. https://doi.org/10.1021/ie048751n

Tronci, S., Neer, P. V., Giling, E., Stelwagen, U., Piras, D., Mei, R., Corominas, F., & Grosso, M. (2019). In-line monitoring and control of rheological properties through data-driven ultrasound soft-sensors. *Sensors (Switzerland)*, *19*(22). https://doi.org/10.3390/s19225009

Understanding LSTM Networks—Colah's blog. (s.d.). https://colah.github.io/posts/2015-08-Understanding-LSTMs/

Wang, P., Zhang, J., Wan, J., & Wu, S. (2022). A fault diagnosis method for small pressurized water reactors based on long short-term memory networks. *Energy, Elsevier, vol. 239(PC)*. https://ideas.repec.org//a/eee/energy/v239y2022ipcs0360544221025469.html

What are Neural Networks? - United Kingdom | IBM. (s.d.). https://www.ibm.com/uk-en/cloud/learn/neural-networks

Wilkinson, J. D., & Hudson, H. M. (1992). *Improved NGL Recovery Designs: Maximise Operating Flexibility and Product Recoveries*.

Yu, C. C., & Luyben, W. L. (1987). *Control of multicomponent distillation columns using rigorous composition estimators. 104*, A29–A69.

Yuan, X., Li, L., & Wang, Y. (2020). Nonlinear Dynamic Soft Sensor Modeling With Supervised Long Short-Term Memory Network. *IEEE Transactions on Industrial Informatics*, *16*(5), 3168–3176. https://doi.org/10.1109/TII.2019.2902129

Zamprogna, E., Barolo, M., & Seborg, D. E. (2005). Optimal selection of soft sensor inputs for batch distillation columns using principal component analysis. *Journal of Process Control*, *15*(1), 39–52. https://doi.org/10.1016/j.jprocont.2004.04.006

Zhang, S., Liu, C., Jiang, H., Wei, S., Dai, L., & Hu, Y. (2015). *Feedforward Sequential Memory Networks: A New Structure to Learn Long-term Dependency*. https://doi.org/10.48550/arXiv.1512.08301

Zhu, W., Chebeir, J., & Romagnoli, J. A. (2020). Operation optimization of a cryogenic NGL recovery unit using deep learning based surrogate modeling. *Computers and Chemical Engineering*, *137*. https://doi.org/10.1016/j.compchemeng.2020.106815

Zhu, X., & Ji, Y. (2022). A digital twin–driven method for online quality control in process industry. *The International Journal of Advanced Manufacturing Technology*, *119*, 1–20. https://doi.org/10.1007/s00170-021-08369-5

Acknowledgements

I would like to express my gratitude to Prof. Roberto Baratti for providing me with the opportunity to pursue this PhD. His patience, kindness, advice and guidance that have been instrumental in my academic journey. I am also deeply grateful to Prof. Stefania Tronci for her support, availability, kindness, and listening ear during the best and worst moments of my research.

I owe a heartfelt thanks to my parents, who have endured me throughout these three years, as well as my friends, siblings, and sister-in-law, who have been a constant source of valuable advice. I am also grateful to my niece and nephew, whose mere existence has brought joy to my life.

I would like to thank all my colleagues at the Department of Mechanical, Chemical, and Materials Engineering, particularly Massi, Fabio, Andrea, Simone, Damiano, and Mariano. But most of all, I would like to express my gratitude to fellow 'Dottorande Disperate' (just like me) Silvia and Giulia, who have made this journey less lonely and more colourful. Together, we have supported each other through thick and thin.

I would like to thank my 'Finnish' flatmates, Mitzuki and Bunta, and my colleagues Minho and Augusto, who have made a freezing place more warm and friendly.

I am sincerely grateful to Prof. José Romagnoli for being careful and looking out for me during my time at LSU. I would also like to thank Luis and Karla for warmly hosting me in their home, as well as all my colleagues at the LSU PSE group: Estelle, Keshani, Zach, Teslim, and Miriam. A special thanks goes to my friend Jhonattan, who has been my closest companion during my stay in Baton Rouge and has shown me the customs of Louisiana.